Validation of a Lattice Boltzmann model for snow transport and deposition by wind

Dissertation

submitted to and approved by the

Department of Architecture, Civil Engineering and Environmental Sciences
University of Braunschweig – Institute of Technology

and the

Faculty of Engineering
University of Florence

in candidacy for the degree of a
Doktor-Ingenieurin (Dr.-Ing.) / Dottore di Ricerca
in
“Mitigation of Risk due to Natural Hazards on Structures and Infrastructures”

by
Sara Giangreco
born 28.07.1979
from Tricase (LE), Italy

Submitted on	25. August 2010
Oral examination on	28. October 2010
Professorial advisors	Prof. M. Krafczyk
	Prof. V. Sepe

2010

Abstract

Risk management became an important issue for many disciplines such as finance, insurance industry or mechanical and civil engineering. In the general framework of risk management, risk analysis and hazard prediction are fundamental preliminary steps. This contribution addresses the prediction of snow-wind hazard resulting from coupled dynamics of snow transport and deposition by wind, which is the key to the prediction of snow load profiles on buildings. The target of this work is the development of a detailed Computational Fluid Dynamics (CFD) model and its validation by means of wind tunnel data available for representative model geometries. This approach for load analysis allows to investigate problems, which are not sufficiently standardized in terms of design codes. For this purpose, a two dimensional numerical large eddy simulation (LES) model for transient snow transport by wind is suggested. The model based on the lattice Boltzmann method (LBM) has been developed and validated. The lattice Boltzmann method presented utilizes the Multiple Relaxation Time (MRT) model and fluid/wall boundary conditions of second order accuracy. In the current approach, dry snow is modelled as a continuous component, which is being advected by the turbulent transient flow field. Snow deposition and erosion are controlled by imposing rules for the influence of wall shear stress and equilibrium approaches for the terminal velocity of snowflakes. The numerical method is compared to the experimental studies which have been carried out by L. Sanpaolesi et al, [22], in the "Jules Verne" Climatic Wind Tunnel of Nantes, France. These validation studies will be presented including sensitivity studies for various model parameters. Finally, potential extensions and shortcomings of this approach are discussed.

Kurzfassung

In Disziplinen wie beispielsweise dem Finanz- und Versicherungswesen, dem Maschinenbau oder dem Bauingenieurwesen spielt das Risikomanagement eine grosse Rolle. Im Gesamtkonzept des Risikomanagements sind die Risikoanalyse und die Prognose der Gefährdung fundamentale Ausgangsbausteine. Dieser Beitrag behandelt die Vorhersage der Schnee-Wind-Gefährdung resultierend aus gekoppelten dynamischen Prozessen von Schneetransport und -ablagerung zur Vorhersage von Schneelastprofilen auf Bauwerken. Ziel dieser Arbeit ist die Entwicklung eines CFD-Modells und dessen Validierung an Ergebnissen experimenteller Windtunnelversuche, die für repräsentative Modellgeometrien verfügbar sind. Dieses Analyseverfahren erlaubt außerdem die Untersuchung von Problemen, die in den Bemessungsnormen nicht ausreichend standardisiert sind. Zu diesem Zweck wird ein zweidimensionales numerisches Large-Eddy-Simulationsmodell (LES) für den transienten Schneetransport infolge Wind vorgeschlagen. Das Modell, das auf der Lattice-Boltzmann Methode basiert, nutzt das Multiple Relaxation Time (MRT) Modell und Fluid-Wand-Randbedingungen zweiter Ordnung Genauigkeit. Im vorliegenden Verfahren wird trockener Schnee als kontinuierliche Komponente modelliert, der von einem turbulenten transienten Strömungsfeld bewegt wird. Schneeablagerung und Erosion werden durch den Einfluss der Wandschubspannungen und Gleichgewichtsansätzen für die Schneefallgeschwindigkeit modelliert. Das numerische Modell wird mit experimentellen Studien verglichen, welche von L. Sanpaolesi im Jules Verne-Klima-Windtunnel von Nantes in Frankreich durchgeführt wurden. Diese Validierungsuntersuchungen sowie enthaltene Sensitivitätsstudien für verschiedene Modellparameter werden vorgestellt. Schließlich werden Möglichkeiten der Erweiterung dieses Verfahrens sowie Mängel diskutiert.

Acknowledgments

This work is the result of the real help and moral support of many people, I hope to succeed in thanking them all.
First and foremost my gratitude goes to Prof. Manfred Krafczyk for his continuous availability, for his patient support and dedication in teaching me the state of the art of my research subject and for his encouragement with which my thesis has been brought to success. Thank you for believing in my abilities, for the attention to my difficulties and for finding constructive solutions.
Another person whom I can never thank enough is Dr. Sebastian Geller who was, at different stages of this work, a reliable help to finish it. He was valued for his scientific experience and his moral support.
I am profoundly grateful to Prof. Udo Peil for the support and the believe in me, the fruitful discussions and above all for his great respect for my work.
Thanks also to Prof. Vincenzo Sepe for introducing me in this doctoral research and for giving me the opportunity to live this important experience.
I would like to express my gratitude to Dr. Mathias Clobes for welcoming me at the Stahlbau Institute of Braunschweig and for sharing and passing on me his scientific experience, in spite of my linguistic limits.
I also want to thank Prof. Claudio Borri for his efforts, along with Prof. Peil, in coordinating this international PhD, because they have given me this opportunity.
The discussion and conversation with Prof. Renato Ricci, Prof. Massimo Majowiecki, Prof. Piero D'Asdia, Prof. Luca Sanpaolesi and Dr. Luca Artipoli were useful during this research and the support of Prof. Massimiliano Gioffrè and Prof. Gianni Bartoli was instrumental in concluding this work.
Furthermore, I would to like to thank Prof. Philippe Delpech for his experimental data and research materials, and for welcoming me, for a brief stint, at CSTB of Nantes giving me the opportunity to live a fascinating experience of an experimental research.
I wish to extend my thanks to all my colleagues at the iRMB institute for providing an appreciated atmosphere, for valuable discussions and, primarily, for offering me their help whenever I needed it.
I am thankful to all my friends and my colleagues of this PhD, which often have been my second family for helping me with their support and providing a comfortable and lovely environment.
Last but not least I want to express my gratitude to thank my family who have supported me all the time and for understanding my sporadic presence at home during important times, they have been my strength.
Thank you for the research founds:
University La Sapienza in Rome;

Institute of Steel Construction in Braunschweig;
Institute für Computational Modeling in Civil Engineering in Braunschweig.

Sara Giangreco
Specchia, August 2010

List of Figures

List of Tables

Contents

1 Introduction

1.1 Scope

This dissertation presents an original numerical simulation technique of the generic problem of wind-snow interactions. The aim is to provide a cheap tool to assess the load distribution induced by snow on ordinary buildings. To model fluid the so-called lattice Boltzmann approach has adopted.
The main parts of the work presented in this thesis are three:

- The implementation of a D2Q9 (two dimensional nine velocity distribution) model to simulate snow transport by wind. The first part focuses on the physical and numerical modeling aspect to describe the behavior of snow transport, the implementation of the algorithms to express these phenomena, and the flow properties at the boundaries.

- The central part presents some of the validation examples, which were carefully examined during the development of the model and code implementation. The model performed is validated through oversimplified test cases in terms of the geometry used to generate the numerical grid, and in terms of definition of flow. Severals experiments are performed to estimate each single mechanism of transport, to determine the effective parameters and constitutive relationships these simple cases studied are performed with coupled problem of deposition and erosion.

- The parameters optimization is obtained with comparisons of numerical results and experiments. A convergence study is described for different shapes of buildings. The last section presents the results, the performances are measured and analyzed.

The model solves coupled actions of snow and wind on structures in two-dimensions.

1.2 Motivation

The motion of particle in fluids is a physical phenomenon frequently occurring in nature. For example, water transports sediment in rivers, wind moves snow particles on mountains or sand particles in the desert.

Today, with the increasing power of computers, one has more and more recourse to them to simulate physical phenomena. This implies a virtual description of the phenomena which has to be as close as possible to reality. Compared to scale models, computer simulations present many advantages (e.g. they are easy to modify and handle, and are also cheaper). Also, these virtual simulations and their numerical models bring a better understanding, allow us to make predictions more accurate and, sometimes, offer an explanation of the mechanisms. Last twenty years they have witnessed extensive embracing of Computational Fluid Dynamics (CFD), which is one of the branches of fluid mechanics that uses numerical methods and algorithms to solve and analyze problems that involve fluid flows.
In this thesis, we focus our attention on snow transport and deposition by wind occurring on the roofs of infrastructure.
In most snowy regions, the combination of wind and snowfall often leads to unwanted snow depositions in lees created by obstacles or other places where wind reduces its transport capacity. Snow transport is mainly driven by this interaction between wind, topography and vegetation, but also interactions between moving snow particles, humidity, temperature etc... affects the overall transport. In all cases wind is the primary snow drift parameter (Pomeroy, Gray 1997).
Special considerations for snow drift are often necessary during planning of structures, new residential, roads, to reduce disadvantages or to utilize advantages of the cold climate. In the design phase of new structures and during the analysis of the existing configuration, it is therefore important to determine the configuration and magnitude of snow loads, that can exhibit marked variability inherent non-linearity of the coupled process as can be observed in Figure (1.2.1).
.

Figure 1.2.1 – Ordinary building, Italy.

Dangers arising from inadequate provision against snow loads are nevertheless real, as amply demonstrated by frequent occurrence of building collapses. Unfortunately in some cases, such collapses have brought about loss of life.

The current Building Codes [22] provide minimum design loads for roofs which are based primarily on field observations made on a variety of roofs and on a statistical analysis of ground snow load data. There are, however, numerous situations where the coupling of different climatic actions are not well covered by the general provisions of the codes. In order to increase the reliability level of the design process of structural systems, very careful load analysis must be performed to control these phenomena.
Physical experiments in wind tunnels, water flumes and in full scale are still used for prediction of snow drifts. Unfortunately, these kinds of experiments are time consuming, expensive and not easily available for the common engineer, so the need for a more commonly available tool for predicting possible snow drift formations is certainly present. Besides, a model in laboratory is complicated as the relevant dimensionless parameters such as Reynolds number and material parameters cannot easily be met due to inherent downscaling effects. Hence, a numerical model can contribute to a better understanding of these phenomena.
The main objective of this work is to develop a numerical model and validate it through the comparison with experimental results. The goal is to analyse wind and snow drifting conditions on different types of simple structures, and to provide an inexpensive tool to assess the load distribution induced by snow on ordinary buildings. The numerical simulation also acts as a low cost counterpart to experimental wind tunnel investigations of non-standard buildings, like stadium and arena.
The numerical model developed at the Institute for Computational Modeling in Civil Engineering of Braunschweig, Germany, adapts Large Eddy Simulation (LES) by computing only the resolved structures and modeling the effect of the unresolved scales on the effective ones.
The experimental tests carried out in the "Jules Verne" Climatic Wind Tunnel of Nantes, France, developed for an European project by L. Sanpaolesi et al, [22], of the University of Pisa, Italy, are used to calibrate the available numerical model parameters. The numerical-experimental comparison selects building configurations, which might be of primary importance in the design codes.

1.3 Outline

First (1.1-1.2) the topic, which is developed in this thesis, is introducted and then motivations of this choise in doctorate of "Risk Management on the Built Enviroment". The objectives and the main research institutes that are involved in this project are also mentioned. In chapter (2) a general framework for Risk Management is described through the formulation of many different definitions of Risk, with regard to the Risk Management Framework (RMF) developed by the research group of the International Graduate College (IGC 802) [52] in an attempt to create a unified language for Risk Management. For complex problems, that are for instance not standardised, RM provides a general approach. The specific importance of the different climatic actions on the structures are highlighted. A risk based design can be done which is usually more

economic and more accurate than the standards. New effects can be taken into account and implemented into the design. The investigation regards the structural load analysis considering the wind-snow hazard. The general risk management methodology of [52] is modified in a reasonable way to consider also the impact of wind-snow on the final load of building, the wind effect changes the profile of snow deposited on building, which represents a dynamic obstacle in the flow filed. Under the wind-snow interaction the snow cover is growing in deposition zones, and the new shape therefore influences the local velocity field, generating the load hazard. Hence, the hazard-load analysis is added to the general scheme of Risk Management (2.4.1).
Chapter (3) proposes an introduction of the physical proprieties of wind and snow, the classification of these actions considering different phases in space and time. In the central part of this chapter the preliminary notions of mechanisms of snow transport by wind are explained. After reviewing the state of the art related to the different snow drifting models the approach used in this thesis is presented. The numerical model to simulate wind-snow interaction (i.e. the **VirtualSnow** model), is calibrated and validated through the comparison between experimental and numerical results, as showed in chapter (7). The description of the wind tunnel test campaign carried out in the "Jules Verne" Climatic Wind Tunnel of Nantes, is reported in chapter (4). The scientific work, developed under the commission of the European communities in 1997, is aimed at improving the scientific knowledge and models for the determination of snow loads on buildings, to product a sound common scientific basis which can be accepted by all European countries involved in the drafting of Eurocodes. Several types of structures are tested and the discussion includes the influence of the experimental parameters on the results.
In chapter (5) a brief description of fluid dynamics is given. Some fluid dynamics essentials and the main traditional numerical models are introduced. The chapter ends with a model comparison. Chapter (6) describes the salient features of the **VirtualSnow** model, the flow settlement conditions and the rules describing the behaviour of snow (deposition, erosion and toppling). To model virtual snow the flow concentration dynamics, governed by advection, diffusion and gravity are computed with the lattice Boltzmann method in combination with an LES - turbulence model. The snow cover is dynamic by coupling changes in geometry to the flow. The model is programmed by considering a vector of cells rather than a multidimensional array. Such a vector implementation implies to add neighborhood information to the cells. The major advantage is that this vector data structure is usable for any lattice topology and dimension. The validation process of the code is described step by step in chapter (7). First we discuss oversimplified cases in terms of geometry, definition of flow, grid discretization and decoupled mechanisms of snow transport. After that we consider more complicate cases to address real experiments presented in chapter (4). The comparison for different shape of buildings between numerical and experimental results is presented in chapter (7). Finally, in chapter (8) some general conclusions are drawn and an outlook on future work is given.

2 Risk management methodology and risk reduction for structures under combined wind-snow actions

The concept of risk management (RM) has become widely accepted in the last years, being applicable to a huge variety of activities, decisions and operations, involving public as well as private enterprises, groups or single individuals. The present chapter aims at describing the procedure for RM developed within the IGC 802 [52], which has been adopted in the present dissertation as the backbone of the methodology proposed for managing risk on buildings due to snow transport and deposition by wind. The chapter ends with the contribution of the present research work to mitigate the risk in this field, additional conclusions are drawn in chapter (8).

2.1 General remarks

The relevance of risk of buildings during a wind-snow storm is evident to everybody after several structure collapses each years, when the richest and most technological countries of the world showed their vulnerability and non-preparedness with respect to such an event. The transport of snow and its subsequent redeposition as a drift is a primary cause for roof collapse in could climate. That is, roof collapse caused by relatively large, concentrated loads that form at a drift accumulation area is more common than collapse caused by more moderate uniform loads acting over the whole roof. Information from the insurance industry indicates that in the past about 30% of all structural losses from snow in United States were due to unbalanced drifting [51]. During particularly snowy winters, hundreds of such losses can be expected. O' Rourke describes an extreme case that occurred in the Boston, Massachusetts, area in 1978 in which the maximum load caused by the drift (13.4 kPa) was more than 18 times the ground load (0.7 kPa).
Available data are already quite eloquent, for example the collapse of Bad Reichenhall Ice hall, Germany, showed in Figure 2.1.1.

Figure 2.1.1 – Collapse Bad Reichenhall Ice-hall, Germany.

Figure 2.1.2 – Collapse Bad Reichenhall Ice-hall, Germany.

In the town of Bad Reichenhall, the roof of a 1970s-built ice rink collapsed, fifteen people were killed. The structure was in use until the disaster occurred on 2nd of January 2006. Police conducted an investigation into the cause of the collapse. There are a large number of reports indicating structural weaknesses in the building and discussions had been held some years earlier in the town council over the necessity of either completely renovating or pulling down the hall. Building experts agreed that the volume of snow was sufficient to cause the 60-x-30-m roof to collapse, considering also the material deterioration of the structure. Snow loading on building roofs represents an important design consideration in particularly in low-rise construction and very careful analyses

are necessary.
After this panoramic view of risk management, related to safety of buildings, it is important to remember that this research work provides an advanced tool to analyze wind-snow hazard during the design phase.
In the next section, first of all different definitions of risk are presented and discussed. Thereafter, a methodology is described that shows the relation of the different definitions as well as a reasonable concept to manage disaster risk. Moreover, the concept is modified to apply it to the current problem of this work.

2.2 Different definitions of Risk

Risk management is a quite modern concept used in many fields as medical science, finance and insurance industry, mechanical engineering and also to manage disaster risk. Wind storms, floods, earthquakes, fires and other natural disasters as well as miscellaneous catastrophes that occur worldwide are very different in nature and imply various impacts on the affected surrounding region. To deal with such disasters natural scientists, engineers, economists, politicians and other stakeholders are involved. All of these show the high multidisciplinary application and the different histories in developing RM of the different fields. Almost each of them developed their own understanding of disaster related terms.
As a consequence, a huge variety of definitions is existing and the communication within the disaster management community is often accompanied by misunderstandings and confusion. A consistent communication in disaster management is essential for an efficient cooperation of various disciplines and coordination of the important sub-steps in the risk management chain. The results of an extensive literature review are shown in the following. Basically, five widespread groups of definitions regarding disaster risks can be extracted and are categorized subsequently [52]:

- Risk = Hazard times Vulnerability **Group(1)**
- Risk = Hazard times Vulnerability · Exposure **Group(2)**
- Risk = Probability times Damage **Group(3)**
- Risk = Probability times Loss **Group(4)**
- Risk = Probability times Consequences **Group(5)**

Definitions of disaster risk management related terms are provided in a glossary of [52]. For these groups, some citations are given below as well as several further references.

Group(1):
"Risk is the product of hazard (H) and vulnerability (V) as they affect a series of elements (E) comprising the population, properties, economic activities, public services, and so on, under the threat of disaster in a given area" (Alexander, D. 2003) [7]. Further

references: [24], [61], [3], [23].

Group(2):
"Risk is associated to the disaster as a product of both the exposure to the hazard (natural event) and the vulnerability of objects (society) to the hazard. It suggests that three main factors contribute to disaster risk: hazard, exposure and vulnerability." [74] Further references: [4], [44], [11]

Group(3):
"Risk is an expression of possible loss over a specific period of time or number of operational cycles. It may be indicated by the probability of an accident times the damage in dollars, lives, or operating units." [36] Further references: [35], [2].

Group(4):
"A state of uncertainty where some possible outcomes have an undesired effect or significant loss. A set of measured uncertainties where some possible outcomes are losses, and the magnitudes of those losses - this also includes loss functions over continuous variables [1]. Further references: [65]

Group(5):
"Risk is the probability of an event multiplied by the consequences if the event occurs." [25] Further references: [59], [40], [58].

In relation to the specific case studied in this thesis, wind-snow hazard is increasing because of climate changes, the planet is globally warming, more energy is consequently available in the atmosphere and as a result the frequency and probably the intensity of extreme events like snow storm or windstorms in general have sensibly increased. This trend is expected to continue in the next decades and for instance it will probably be necessary to design structures with different wind loads depending on the year of construction and expected lifetime [11]. Exposure is increasing as well due to the migration of population, goods and facilities into hazardous areas, where many mega-cities were founded in the last decades. Finally new structures tend to be lighter and consequently more vulnerable to wind. The diffusion of light and high-resistance materials leads the construction industry in this direction. In addition, always more challenging designs are realized (large flexible roofs, long-span bridges, high-rise buildings, etc.) which requires that wind-snow effects are considered as carefully as possible.
Very often, the existing definitions of risk available in the literature do not use clear mathematical equations to determine the risk. Frequently, risk is described as a function of several terms. The before collected risk groups Group (1)-(5) have to be understood in this sense and not strictly mathematical. The main task of the groups is to assign the huge variety of existing definition to reasonable groups with similar meaning and estimation strategies. The wide range of understanding of risk and the meaning of included

terms is shown well in the following definition.
"Risk is a combination of the probability or frequency of occurrence of a defined hazard and the magnitude of the consequences of the occurrence. More specific, a risk is defined as the probability of harmful consequences, or expected loss (of lives, people, injured, property, livelihoods, economic activity disrupted or environment damaged) resulting from interactions between natural or human induced hazards." [26].
Several definition groups are included in this single definition. It results mainly from the different means of damage, loss and consequences. This can be observed for many different risk definition in the literature. It can be pointed out that the last three groups may be summarized to one, if the three terms (damage, loss and consequences) have similar meaning, that is the result of a disaster. Moreover, all above given risk definitions of the five groups as well as the quoted verbal definitions show that the diverse meanings of risk are mainly caused by the different understandings of the terms hazard, vulnerability, exposure, damage, loss and consequences. The meaning margins and intersecting between the references are perceptibly smeared and foggy.
An advanced disaster management concept of [52] is elucidated in the next section. Important sub-steps of risk management are included in this methodology. The theoretical background, that is sufficient to illustrate how the above listed definitions interrelate, is explained and definitions of the risk defining terms are given.

2.3 Risk management methodology

The necessity to have a reasonable clarified base of risk management terminology is shown in the previous part. For the research group International Graduate College such a base is given and used also in this work. The methodology is developed in [52]. Subsequently, this basic concept is introduced regarding the mentioned sources to give the fundamentals of risk language used in this thesis.
As illustrated in Figure (2.3.1) the three main components of the framework are given by risk identification, risk assessment and risk treatment and are performed sequentially throughout the risk management process, accompanied by a risk review step and continuous risk monitoring. The risk review process is assigned to the task to constantly include all new information, knowledge and experience about the risk and to indicate its evolution within the process over time. Thus, the risk is updated on a regular basis. It should be emphasised that the risk review process is only performed for risks that have already run through the whole process at least once. Consequently, in each risk review iteration the effectiveness of possibly implemented risk reduction interventions is indicated. The risk monitoring procedure in contrast, captures the exchange of information of all persons actively or passively involved or participating in the risk management process. This exchange of information is necessary to guarantee a smooth collaboration between interdisciplinary researchers and to discover new hazards due to the ever changing environment.

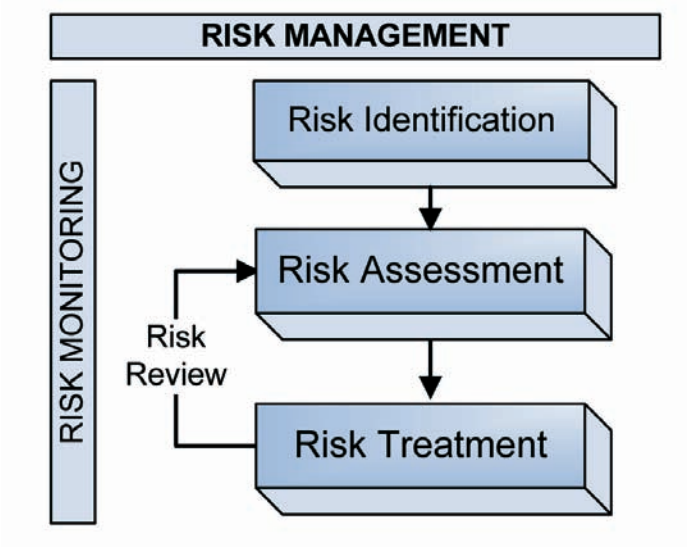

Figure 2.3.1 – The general risk management framework, [52]

2.3.1 Risk identification and Risk assessment

The prerequisite for performing the risk identification phase and therefore to initiate the operation of the risk management chain is the condition of being aware of a dangerous situation. The risk identification step leads to an answer to the question "what can happen and where?"
Differently from the case of wind storm records, a database of wind-snow interaction phenomena i.e. maps relate snow intensity precipitation to dominant direction of strong wind and mean value of the velocity in each direction does not exist up to now. Structural engineering needs relationships to estimate the potential snowdrift loading. Thus, knowledge about potentially dangerous scenarios arising from wind-snow interaction on constructions may be attained mainly through field observations or reports on past events. For example, the roof over the Montreal Stadium, Quebec is composed of a pretensioned membrane combined with an eccentric cable-stayed system, which leads to a non-uniform structural response under variable static loads. The roof ripped on several occasions due to a design flaw in consideration of static as well as the dynamic effects of wind and snow. In particular the first failure occurred in an apparently unexceptional weather condition. Hence, first of all the boundaries of the model domain have to be circumscribed by defining the system under analysis. After the identification of risky situations, the RM process proceeds with the following steps. First, the system to be investigated has to be delineated within the model domain, which can be a single building (as in the present work) or infrastructure or structural element, but in general also a city, a region or even a whole country, depending on the type of natural disaster under consideration. It should be noted, that any component in a system can be modelled as a system itself. Secondly, all sources of events that may endanger the functionality of

the system have to be identified. These events are named hazards.
With reference to the aforementioned case study, the Olympic Stadium of Montreal, both the occurrence of wind storm event and the snow storm event may be recognised as the hazards affecting the system, similarly to the topic of the present research.
As soon as this analysis is completed for a particular location, one proceeds with the risk assessment phase.
Risk analysis:
The risk analysis procedure (2.3.2) represents the most sophisticated part of the risk assessment phase, whose major objective lies in the quantification of the risk defining parameters and finally the risk itself, most desirably in monetary units per time unit (i.e. $\$/year$). In order to reach this ambition, first of all a hazard analysis is being performed where the intensity and frequency parameters of each identified hazard type with respect to the predefined system are estimated. Once the hazard data are quantified, it has to be analysed, which components of the system are exposed, i.e. potentially endangered by the impact of the hazard. In this way, a subdivision of the system into elements at risk (EaR) and elements at non risk (EaNR) is performed, depending on the hazard under consideration. As the EaNR are by definition not exposed, they are not threatened by the hazard and can therefore be excluded from the further analysis. An EaR on the contrary, represents a building or another arbitrary infrastructure element that is characterised by several parameters that have to be determined. Among these are precise location parameters within the system, information about the functional use (residential, commercial, industrial), occupancy (inventory of contents, number of people living or working inside) and construction type (building material, number of stories, construction year). A detailed discussion about EaR parameters is provided in Grossi et al. [7]. Furthermore, to facilitate the analysis, EaR with similar characteristics can be grouped together into EaR classes, depending on the hazard under consideration. Then, further analysis can concentrate on one typical representative out of each EaR class, assuming that all other EaR of the same category will show similar behaviour.

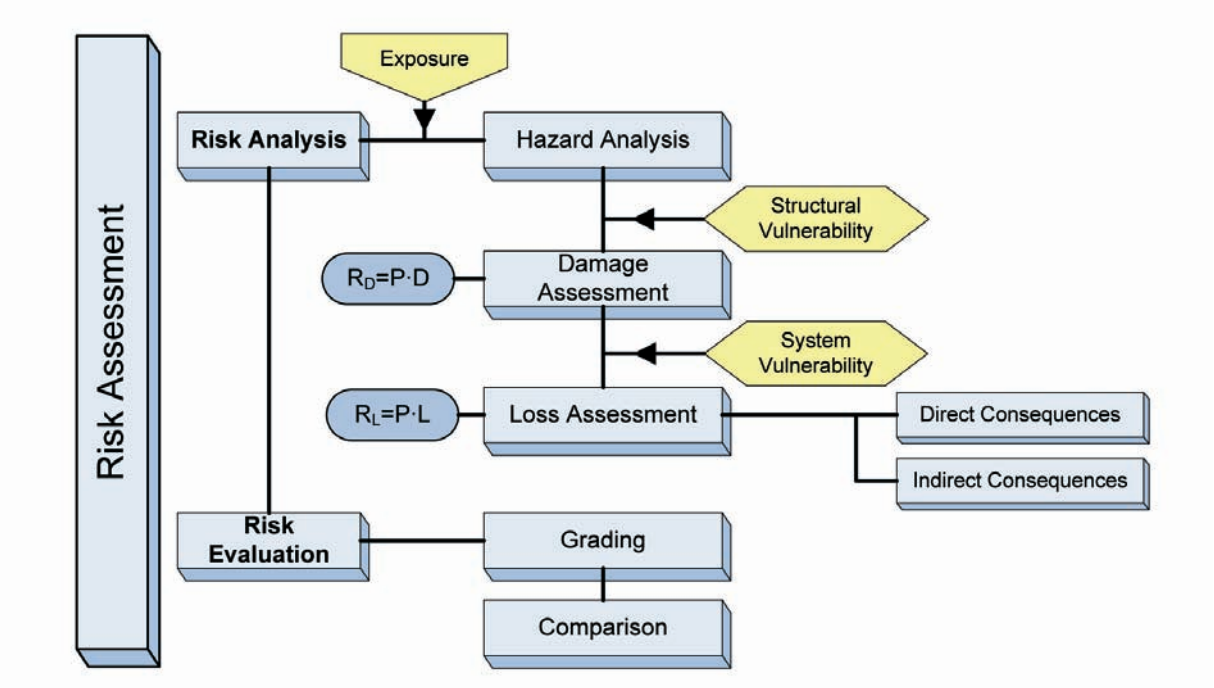

Figure 2.3.2 – The risk assessment phase, [52]

After all the EaR (classes) have been identified and clearly delineated, the structural behaviour of each EaR (class) has to be predicted depending on the hazard load. The damage module of an EaR is strongly dependent on the structural response of the EaR and captures physical harm only. It can be expressed by a large variety of measures, e.g. water height, crack width, storey drift, which are used to derive damage states. It has to be clearly emphasised that damage is not measured in monetary values. The relation between the hazard intensity and the resulting damage is called structural vulnerability. Thus, the structural vulnerability is an EaR (class) specific characteristic that indicates the degree of physical susceptibility towards the impact of the hazard.
Subsequent to the prediction of the structural behaviour of all EaR (classes), the consequences for the system that might go in line with a given level of damage of the exposed elements have to be analysed. For this investigation the characteristic parameters of each EaR (class) have to be taken into account. It is distinguished between direct consequences, that occur simultaneously to the time the disaster takes place and indirect consequences, that occur with a time shift as a result of the direct consequences. Whereas direct consequences are in a straight line linked to the coping capacity of the system, i.e. the ability to withstand the natural forces and to provide immediate help, indirect consequences are linked to the resilience, i.e. the capacity to remain functional and recover from the disaster. In addition, each consequence class is further subdivided into tangible or economic consequences, that are directly measurable in monetary terms and intangible consequences, that are not directly appreciable, e.g. injuries and fatali-

ties, pollution of the environment, loss of cultural social and historical values etc. (2.3.2) provides an overview of the consequence division.
After all possible consequences for each EaR (class) and thus for the system have been determined, loss appraises and eventually accumulates all direct and indirect consequences at the time the disaster takes place. In this respect, the indirect consequences that occur later in time have to be discounted on basis of a properly defined discount rate that is specific for each consequence class. In this context, system vulnerability is an EaR (class) specific characteristic, that links the hazard parameters directly to the loss and indicates the total potential the hazard has on the EaR (class). Thus, it indicates the physical susceptibility of the EaR (class) itself, its contents as well as the resulting degree of disruption of its functionality within the system. Consequently, the structural vulnerability is included in the broader concept of system vulnerability.
The risk analysis phase terminates with the quantification of risk where all the previously collected information is comprised. It is distinguished between two different types of risk. Firstly, risk can be calculated by taking the product of the annual probability of occurrence or exceedance of the hazard or damage multiplied by the expected damage that goes in line with it.

- Structural Risk = Probability x Damage [Damage measure / year]

This is being referred to as structural risk. Evidently, the structural risk is of primary importance for engineers in order to predict the behaviour and the response of a structure or structural element under potential hazard load. The second way to express the risk is to take the product of the annual probability of occurrence or exceedance of the hazard or loss and the expected loss.

- Total Risk = Probability x Loss [Loss unit / year]

It is being referred to as total risk. The total risk may comprise all consequences, both tangible and intangible, if a reasonable way has been found to convert the primarily non appraisable harms into monetary units. Alternatively, this transformation of intangible outcomes does not need to be done and the total risk can be split according to the respective consequence classes to indicate their relative contribution to risk. In any case the total risk is more exhaustive than the structural risk as the full hazard potential to the system is taken in account.

- Risk evaluation:

Subsequent to the termination of the risk analysis procedure, the risk evaluation phase is initiated. The purpose of risk evaluation is to make the considered risk comparable to other competing risks to the system by the use of adequate risk measures. In this context, so called exceedance probability curves have found wide acceptance as a common tool to illustrate risk graphically. In an exceedance probability curve the probability that a certain level of loss is surpassed in a specific time period is plotted against different

loss levels. Hereby, the loss to the system can be specified in terms of monetary loss, of fatalities or of other suitable impact measures. An insightful overview of common risk measures and tools to compare risks is provided in Proske [11]. Finally, after having analysed the risk on basis of adequate risk measures, it may be graded into a certain risk class, depending on individual risk perceptions.

2.3.2 Risk treatment

After the risk to the predefined system has been analysed and graded into a risk class, the last procedure of the risk management framework, the risk treatment phase, begins to operate. This procedure is assigned to the task to create a rational basis for deciding about how to handle the risk in the presence of other competing risks. Based on several analytical tools from decision mathematics, economics and public choice theory, a decision whether to accept, to transfer, to reject or to reduce a given risk can be derived. In the latter case, risk mitigation initiatives are implemented. Figure (2.3.3) visualises the process of risk treatment schematically.

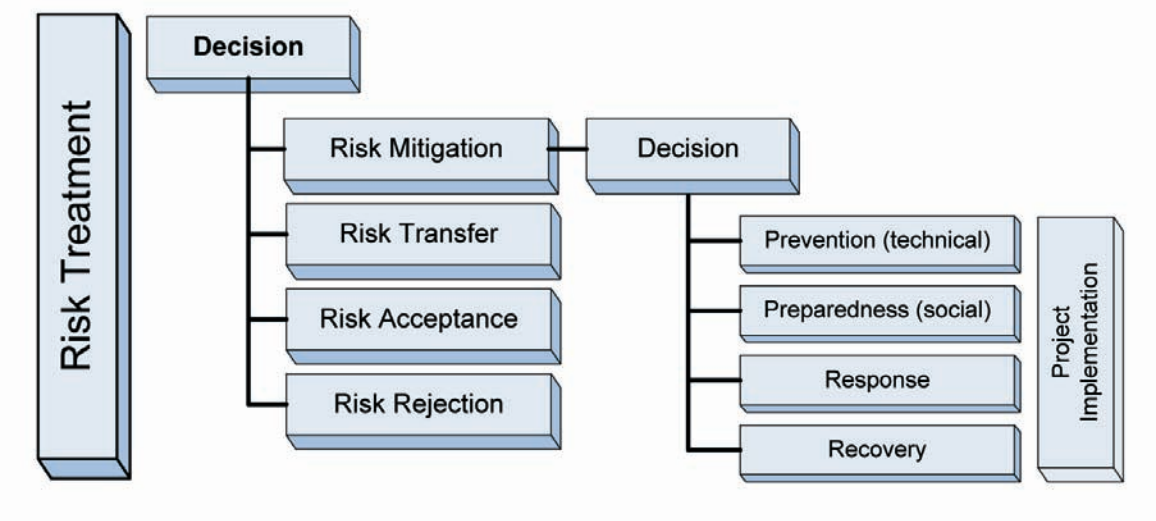

Figure 2.3.3 – The risk treatment phase, [52]]

If the risk is to be mitigated, decision makers are able to choose among several options to implement a risk reduction project. All the possible risk reduction strategies have in common that they reduce the vulnerability of the system. Depending on the specific strategy that is chosen, they can either reduce structural vulnerability by increasing the resistance of structures or system vulnerability by strengthening the system to recover from the disaster as quickly as possible. The strategies are subdivided with respect to the time the risk reduction project is implemented.

Firstly, so called pre-disaster interventions, such as prevention and preparedness, are available. Prevention includes technical measures like structural strengthening, that have to be performed with an accurate time horizon before the disaster takes place. Typical examples are snow storms, earthquakes or volcanos. Preparedness in contrast contains all social activities, e.g. evacuation plans and emergency training, that are necessary to limit harm shortly before the disaster takes place.
Secondly, post-disaster strategies can be pursued to reduce the risk. Among these, response covers all activities that are performed immediately after the occurrence of the disaster, such as the organisation of help and shelter for the injured and harmed as well as the coordination of emergency forces. Recovery on the contrary, subsumes all activities that need to be taken until the pre-disaster status of the system is restored again.
Obviously, also a combination of the mentioned possibilities can be applied to mitigate the risk.

2.4 Application of the risk management methodology

This section describes how the above explained RM process can be applied on the current problem of wind-snow hazard on buildings. The RM process, developed by IGC 802, is modified in a reasonable way to consider also the impact of the action due to wind-snow interaction phenomena on the final load of buildings.

2.4.1 Wind-snow hazard analysis

Concerning the large sphere of risk management this research work focuses on hazard analysis, that is mainly on the step of risk analysis in the process of risk assessment, see Figure (2.4.1). As already pointed out, wind-snow engineering as a modern discipline is fairly young and risk-consistent approaches in this field are still not very well codified. Then, if we concentrate on wind-snow interaction phenomena, to perform risk analyses and to conceive risk mitigation planning is even much more difficult, since this phenomena is already quite difficult to treat in a traditional, deterministic way. The ambitious attempt of this work is to include in risk analysis wind-snow hazard study and stability under load hazard resulting from these actions. Two contributions in this direction are given: the first one is a sort of pre-design study of wind-snow interaction, which is related to risk mitigation through code implementation; the second one is the quantification of snowdrift intensity. Snow and wind are two different climatic actions that are usually considered separated from each other. This assumption is only correct, if these actions occur not combined. Snow is a live load acting vertical pressure on a structure. Wind is a live load as well that can act from different directions on the building. For both loadings, separated hazard analyses can be carried out, simply by wind and snow maps of the design codes and their load application rules. The results of such hazard analyses

are the wind velocity and the snow depth on the ground. However, during a snowstorm the presence of strong wind is nevertheless real and interaction effects can become important. Therefore, the actions of wind and snow have to be studied simultaneously to define the environment field of the structure, this goes in line with interactions of both hazards and will be called wind-snow hazard in the following. Of course, the occurrence of wind and snow can be analyzed more precise to characterize roof snowdrift loading, for instance by means of meteorological studies, measurements in situ, experimental tests and numerical models. For very important structures this may be done but structural engineering need tools relatively easy to use and yet reasonably accurate.

2.4.2 Resulting hazard load

Wind-snow hazard includes the mechanisms of transport of snow by wind taking into account also the relation with the obstacles, here the construction. It is explained more in detail in chapter (3). The general RM methodology of (Pliefke et all. 2007) [52] is modified in a reasonable way to consider the hazard load analysis. The snow pack deposited on the roof after a snow storm generates a new obstacle shape that of course influence the wind field and the final load distribution profile. In Figure (2.4.1) the hazard-load analysis is added to the general RM methodology.

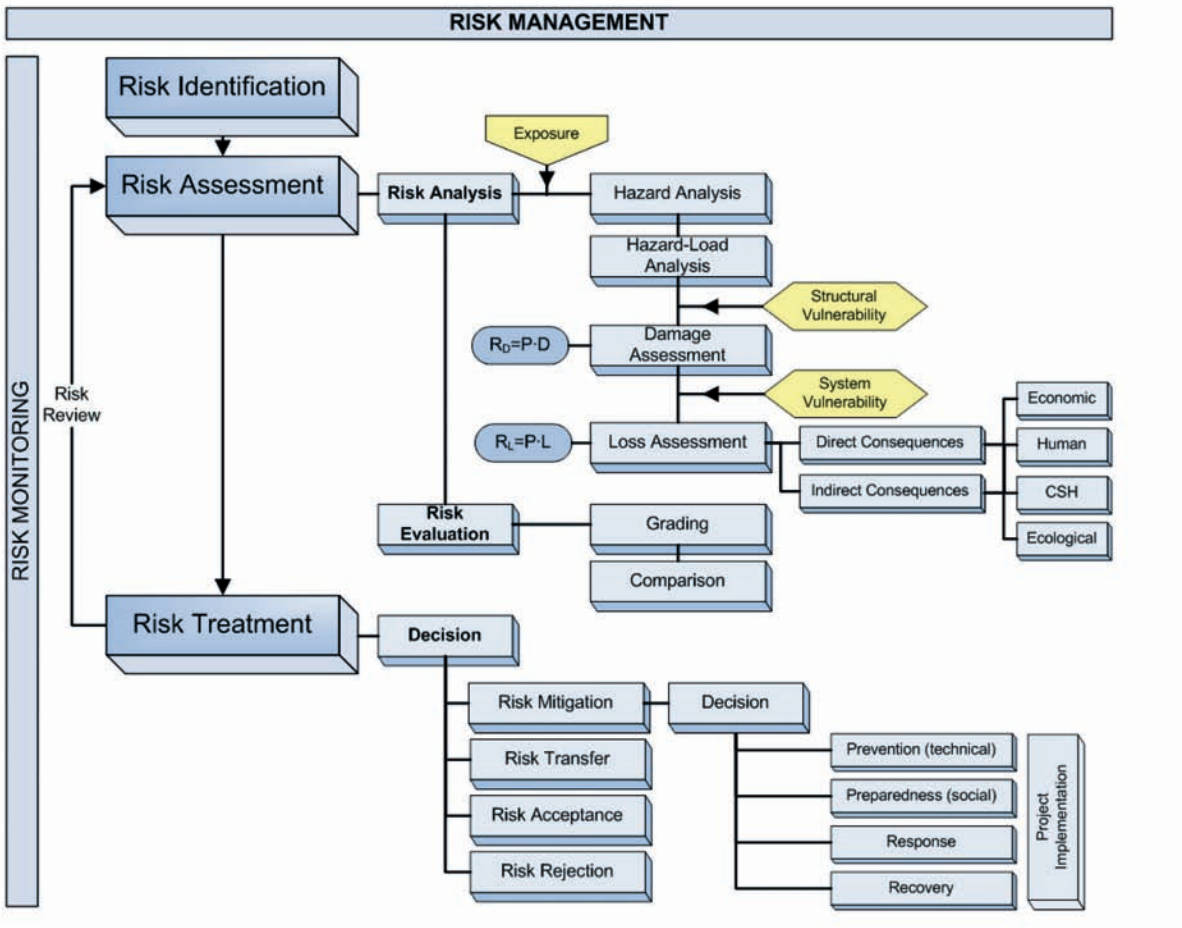

Figure 2.4.1 – Modified risk management process.

For the advanced hazard-load analysis, which is the main part of this thesis, a sophisticated procedure is applied by means of an innovative numerical CFD model.

2.4.3 Risk reduction for structures under wind-snow actions

The risk of collapses goes in line with the lack of knowledge regarding potential loading on a structure caused by snow, wind and its interaction. Finally in a catastrophic scenario due to a natural event, the collapse or the serviceability failure of important structure can make the disaster response extremely difficult concerning emergency plans and humanitarian assistance. Obviously, insufficient information of possible snow and wind action may lead to disasters. A contribution to close this gap is given by the approach and method of this thesis. Complete extensive experimental investigations can be very expensive and time-consuming and often wind-tunnel tests are performed only

at the last design stage as final validation. Therefore for structural engineers it could be very useful to dispose of an instrument able to highlight or to exclude with a certain degree of reliability the possibility of instabilities, without performing wind-tunnel tests, at least at pre-design stages. The design of ordinary structures is usually performed regarding construction codes with inadequate and partly insecure assumptions of the loading. These may lead to a wrong assessment of the risk.
For existing structures a so-called risk monitoring with the new information can be done. In the present research work we limited our attention to stability for structures under non uniform load and we tried to set up a simplified method of calculation which could be used in order to understand if a given structure, for a specified level of the hazard, is safe enough (wind-snow interaction is definitely not a problem) or the design must be definitely modified or if wind tunnel tests are needed in order to better assess the actual vulnerability of the structure. This tool could be useful to better design conventional buildings and in this sense we can speak about a pre-design study, which could help to improve the codes, therefore as a measure of risk mitigation.

3 Basic concepts in snow transport modelling

In this chapter the mechanics of snow drifting process are outlined and the requirements for physical modelling are summarized. It will be seen that these cannot all be satisfied in practice and every modelling method therefore involves some compromises. The current approach to modelling snowdrift is discussed in the light of the requirements, more detailed aspects concerning the physical equations and the implementation will be present in chapter (6). The chapter is divided in three parts: first we discuss the characteristics and classification of winds and snow actions, and then the preliminary notion of mechanisms of snow transport by wind are presented, followed by snow drifting models.

3.1 Characteristics and classification of winds

3.1.1 Geostrophic winds

Firstly, fundamental proprieties of stratified planetary boundary layers are outlined, starting to describe the wind surface high up in the troposphere where geostrophic winds are blowing, see Figure (3.1.1) [62]. The motion of air is frictionless and the only force that balances the pressure gradient in the flow is the Coriolis force, which results from the earth rotation. Viscosity effects are neglible and ideally no turbulence is present. All fluid parcels in the same vertical column move in harmony, for example there is no vertical displacement of air.

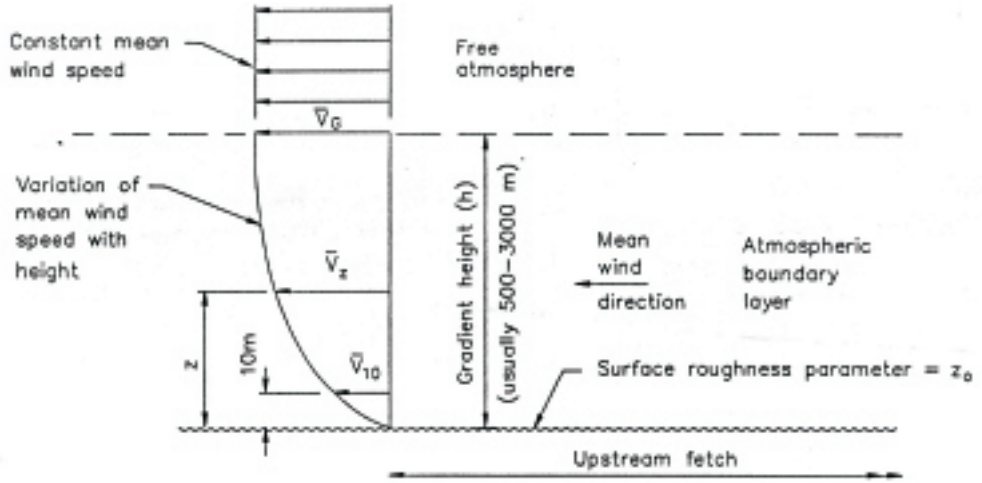

Figure 3.1.1 – The troposphere. The geostrophic wind, $\overline{V}G$, and the boundary layer wind, $\overline{V}Z$, [62].

The wind is not flowing across the lines of constant pressure (isobars), but along them. This is the most important feature of geostrophic flows.
Below the free atmosphere, the earth excerts friction on the wind, causing the speed to gradually reduce to zero at the ground surface. As a result, a layer where viscous effects in the flow are important develops in the lowest 400 - 1000 m of the atmosphere. This is the surface boundary layer or the Ekman layer. The flow must now be described by also including the inertia terms, time dependency and viscosity terms due to the vertical velocity gradient, the atmospheric motion equations are [19]:

$$\frac{\partial u}{\partial t} + u \cdot \frac{\partial u}{\partial \mathbf{x}} + v \cdot \frac{\partial u}{\partial \mathbf{y}} + w \cdot \frac{\partial u}{\partial \mathbf{z}} - fv = \frac{1}{\rho_0} \cdot \frac{\partial p}{\partial \mathbf{x}} + V \cdot \frac{\partial^2 u}{\partial \mathbf{z}^2} \tag{3.1.1}$$

$$\frac{\partial v}{\partial t} + u \cdot \frac{\partial v}{\partial \mathbf{x}} + v \cdot \frac{\partial v}{\partial \mathbf{y}} + w \cdot \frac{\partial v}{\partial \mathbf{z}} - fu = \frac{1}{\rho_0} \cdot \frac{\partial p}{\partial \mathbf{y}} + V \cdot \frac{\partial^2 v}{\partial \mathbf{z}^2} \tag{3.1.2}$$

$$\frac{1}{\rho_0} \cdot \frac{\partial p}{\partial \mathbf{z}} + g = 0 \tag{3.1.3}$$

where

- f = Coriolis parameter, varying with longitude, $f \approx 10^{-4}[1/s]$
- g = gravity
- u,v,w = velocity components in the horizontal x-y plane, and vertical axis (z)
- ρ_0 = air density
- p = pressure
- V = kinematic viscosity of air

The effect of wind speed gradients and viscosity on the flow is a motion of flow fluctuating in time and space, called turbulence. Close to the ground, the shear stress due to turbulence is much higher than the molecular shear stress. It is therefore usual to replace the molecular kinematic viscosity by a turbulent viscosity, V_T, according to the Boussinesq approximation.
The wind flow in the lowest levels of the atmosphere is further influenced by the presence of the ground. This influence is not only from the large scale landscape and smaller terrain formations but also due to the surface structure of the ground, e.g. the vegetation or surface texture. On the length scales of interest to the current study ($L \approx 10^2 m$) it is reasonable to neglect the Coriolis terms from the calculations. This is possible because the flow structure in the lowest 10% of the boundary layer is not significantly affected by Coriolis force.
On the other hand, the set of equations must be expanded to include also the viscous terms for horizontal wind speed gradients, since these can have a magnitude comparable to the vertical gradients in complex landscape. Another simplification used here is the assumption of small density variations in the vertical direction due to thermal stratification of the air. The equation for conservation of mass in a constant density flow thus actually describes conservation of volume:

$$\frac{\partial u}{\partial x} + \frac{\partial v}{\partial y} + \frac{\partial w}{\partial z} = 0 \tag{3.1.4}$$

3.1.2 The logarithmic wind profile

At the ground surface the wind velocity actually becomes zero. This is the so called no-slip condition. The no-slip condition results in shear stress of the flow, and a high vertical velocity gradient. Looking at two-dimensional flow in the x direction only, the following equation known as the logarithmic wind profile [67], the equation describes the vertical wind speed development over a flat surface in a neutrally stable atmosphere:

$$u(z) = \frac{u_*}{k} \cdot \ln \cdot \frac{z}{z_0} \tag{3.1.5}$$

where

- u_* = friction velocity is $\sqrt{\frac{\tau}{\rho_f}}$
- τ = is the fluid-induced shear stress (sum of turbulent and molecular shear stress)
- ρ_f = denotes the density of fluid
- k = Karman´s constant $(= 0,4)$
- z = is height above ground
- z_0 = roughness height

The equation describes the vertical wind speed development over a flat surface in a neutrally stable atmosphere, i.e. when the potential temperature is constant with height. A fairly rough or vegetated surface is represented by a high roughness parameter, z_0, and opposite for a smoother surface. Mobile surfaces, such as an erodible snow cover or the sea water present a roughness height varying with the friction velocity:

$$z_0 = c \cdot \frac{u_*^2}{g} \tag{3.1.6}$$

According for fresh cold snow the value c = 0.015 was found by Joffre (1982) and 0.018 by Schmidt (1982).
Over surfaces densely covered with large obstacles, such as forest trees or houses, (3.1.2) has to be corrected to adjust to the mean height at where the aerodynamic drag acts. This demands introduction of the displacement height, d, which shifts the logarithmic profile upwards (3.1.2):

$$u(z) = \frac{u_*}{k} \cdot \ln\left(\cdot\frac{z-d}{z_0}\right) \tag{3.1.7}$$

Typical values for d can be around 0.7 times the height of the obstacles on the ground, depending on their shape and spacing [13].

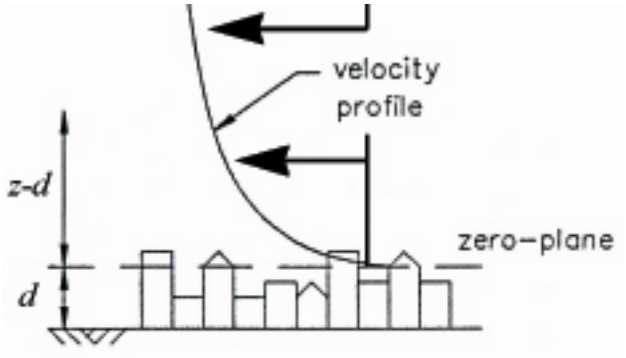

Figure 3.1.2 – The shift in the zero-plane for the logarithmic wind profile, [19].

3.1.3 Internal boundary layer

The previous section emphasised how the surface roughness influences the local wind speed. Over a given fetch, changes in surface roughness will therefore reflected in changes in the wind profile. As the surface roughness changes, an internal boundary layer starts to develop and grows deeper along the new fetch.
Stull (1988) presented the following parametrization for the growth of the internal boundary layer depth during neutral conditions. The situation is illustrated in Figure (3.1.3)

$$\frac{\delta}{z_{01}} = \left[0.75 + 0.03ln \cdot \left(\frac{z_{02}}{z_{01}}\right)\right] \cdot \left[\frac{x}{z_{01}}\right]^{0.8} \tag{3.1.8}$$

where

- δ = depth of the internal boundary layer
- z_{01} = roughness length upwind of the border
- z_{02} = roughness length downwind of the border
- x = distance from the border along the new surface

This equation is useful for estimating the suitable position and elevation for wind speed gauges.

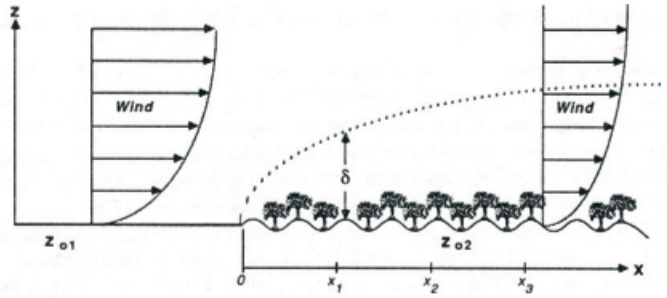

Figure 3.1.3 – Explanation of the parameters of eq. (2.12), by Stull (1988), [67].

3.2 Characteristics and classification of snow

This paragraph presents the fundamental features that determine the physical characteristics of a snow mass distinguishing the snow deposited on a surface from the falling snow.

3.2.1 Deposited snow

The physical properties of snow on the ground may differ greatly from the ice crystals in the snowfall events.
Physical properties of snow change over time. Furthermore, snow properties can vary widely over small distances, both vertically within a snowpack and horizontally over space. A snow cover is generally composed of layers of different types of snow, each of which is more or less homogeneous within its own boundaries. Snowpack stratigraphy is the result of a combination of processes, which include: individual snowfalls each with different meteorological conditions, meteorological conditions between snowfall events which can form melted areas due to sun irradiations and wind crusts, and different rates and types of grain growth after snow accumulates in the snowpack.
Snow deposited on the ground is a complicated mixture of water in three phases: ice,

liquid water, and water vapor. The primary distinctions between types of deposited snow are based on physical characteristics summarized in the following list [43]:

- Temperature
- Hardness
- Water Equivalent
- Depth
- Density
- Impurities
- Albedo
- Strength
- Grain Shape
- Grain Size
- Liquid Water Content

Snow grains can become bonded to their neighbors. This process is called sintering. These bonded snow grains act as an ice skeleton to provide structural strength to the snowpack. Snow strenght depends on the stress state (compressive, shear), stress rate, strain and strain rate. One of the most important characteristics of the snowpack are the size and shape of individual snow grains. Grain shape and size tells us about the history of the snowpack at that site. Grain shape and size provide important information about snow stability and transport by wind.

TERM	SIZE(mm)
Very Fine	<0.2
Fine	0.2 - 0.5
Medium	0.5 -1.0
Coarse	1.0 - 2.0
Very Coarse	2.0 - 5.0
Extreme	<5.0

Table 3.2.1 – Classification of the snow grain size, [43].

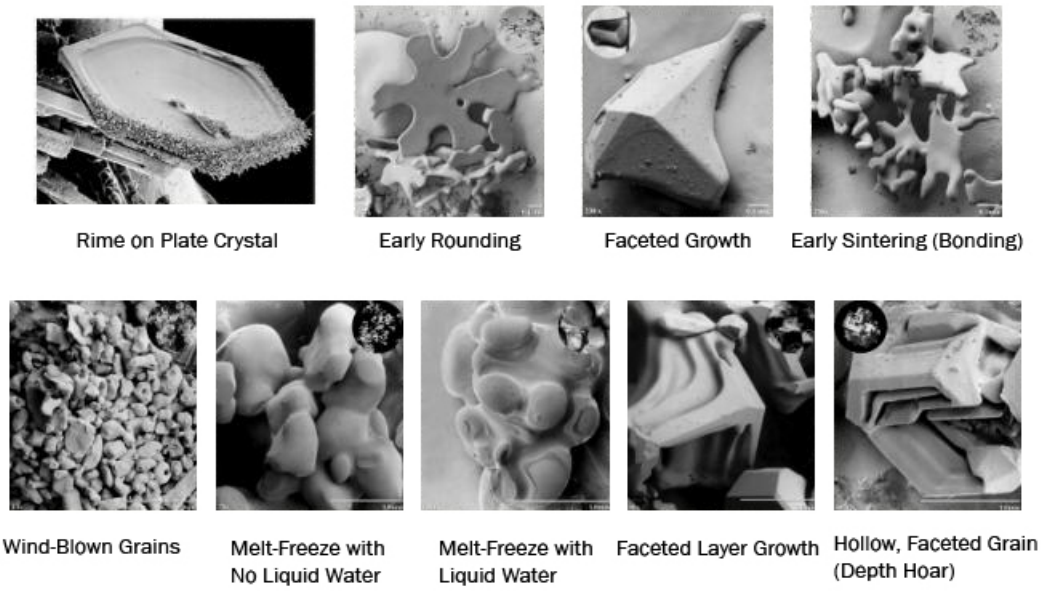

Figure 3.2.1 – Snow grain shapes classification, [43].

3.2.2 Falling snow

We will use the term blowing snow to refer to aeolian transport of snow particles at all heights without distinction between blowing snow, which is at or above eye level, and drifting snow, which is closer to the ground (as defined in Atmosphere Environment Service, 1977). The properties and characteristics of falling snow change constantly as a function of energy fluxes, wind, mixture, water vapor, and pressure.
Snow particles are transported by the wind, they become progressively smaller and more rounded from fragmentation, abrasion, and evaporation, for example, high wind speeds near the surface may break ice crystals into smaller pieces. Further disintegration of the original snow crystals may occur as the crystals are bounced and dragged over the snow surface in the turbulent boundary layer. After being reduced in size and shaped more symmetrically through interactions with wind, the individual crystals may be packed more closely to produce a much denser surface layer than would otherwise occur. The concentration of snow particles at a given height above the surface increases with wind speed. At wind speeds of 100 km/h, for example, 50% of the total blowing snow is more than 1 m above the surface, and 30% is above 2 m.
Based on the results at various heights, a schematic of the blowing snow density profile is proposed, as shown in Figure (3.2.2) [43].

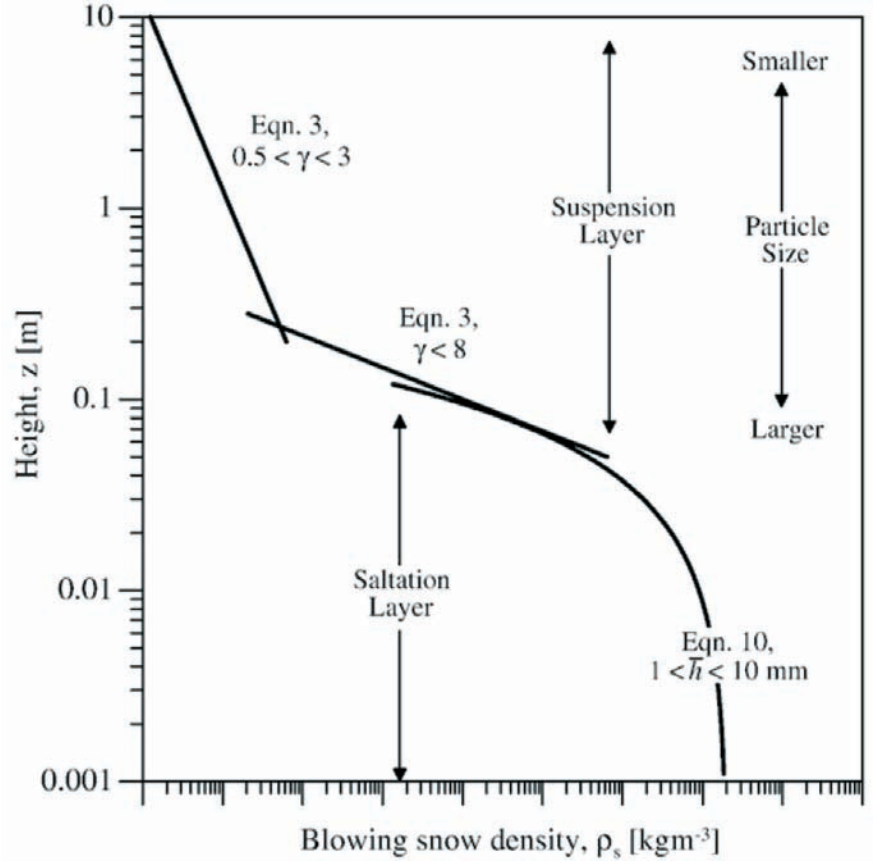

Figure 3.2.2 – A proposed schematic of the blowing snow density profile, [43].

When wind across a snow surface exceeds some threshold speed start the saltation process, the wind dislodges particles and eject them into the flow. A best-fit to the mass density profile in the saltation layer is derived, assuming a half-normal distribution of the vertical ejection velocity of saltating particles. Within the saltation layer, the observed vertical profile of mass density is found to be proportional to the function $exp\left(-0.61 \cdot \frac{z}{\bar{h}}\right)$, where $\bar{h}$ is the average height of the saltating particles. For the range of conditions studied, $\bar{h}$ varies from 1 to 10.4 mm, while the extent of the saltation layer varies from 17 to over 85 mm. At greater heights, $z > 0.2m$, the blowing snow density varies according to a power law. Between these saltation and suspension regions, results suggest that the blowing snow density decreases following a power law with an exponent possibly as high as $\gamma \approx 8$. Snow is deposited where surface shear stress decreases with distance downwind, and erosion occurs where shear stress increases, as described in section (3.3.2).
In blowing snow the particle size decreases with height above the surface, with mean diameters ranging from about 0.2 mm at a height of 5 cm, to about half this size at 1 m. There is little entrapped air in the ice, and the specific density of the particles is

typically about $0.9kg/dm^3$.

3.3 Mechanisms of snow transport by wind

3.3.1 Particle motion

In the following section the relationship between the snowdrift and wind flow patterns will be analyzed. When the wind blowing over the bed of snow particles becomes sufficiently strong, the snow drift is initiated. The surface particles are set in motion when the drag and lift forces caused by wind are strong enough to overcome gravity and particle cohesion. The value of wind speed (or the corresponding shear stress) that needs to be exceeded for this process to start is called the fluid threshold. The raising of initially motionless particles from a bed into the airflow by fluid forces is referred to as aerodynamic entrainment. In snow drift, a distinction can be made between three different transport modes: creep (surface), saltation and suspension [8], like shows the figure (3.3.1).The transition between the different transport modes is continue.

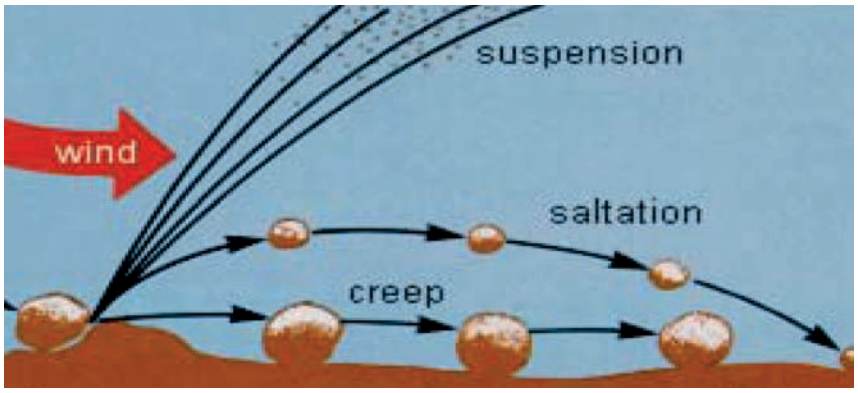

Figure 3.3.1 – Transport modes of blowing and drifting snow.
Creeping h $0.001m$; saltation 0.001<h<0.4m; suspension 0.05<h<100m, [43]

The grain transport that takes place closest to the surface is referred to as creep. Several definitions of creep are possible; in the following creep will be defined as the motion of grains which are still in contact with the bed. This type of transport is mainly caused by the impact of saltating grains motion. The forces acting on the grains are gravity and inter- particle forces. Although the number of particles traveling in this transport mode is large, the contribution to the transport rate is small due to the short displacement length. Typical grain sizes are of the order of 1 mm.
When the particle are lifted from the bed, they enter the transport mode called saltation.

In the saltation layer particles follow ballistic trajectories. When they return to the bed, they may rebound or eject new surface grains in the air. Initially, this process causes a fast increase in transport rate. However, due to the growing number of particles in the air momentum is extracted from wind. This feedback mechanism leads to the rapid development towards an equilibrium state. In saltation the most significant forces acting on the particles are drag and gravity. The effect of turbulence on the particle trajectories is negligible. The typical grain diameters in the saltation mode are $0.05 - 0.5mm$. Most of the snow transport occurs in this mode, whereas the volume fraction of the snow particles is in the range $10 - 5\%$ to $10 - 3\%$. Furthermore, for high wind speeds the height of the saltation layer can reach about 0.1 m. Saltation starts at wind speeds u10 (wind speed measured at 10 m height) of about $5 - 8\frac{m}{s}$, whereas the different transport modes contribute to the snowdrift as listed in table [30].
For small grains or for strong winds the shape of the particle trajectories may be modified by turbulent fluctuations. This type of transport is generally referred to as modified saltation. For this situation the turbulence causes a fluctuating drag on the particles. The initial conditions (i.e. ejection velocity and ejection angle) still have a significant influence on the particle motion.
At high wind speeds, particles may also be picked up by turbulent eddies and transported over larger distances without contact with the bed. This transport process is called suspension. Suspended particles move on a random path through the flow, and may almost follow the trajectories of the fluid parcels. This mode is referred to as Langrange transport. The typical volume fractions are lower than 10^{-4} and the grains are usually smaller than in the saltation layer. The height of the suspension layer in atmospheric turbulence may be up to several tens of meters. It should be noted that snow particles in the air from precipitation are also regarded as being in suspension.

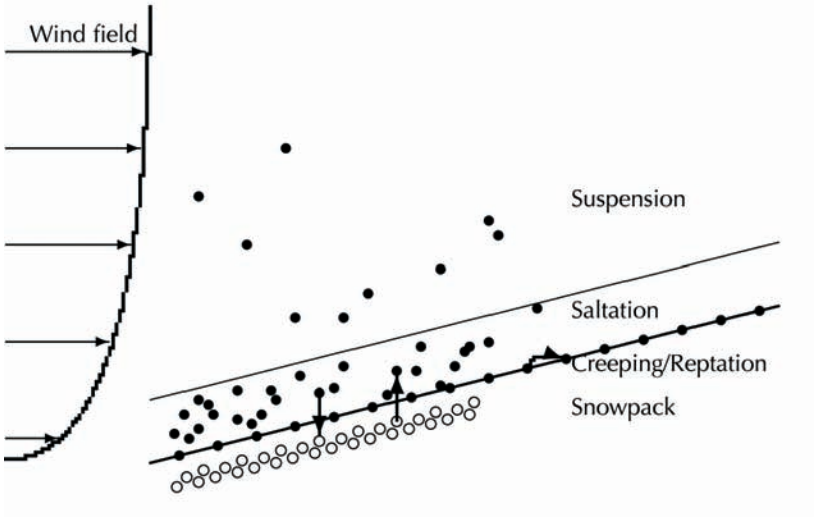

Figure 3.3.2 – Snowpack indicates the structural snow cover, open circles designate grains bound on the snowpack and full circles designate grains in motion [43].

TRANSPORT MODE	DISTRIBUTION OF TOTAL %
Surface creeping/replation	5 - 25
Saltation	50 - 75
Suspension	3 - 40

Table 3.3.1 – Distribution of total snow mass transport: the values vary with wind speed.

The transport processes discussed above lead to an evolution of the snowpack. The snow cover is growing in deposition zones, and the new shape therefore influences the local velocity field. The snow depth is reduced in erosion zones due to particle entrainment and deposition zones when saltation exceeds saturation. The numerical approach of these phenomena is discussed in the next section.

3.3.2 Evolution of snowpack due to deposition and erosion processes: approach to models

Wind-inducted drifting can produce snow accumulations many times greater than those due to snowfall alone. Erosion and deposition of solid particles is often a phenomenon of considerable importance. Erosion occurs where the amount of snow of material transported by saltation increases with downstream distance and deposition occurs where the opposite is true.

In the following, previous work on snowdrifts is outlined, [12], [50].
Bagnold (1941) [12] laid the foundation to understand aeolian snow and sand transport. He derived an empirical relation between the fluid-induced shear stress and a logarithmic wind profile Prandtl, (1965), equation (3.1.5).
From measurements, Bagnold obtained some erosion and deposition criteria which depend on a critical shear stress. For the erosion and accumulation processes, he found:

$$(u_*) = (A_{i,e}) \cdot \sqrt{\frac{\rho_p - \rho_f}{\rho_f} \cdot g d_p} \tag{3.3.1}$$

where

- u_* = threshold friction velocity of impact and erosion
- $A_{i,e}$= empirical parameters
- ρ_p= particle density
- d_p= particle diameter
- g= gravity acceleration

This formula were verified by Nishimura and Hunt (2000) [50] in wind-tunnel measurements.
Anderson and others [9] gave a more formalized classification of snow and sand transport. Anderson estimated a linear dependence between the number of entrained grains per unit time and per unit area and the shear stress induced by the fluid. Additional work, based on work by Bagnold [12] and Owen [46] on the saltation transport mode, was done by Pomeroy and Male [53], who derived semi-empirical functions of the height of the saltation layer, the mass flux in the saltation mode and the saturation concentration in saltation.
Unlike the previous approaches the "VirtualSnow" model solves concentration of fluid and not simulates the single particles. Therefore, we do not try to represent a specific grain of snow with relative particle diameter, but estimate the concentration of fluid mass for each cell of a discrete lattice. The properties of fluid change under the combined effect of the local fluid velocity field and gravity. A simple set of rules, detailed in section (6.5), is sufficient to catch the main ingredients of particles motion (saltation, creping, sunspension) under the action of a fluid. The model is based on the balance equations for interpenetrating phases, hence we account for the snow particles in saltation and suspension as a continuous phase. The saltation and the suspension layers are not separated numerically. The erosion and deposition process is a function of the snow concentration, the surface normal and shear stress, the particle fall velocity and threshold surface shear stress. One important advantage of our model is the inclusion of important physical concepts such as modelling the snow phase or the evolution of the snowpack due to erosion and deposition processes.
In the following scheme the flowchart of the numerical snowdrift model.

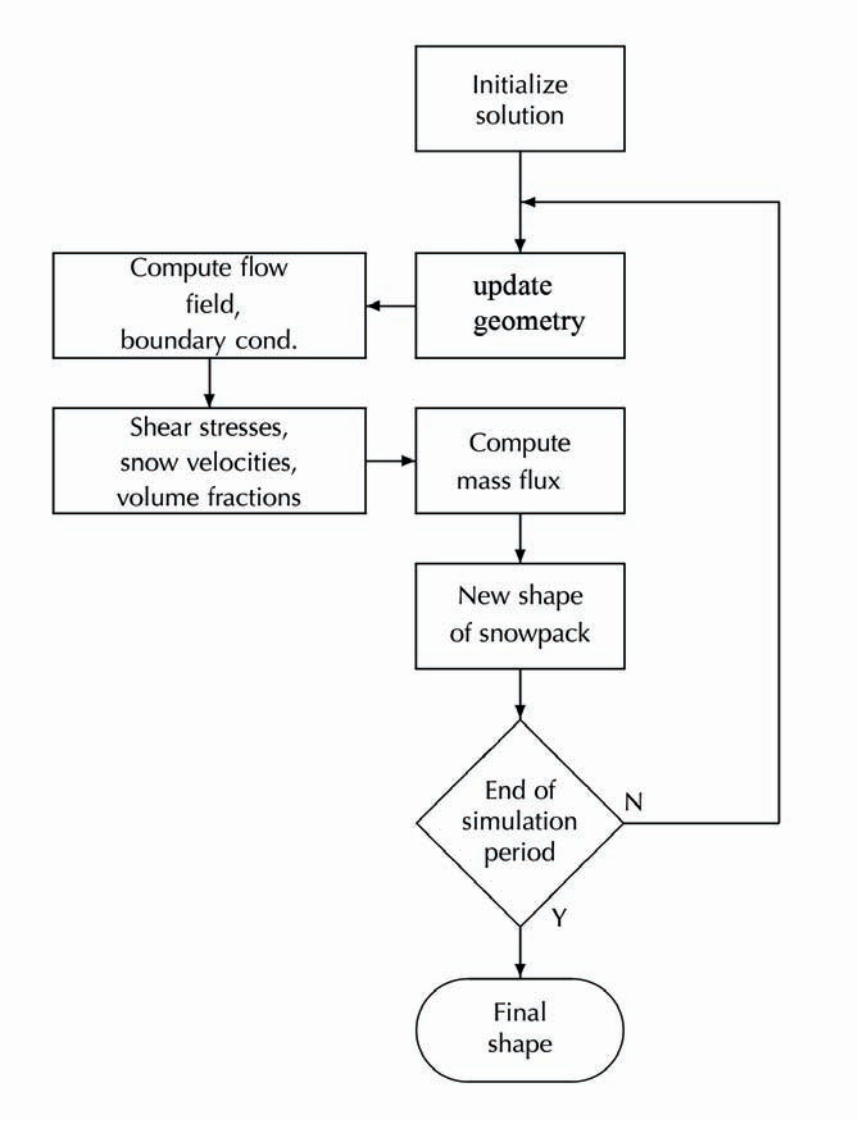

Figure 3.3.3 – Flowchart of the numerical snowdrift model [60]

4 Experimental investigation to validate the numerical model

4.1 Motivation of these tests

The numerical model to simulate snow transport by wind developed in this research work is validated through the comparison with experimental results described in this chapter. The experimental tests, carried out under the commission of the European communities in 1997, is aimed at improving the scientific knowledge and models for the determination of snow loads on buildings to product a sound common scientific basis which can be accepted by all European countries involved in the drafting of Eurocodes, [22]. A wide range of roof types common throughout the European countries were examined through an extensive wind tunnel test campaign developed in the "Jules Verne" Climatic Wind Tunnel of Nantes, France. The comparison between experimental and numerical results will be discussed in chapter (7).

4.2 Jules Verne Climatic wind tunnel

The "Jules Verne" Climatic Wind Tunnel was built in order to conduct full-scale experiments. It has two independent circuits, see Figure (4.2.1): the first is a dynamic circuit and the second one, called the thermal circuit, is able to create hot or cold climates (from $-25\,^{\circ}\mathrm{C}$ to $+50\,^{\circ}\mathrm{C}$) with snow, sun, rain, freezing rain or frost. The temperature, the relative humidity (from 30% to 95%) and the wind speed are controlled. In this circuit, the test section has the following dimensions: length, 27 m, height, 8 m and width, 10 m.

The total electrical power necessary to run the thermal unit is 3000 kW spread in 1000 kW for the fan and 2000 kW for the cooling system.

Snow is produced by snow guns that project compressed air and water in the ambient air of the wind tunnel in order to obtain ice droplets. The experimental devices of the climatic wind tunnel are able to create snow mantles of about 100 mm/h on a 200 m^2 area. The quality of the snow produced is adjustable by controlling the air and water flows in the snow gun.

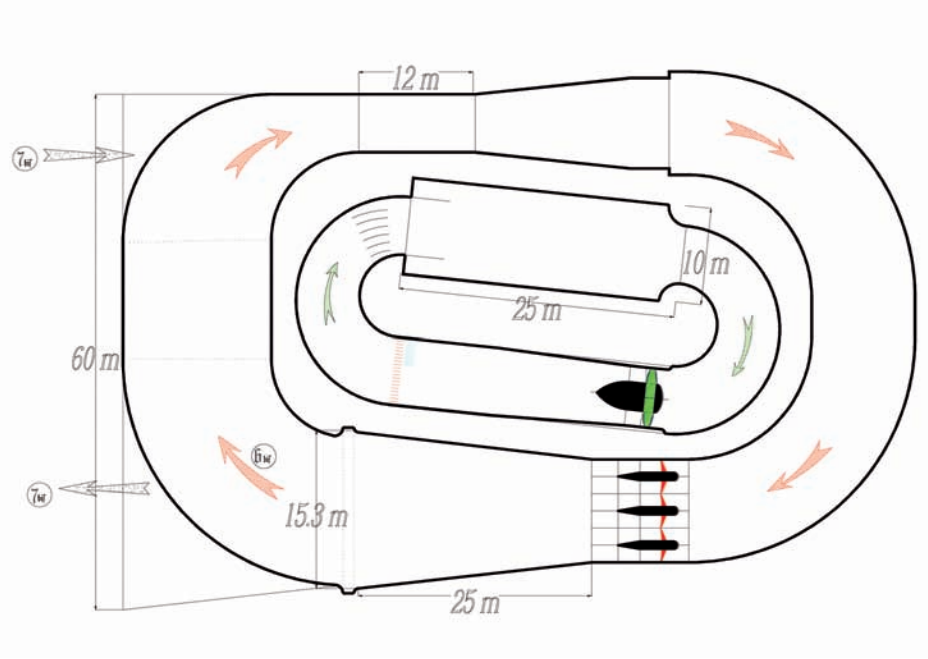

Figure 4.2.1 – "Jules Verne" Climatic Wind Tunnel, floor view [57]

Figure 4.2.2 – "Jules Verne" Climatic Wind Tunnel, internal view

4.3 Experimental parameters

In the experimental campaign considered to validate the numerical model a test duration of one hour represents a long real snowstorm event. Four different buildings shapes were tested with a model scale of 1/10. A full scale wind velocity Vhp = 12.5 m/s is considered

for a model wind velocity Vhm = 4 m/s for all shape of buildings, the area covered by snow is about 4 m x 4 m.
The air temperature in the wind tunnel, about -10 °C, provides artificial "dry" snow, to give an influence to aerodynamic effects. This characteristic of the snow produced in the wind tunnel is actually determined by the volumetric air/water ratio (liquid water content less than 4% in volume), injected in the snow gun for a particular wet bulk temperature. The liquid water content measurements of the snow were made both on the floor near the building model and on the model itself. For all experiments the humidity regulation systems was switched off. Snow density of 360 kg/m3 is measured using a PVC cylinder. This cylinder is pushed horizontally in the snow cover, snow is cut at each end of the cylinder and the cylinder is weighed. Measurements are made on the ground, windward and leeward of the model, and on the roof if there is enough snow.
To simulate the snow accumulation at reduced scale it is first necessary to reproduce mean and turbulent flow. In addition, it is necessary to achieve similarity of particles trajectories. Similarity conditions can be listed as follows:

- Similarity of the mean and turbulent flow
- Similarity of local flow behaviour (Re > 10000 for sharp-edged buildings)
- Similarity of the bulk hydraulic properties of the snow phase (threshold friction velocity u_*t, terminal fall velocity w_f, density ratio $\frac{\rho_s}{\rho}$ where ρ_s is snow density and ρ air density)
- Saltation hop length l of model snow particles significantly smaller than the overall dimensions of the roof (l « H and l « L where H and L are characteristic roof dimensions).

The snow properties summarised in Table (4.3.1) are considered. The snow properties are realistic with regard to natural European usual snow fall.

PROPERTY	NATURAL SNOW	ARTIFICIAL SNOW
Diameter, $D(mm)$	0.5-5	0.15-0.3
Particle density ρ_s, (kg/m^3)	700 - 50	910
Fluid density ρ , (kg/m^3)	1.22	1.34
Terminal fall velocity W_f , (m/s)	0.03 - 0.5	0.5 - 1.2
Snow cover density (kg/m^3)	100 - 600	315 - 370

Table 4.3.1 – Properties of snow particles of natural and artificial snow [57].

A realistic vertical wind speed gradient and turbulence rate were reproduced at the model scale, see figure (4.3.1). This was done through the investigation of the optimal location of roughnesses in the first part of the test section upwind the test models. The model location was set at about 16 m from the nozzle. The same process to optimize

the model location and the roughnesses location (in the case of the **VirtualSnow** model cylinders randomized in the first part of the numerical tunnel simulate the roughnesses) is conducted to calibrate the numerical model, as explained in section (7).

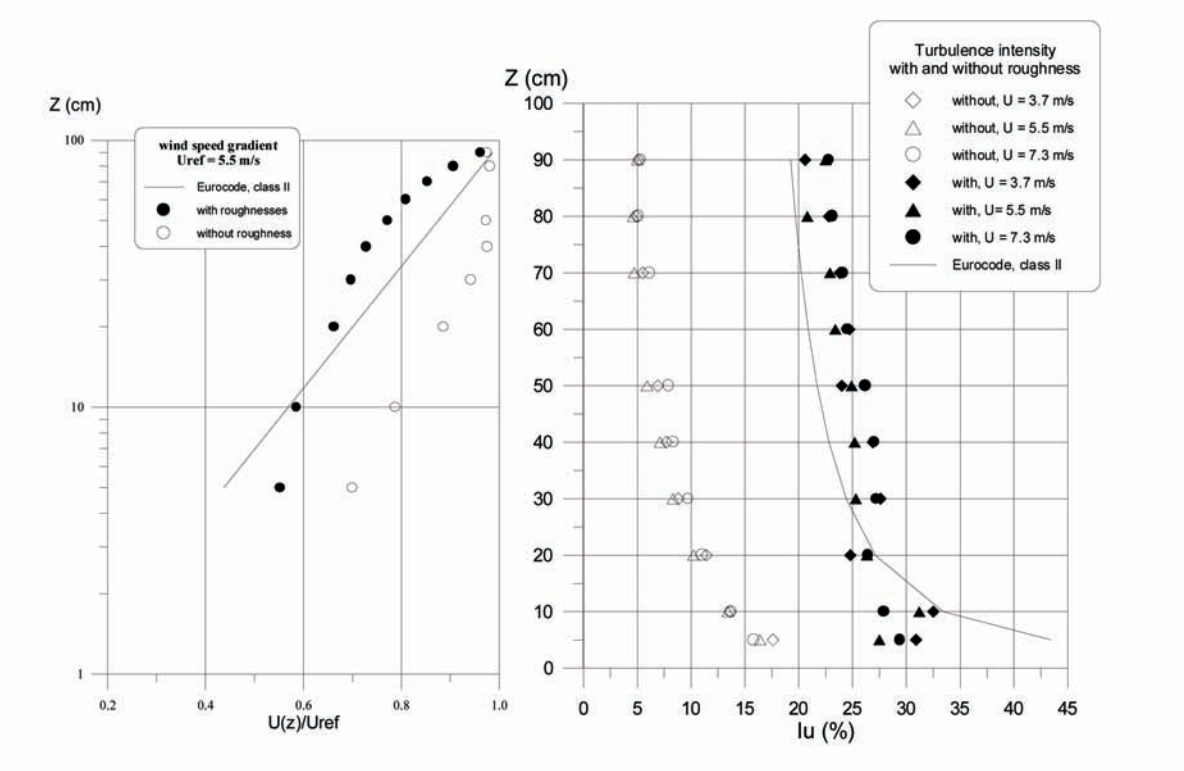

Figure 4.3.1 – Wind speed gradient (left) and turbulence rate (right) initial state (without roughness) and with roughnesses [57]

In the experimental campaign the wind speed measurements were made by using the hot wire technique. The turbulence rate was adjusted over the snow mantle in the test section to be similar to the turbulence over an open field terrain (category II of the Eurocodes), the turbulence intensity is $\cong 20\%$).

4.4 Influence of experimental parameters

To calibrate experiments simple roof shapes tests are performed. This purpose is to analyze the influence of some experimental parameters such as geometrical aspect (effect of model scale and model height), experimentation duration and climatic condition in the wind tunnel (air temperature). Two load cases are generated: uniform loading

(simulation of a snow fall on the models without wind) and snowstorm with wind. In conclusion there is no significant difference between each model with different height or scale. Aerodynamic effects (difference between wind 4 m/s and 3 m/s) are more important.
Tests of snowstorm with wind were carried out with measurement of snow cover every 15 minutes. The results show (Table 4.4.1), that the snow cover increases quite regularly with time.

Test conditions	Cross section surface ratio windward/leeward Duration (h)								Density on the ground Kg/m^3		Density on the roof Kg/m^3	
	1/4h	1/2h	3/4h	1h	1h1/4	1h1/2	1h3/4	2h	windward	leeward	windward	leeward
-10°C,88%	1.16	1.06	0.94	0.72					360	374	400	334
-10°C,88%	0.79	0.80	0.74	0.64	0.65	0.61	0.60	0.63	371	366	400	310
-15°C,83%		0.72		0.59	0.56				390	390	418	352

Figure 4.4.1 – Results of duration tests for two temperature conditions [57]

The ratio between the average depth of the windward and leeward snow cover decreases at the beginning of the test but is becoming constant after one hour, see Figure (4.4.2). It means that the loading reaches a stationary profile. For this reason the test duration was set at one hour. The evaluation of the equivalent prototype snowstorm duration with respect to the model wind velocity and experiment duration is one of the main difficulties of experimental snow load modeling.

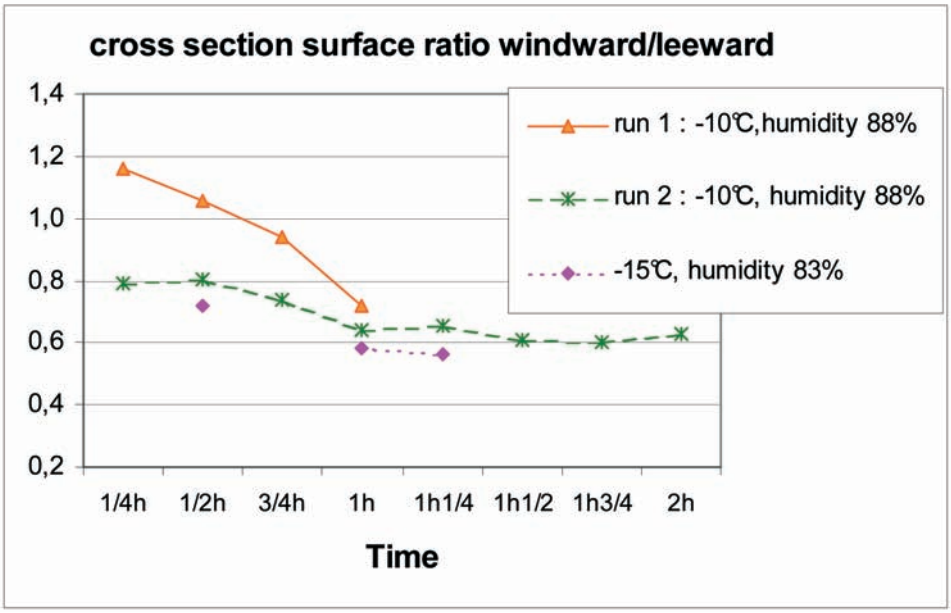

Figure 4.4.2 – Variation with duration test of snow cross section surface ratio windward/leeward on the roof [57]

Measurements of the snow density are carried out for all experimental conditions. Density variations were observed depending on the wind speed or on the location: ground, windward or leeward roof side. In the case of 4 m/s wind, the snow density on the windward side is higher than the density on the ground. This is probably due to the packing of the snow by the wind. In the same wind condition, the snow density on the leeward side is lower than the density on the ground. This is probably due to the way the snow is packed on the roof side by local low speed airflow and eddies. Although the uneven windward/leeward snow drifting is induced by highest wind speed, the snow density measurements tend to compensate the apparent unbalanced snow loads.

4.5 Experimental results

In this section we present the experimental results developed in CSTB Climatic Wind Tunnel used to validate the code.

4.5.1 Definition of length and snow depth

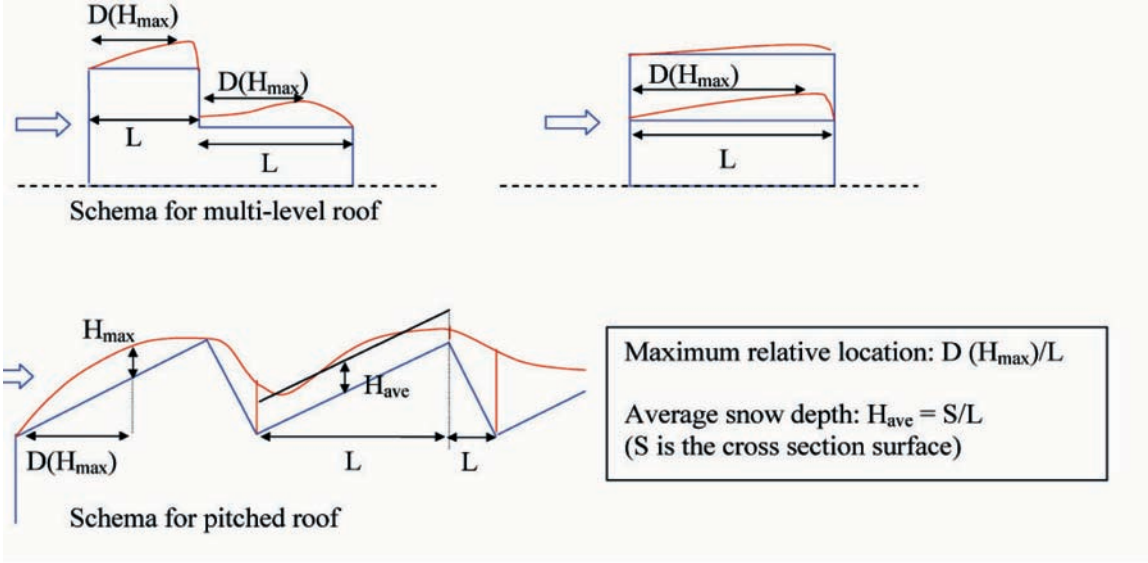

Figure 4.5.1 – Definition of length and snow depth [57]

For each case the average snow depth $Have$ are calculated by dividing snow profile surface by roof length, the maximum snow depth $Hmax$ and the distance from the windward edge $D(Hmax)$. Also the relative position of the maximum snow depth from windward edge is calculated by dividing the distance $D(Hmax)$ by the roof length L. Average snow depth factor $\mu(Have)$ is equal to $\frac{Hmax}{Href}$ and the maximum snow depth

factor $\mu(Hmax)$ is equal to $\frac{Hmax}{Href}$. Only dimensionless snow depth factors are calculated because variations of snow density are not significant.

4.5.2 Definition of geometry

The following Figure (4.5.2) shows the different shapes tested: name, location of the test section and wind direction.

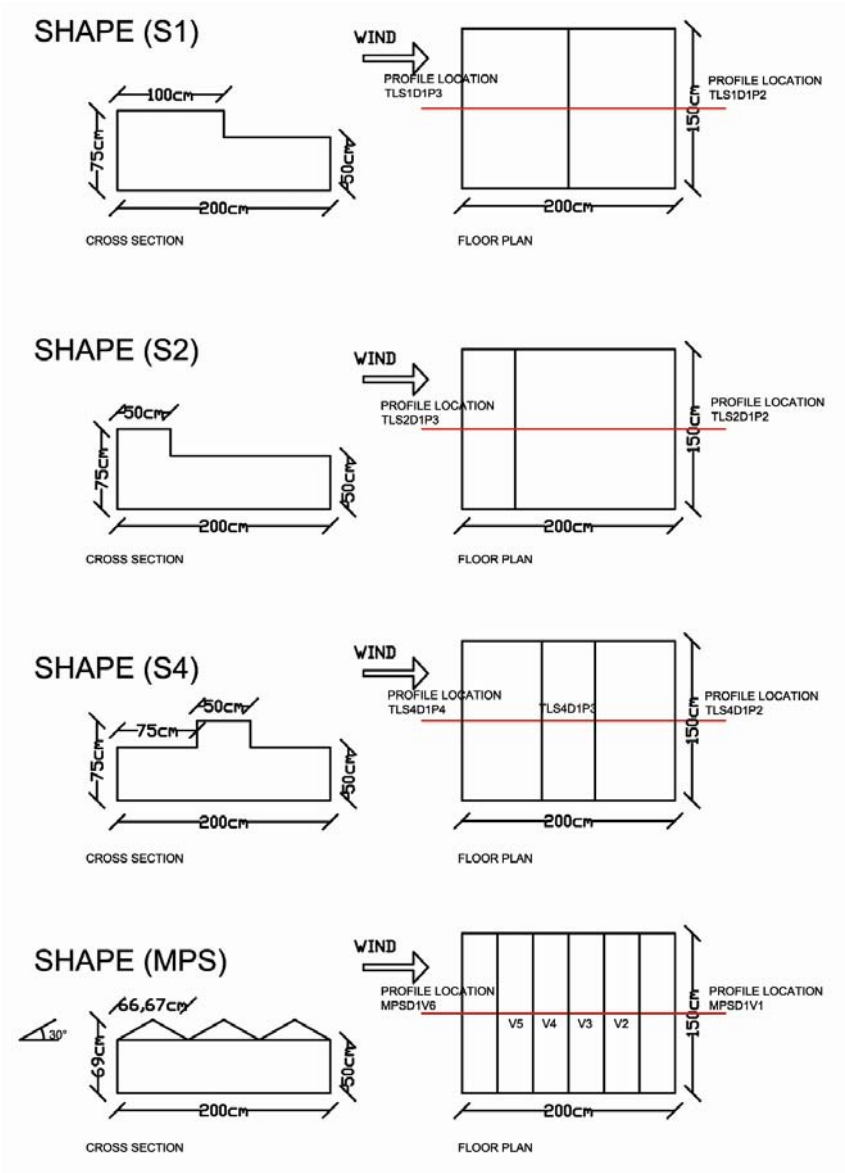

Figure 4.5.2 – Geometry of buildings tested

4.5.3 Results

Name	Wind direction	Hmax (cm)	D(Hmax) cm)	Lroof (cm)	D(Hmax)/L	H ave surface/L	μs ave Have/Href	μs max Hmax/Href
SHAPE(S1) TLS1D2P2	0 °	5	91	100	0,91	3	0,26	0,42
SHAPE(S1) TLS1D2P3	0 °	17	32	100	0,32	13	1,08	1,41
SHAPE(S2) TLS2D2P3	0 °	20	95	150	0,63	16	1,30	1,66
SHAPE(S2) TLS2D2P2	0 °	4	45	50	0,90	3	0,23	0,33
SHAPE(S4) TLS4D1P2	0 °	23	75	75	1,00	8	0,67	1,91
SHAPE(S4) TLS4D1P3	0 °	4	48	50	0,96	2	0,18	0,33
SHAPE(S4) TLS4D1P4	0 °	12	57	75	0,76	10	0,83	1,00
SHAPE (MPS) MPSD1V1	0 °	7	8	33	0,23	6	0,53	0,62
SHAPE (MPS) MPSD1V2	0 °	18	33	33	1,00	10	0,79	1,49
SHAPE (MPS) MPSD1V4	0 °	23	33	33	100	15	1,21	1,92
SHAPE (MPS) MPSD1V3	0 °	19	3	33	0,10	14	1,19	1,54
SHAPE (MPS) MPSD1V5	0 °	23	0	33	0,00	15	1,24	1,92
SHAPE (MPS) MPSD1V6	0 °	14	29	33	0,86	12	1,01	1,18

Figure 4.5.3 – Experimental results [57]

It is observed that there is less snow on the upper part of the two-level flat roof than on the lower part situated either leeward or windward Prediction of snow load profiles on multi-level roof is one of the most complicate open problems. For this reason we decided to compare the "VirtualSnow" model for different configuration of multi-level flat roof. Snow deposition is very sensitive to local flow and that the step in the building shape have an aerodynamic influence on the flow around the building.
The description of the experimental tests will be recalled in chapter (7) to compare the numerical and experimental results for different shape of building.

5 Basic concepts in fluid dynamics

The main goal of the present section is to give the essentials of fluid dynamics in order to have a self-consistent document.
First, the main equations of fluid dynamics are recalled. They are informally presented so as to understand the basic phenomena. More details and rigor can be found in specialized books, see for instance [37].
Second, we review some aspects of turbulence by skimming through Kolmogorov's theory. This will be used to explain two empirical laws which are useful to overview the state of the art of turbulence theory. This presentation does not cover the wide turbulence theory. Yet, it provides answers to basic questions.

5.1 Governing equations of the physical models

The equations that govern the dynamics of fluids stem, from the application of the basic laws of mechanics and thermodynamics to moving deformable media, are the fluid conservation equations: the mass conservation equation, the momentum conservation equation and the energy conservation equation. These equations provide global information about the domain of interest, such as global balances or average values of the fluid variables.
The principle of **mass conservation** establishes that the mass of a fluid volume (a volume that always contains the same fluid particles) is constant. Consider a volume element $dxdydz$. The mass flux through this box leads to the first basic equation of fluid dynamics, the mass-conservation or continuity equation.

$$\frac{-\partial\rho}{\partial t} = \nabla\cdot(\rho U) = \frac{\partial(\rho U_x)}{\partial x} + \frac{\partial(\rho U_y)}{\partial y} + \frac{\partial(\rho U_z)}{\partial z} \tag{5.1.1}$$

where

- $\rho =$ is the fluid density
- $U =$ is the fluid velocity

The derivate $\frac{\partial\rho}{\partial t}$ is the rate of change of density; it can be nonzero because of changes in pressure, temperature, or composition (such as salinity in sea water). We usually consider incompressible fluids (the density does not change in space), equation (5.1.1) leads to the incompressible form:

$$\nabla\cdot U = 0 \tag{5.1.2}$$

In this section the law of **conservation of momentum** will be expressed for inviscid and viscous fluids. If the fluid is inviscid, the momentum equation results are called the Euler equation. On the other hand, when the fluid is viscous, the equation is known as the Navier-Stokes equation. We begin with inviscid flows. The viscous effects are negligible, generally far from the boundaries of the flow field.
The force acting on a control volume of infinitesimal size is composed of a pressure difference on the faces of this volume and a body force due to gravity. This force can be expressed as

$$F = \nabla p + G \tag{5.1.3}$$

where

- $\nabla p =$ is the pressure gradient $\left(\frac{\partial p}{\partial z}; \frac{\partial p}{\partial y}; \frac{\partial p}{\partial z}\right)$
- $G =$ is a gravitational vector

Newton's second law of motion indicates that F is equal to the rate of change of momentum following a fluid particle. It leads to the Euler equation

$$\rho \frac{DU}{Dt} = -\nabla p + G \tag{5.1.4}$$

where

- $\frac{DU}{Dt}$ is a total derivative expressed as $\frac{\partial U}{\partial t} + U \cdot \nabla U$

We now consider the effect of viscosity. It is specific to a fluid and can be interpreted as the attachment rate between fluid particles. The viscosity μ in this equation can be function of the thermodynamic state, and indeed μ for most fluids displays a rather strong dependence on temperature, decreasing with T for liquids and increasing with T for gases.
The shear stress in 2D simulations of an incompressible fluid flow assumes the following expression

$$\tau_{\alpha\beta} = \mu \left(\frac{\partial U_\alpha}{\partial x_\beta} + \frac{\partial U_\beta}{\partial x_\alpha} \right) \tag{5.1.5}$$

where α and β are spatial components, μ is called the dynamic viscosity of the fluid. Note that a fluid which obeys equation (5.1.5) is called Newtonian. The force acting on a fluid element due to a shear stress is the variation of the stress in all the directions.

The viscous force can be added to equation (5.1.4) to give the **Navier-Stokes equation**

$$\frac{DU}{Dt} = \frac{\partial U}{\partial t} + U \cdot \nabla U = -\frac{1}{\rho}\nabla p + \nu \nabla^2 U + \frac{1}{\rho} G \tag{5.1.6}$$

where

- ν is the kinematic viscosity related to the dynamic viscosity by $\nu = \frac{\mu}{\rho}$

The Euler and especially the Navier-Stokes equations are nonlinear partial differential equations, and no general solution has been found yet. Under particular conditions only, analytical solutions can be found. Numerical techniques must be used for other cases. Traditional numerical techniques are mentioned in this chapter, while techniques based on lattice Boltzmann models make up section (6) and in detail in the next chapter.
The total **energy equation** is based on the first principle of thermodynamics: the change of total energy E in a system equals the work done over the system W_{ext} plus the added heat Q_{in}:

$$\Delta E_{system} = W_{ext} + Q_{in} \tag{5.1.7}$$

An equation for kinetic energy of the fluid can be obtained by finding the scalar product of the momentum equation and the velocity vector. Other forms of the mechanical energy equation are obtained by combining the equation of motion with the continuity equation in various ways.

5.1.1 Advection and Diffusion

In nature, transport occurs in fluids through the combination of advection-diffusion responsible of mixing process. Numerical advection-diffusion models are intended to predict the distribution of quantities of heat, dissolved gas, with spatial variability, and reflects two transport mechanisms:

- Advective (or convective) transport with the mean flow;
- Diffusive transport due to concentrations gradients.

Before discussing in section (6.4) the developed lattice Boltzmann method to solve the advection diffusion equation, here a description of the effect of advection and diffusion is given.
Diffusion describes the dispersion of molecules or small particles due to their random (Brownian) motion and the resultant net migration of material from regions of high concentration to regions of low concentration. Stirring (where material gets stretched and folded) expands the area available for diffusion to occur, resulting in enhanced mixing compared to that due to molecular diffusion alone. This helps explain why materials such as milk in coffee diffuse orders of magnitude faster than one would predict based on their molecular diffusion coefficients, [18].
Advection is a transport mechanism of a substance, or a conserved property (such as heat), by a fluid, due to the fluid's bulk motion in a particular direction. An example of advection is the transport of pollutants or silt in a river, in our case snow suspended in air, [18].
Advection-diffusion process are defined by the following equation [5]

$$\frac{\partial s}{\partial t} + u\frac{\partial s}{\partial x} = \nabla\left(D\nabla s\right) \tag{5.1.8}$$

where

- s = is the scalar quantity subject to advection-diffusion
- t = is time
- u = is velocity
- x = is spatial coordinate
- D = is the diffusion coefficient

5.1.2 Turbulence

A flow classificator: the Reynolds number
A flow is, among others, characterized by a single non-dimensional parameter: the Reynolds number Re. It is defined by

$$Re = \frac{UL}{\nu} \tag{5.1.9}$$

where

- U = is the characteristic fluid velocity
- L = is the characteristic length scale of the flow
- ν = is viscosity

A low Reynolds number indicates that the fluid velocity is slow or the length scale is small or the fluid viscosity is high. Hence the flow is smooth. On the other hand, a high Reynolds number expresses that the fluid velocity is fast or the length scale is big or the fluid viscosity is small.
A laminar flow is defined to be a flow with a small Reynolds number whereas a turbulent flow is a flow at high Reynolds number. The Reynolds number separating these two regimes is called the critical Reynolds number. For example, the critical Reynolds number of a flow around a cylinder is around 2300 for a channel flow.
A laminar flow is typically smooth and stationary in time. It means that after the flow settles $U(r;t) = U(r;t+1)$. A turbulent flow presents some instabilities, they appear at certain distance from the obstacle. Hence a layer called boundary layer is formed around the obstacle. The thickness of the boundary layer tends to zero as the Reynolds number tends to infinity. In this boundary layer the viscosity plays a more important role than in the bulk. Van Dyke's book [71] proposes a wide variety of real experiments. Some pictures of a flow around cylinders have been selected. They present a good example of the effect of a Reynolds number variation. These pictures also exhibit the apparition of turbulent instabilities. They are presented in Figure (5.1.1).

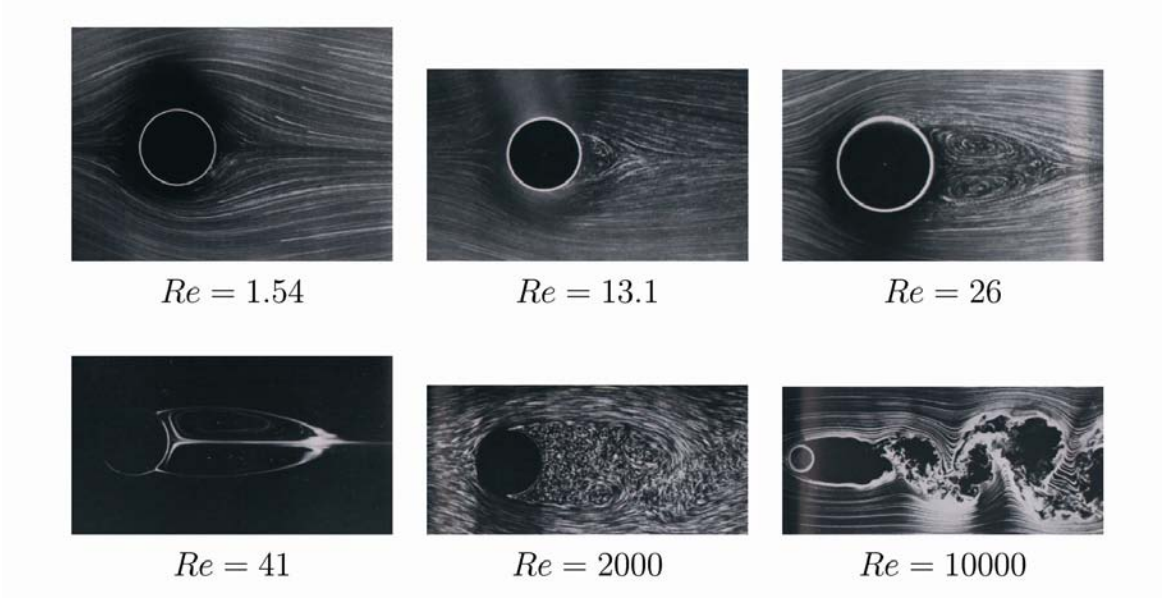

Figure 5.1.1 – Real experiment of a flow past a cylinder at various Reynolds numbers, [71].

.

The Kolmogorov theory shortly visited

In 1941, Kolmogorov proposed his famous theory about turbulence (K41), [29]. This is in agreement with the previous empirical laws and lead to other predictions. The K41 is partially and informally presented here. The reader interested in a complete and rigorous presentation can find some pointers in [29] [42]. Figure (5.1.2) presents the scales and the energy balance of turbulent flows. This phenomenon is usually represented by eddies successively breaking into smaller ones until they reach the dissipation scale. This process is often referenced as the cascade of Richardson.

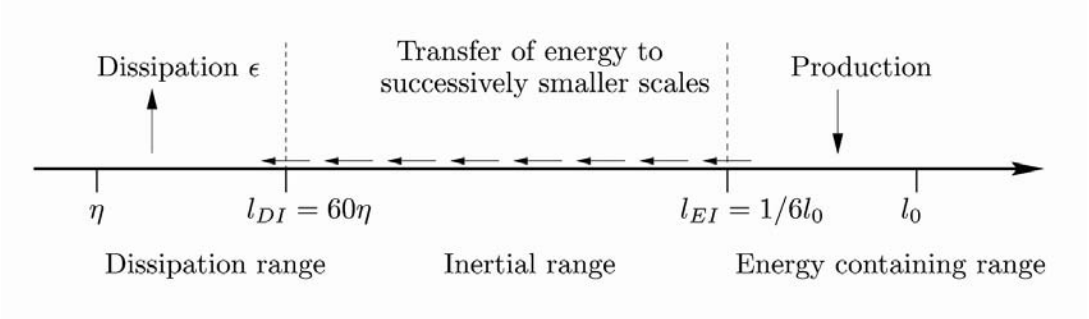

Figure 5.1.2 – Scales and the energy balance of turbulent flows, [29].

.
The energy is introduced in the system between the biggest scale l_0 and $l_{EI} = \frac{l_0}{6}$ (empirically determined). In this context, a scale is the diameter of an eddy. l_0 corresponds to the size of the biggest eddy. For example, if a propeller fan of diameter l_0 would be used to accelerate the fluid it would generate eddies of size l_0. From l_{EI} and $l_{DI} = 60\eta$ (length of the small scale), eddies break into smaller ones and therefore energy is transfered to smaller scales. Finally from l_{DI} and $\eta = (\frac{\nu}{\epsilon})^{\frac{1}{4}}$, energy is dissipated into heat for example. η is the Kolmogorov dissipation scale, η is the viscosity and ϵ is the energy dissipation. The range called energy containing range is defined as the scales between l_0 and l_{EI}. The scales between l_{EI} and l_{DI} are in the inertial range. In this range, direct energy injection and energy dissipation are both negligible. Finally, the dissipation range is defined as the scales between l_{DI} and the smallest scale η. The K41 theory is based on the following hypothesis:

- **H1** In the limit of infinite Reynolds number, all the symmetries of the Navier-Stokes equation, usually broken by the mechanism producing the turbulent flow, are restored in a statistical sense at small scales and away from boundaries.
- **H2** Under the same assumptions as in H1, the turbulence flow is self-similar at small scales, i.e. it possesses a unique scaling exponent h. Thus there exists a scaling exponent $h \in R$ such that $\delta U(r, \lambda l) = \lambda^h \delta U(r, l), \forall \lambda \in R_+$ for all r and all l small compared to the integral scale l_0.
- **H3** Under the same assumptions as in H1, the turbulent flow has a finite non vanishing mean rate of dissipation ϵ per unit mass.

In [29], Kolmogorov found that an exact relation can be derived for $S_3(l)$. He assumed homogeneity (translation invariance), isotropy (rotation invariance) and hypothesis H3. Without any further assumptions he derived the following result from the Navier-Stokes equation.

- **The $\frac{4}{5}$ law.** In the limit of infinite Reynolds number, $S_3(l)$ of homogeneous isotropic turbulence, evaluated for increments l small compared to l_0, is given in terms of the mean energy dissipation per unit mass ϵ (assumed to remain finite and non vanishing) by

$$\left\langle (\delta U_{\parallel}(r, l))^3 \right\rangle = -\frac{4}{5}\epsilon l \tag{5.1.10}$$

The proof of this law is quite hard and not the aim of this section. However a proof can be found in [29]. One of the main results of the K41 theory is the power law for the structure function of order p, Sp(l). Kolmogorov argued that $S_p(l) \propto l^{\frac{p}{3}}$.

Since the K41 theory was proposed, many researchers have protested against it. The major critic is the simplicity of his hypotheses. Among others, Kolmogorov himself introduced important modifications in 1962 [21] taking into account spatial fluctuations in the turbulent energy dissipation, [10] and others have criticized the linear exponent $\frac{p}{3}$ of the longitudinal structure function $S_p(l)$ for $p > 3$ and proposed some refinements. Let

us also mention the notion of Extended Self Similarity (ESS) which extends hypotheses H1 and H2 in the case of smaller Reynolds number.
Although the above presentation was succinct, it is clear that the K41 theory is definitely not complete and is largely supported by hypothesis. Probably because turbulence is a current subject of research and because a complete model describing the whole turbulent phenomenon is still needed. Before to going through an explanation of the turbulence model, let us to define a new concept: eddy viscosity.

5.1.3 Eddy viscosity

In 1877, [21] observed that turbulence greatly (locally) increases the viscosity. So he introduced the concept of eddy viscosity νt in order to quantify this increase. The eddy viscosity is defined as

$$-\langle u_\alpha u_\beta \rangle = \nu_t \frac{\partial \widetilde{U}_\alpha}{\partial_{x\beta}} \tag{5.1.11}$$

where

- $\langle\rangle$is the time average
- α and β are spatial components
- u is the fluctuation of the velocity around the time averaged velocity $\widetilde{U}$ and $\langle u_\alpha u_\beta \rangle$ is Reynolds stress tensor component

This stress is an important quantity because it represents the main contribution to the residual which appears when one uses most numerical techniques. Roughly speaking, the Reynolds stress gives an indication on the flow fluctuation. One can note the similitude between equations (5.1.11) and (5.1.5) indicating why ν_t is considered as a viscosity. The eddy viscosity is typically several orders of magnitude larger than the molecular viscosity. It is important to realize that ν_t is a representation of the action of turbulence on the mean flow and not a property of the fluid. The effective viscosity $\nu_{eff}$is locally the sum of the molecular viscosity ν and the eddy viscosity ν_t.

5.2 Turbulence models

Turbulent flows may be computed using several different approaches. Either by solving the Reynolds-averaged Navier-Stokes equations with suitable models for turbulent quantities or by computing them directly. The main approaches are summarized below.

Reynolds-Averaged Navier-Stokes (RANS) models

- **Eddy-viscosity models** One assumes that the turbulent stress is proportional to the mean rate of strain. Further more eddy viscosity is derived from turbulent transport equations (usually k + one other quantity).
- **Non-linear eddy-viscosity models** Turbulent stress is modelled as a non-linear function of mean velocity gradients. Turbulent scales are determined by solving transport equations (usually k + one other quantity). These models mimic response of turbulence to certain important types of strain.
- **Differential stress models** This category consists of Reynolds-stress transport models (RSTM) or second-order closure models (SOC). One is required to solve transport equations for all turbulent stresses.

Computation of fluctuating quantities

- **Large-eddy simulation** One computes time-varying flow, but models sub-grid-scale motions.
- **Direct numerical simulation** No turbulence modelling what so ever is applied. One is required to resolve the smallest scales of the flow as well.

The range of modelling for certain CFD approaches is illustrated in the following Figure (5.2.1). Turbulent flows are characterized by the formation of structures at many length scales. It is clearly seen, that models computing fluctuation quantities resolve shorter length scales than models solving RANS equations. Hence they have the ability to give more information about the flow field. However they have a demand of much greater computer power than those models applying RANS methods.

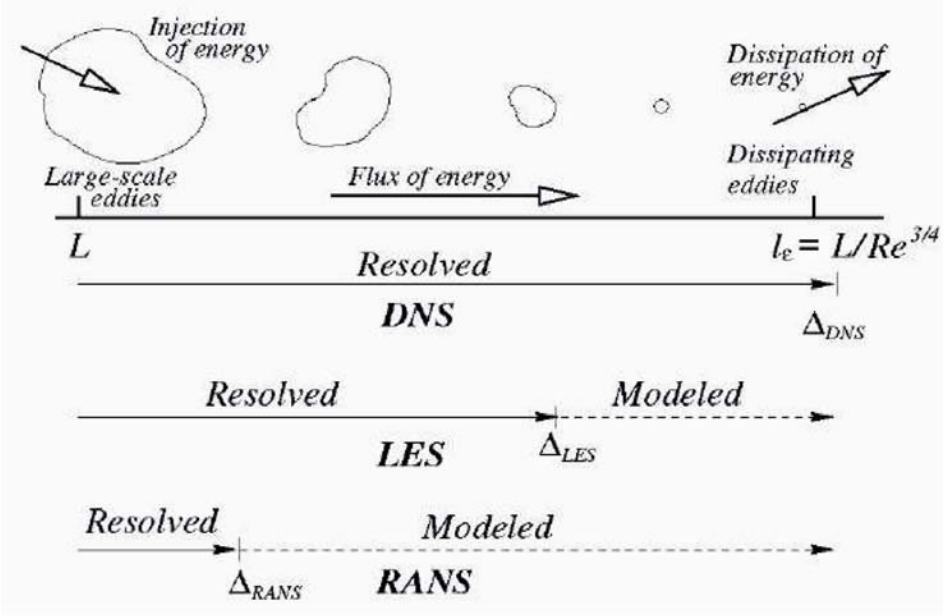

Figure 5.2.1 – Extend of modelling for certain types of turbulent models, [21].

.

The "VirtualSnow" model computes a **Large Eddy Simulation** with a subgrid model called Smagorinsky model. Turbulent flows are characterized by the occurrence of eddies whose size may vary over a large range. The larger eddies contain the main portion of the flow energy. This energy is successively transferred to the smaller eddies, and is eliminated by viscous dissipation in the smallest ones. This process is described by the theory of Kolmogorov in the previous section. In order to obtain an accurate representation of the flow evolution, all structures down to the smallest ones must be representable on the computational grid. With currently available computing resources, it is actually impossible. To face this problem, simulations are often simply run on an underresolved grid. Large eddy simulations simulate the effect of the large eddies in the flow but do not take into account the small ones. The effect of the small eddies is however not neglected. Instead, a new, modified dynamics is executed on the computational grid. This dynamics replaces the effect of the small eddies, had the simulation been executed on a fully resolved fine grid, by a numerical prediction. This prediction is only an approximation to the exact, fully resolved dynamics. The most common of those subgrid models include the notion of an effective viscosity: they predict that the adapted dynamics on the coarse grid implements the Navier-Stokes equation with a time and space dependent viscosity. The Smagorinsky subgrid model relates the effective viscosity to the value of the local strain rate tensor S.
Smagorinsky proposed to define the local stress tensor τ_{ij}^r as

$$\tau_{ij}^r = -2\nu_t \left(\frac{\partial \bar{U}_i}{\partial_{x_j}} + \frac{\partial \bar{U}_j}{\partial x_i} \right) = -2\nu_t \bar{S}_{ij} \tag{5.2.1}$$

where

- ν_t is the turbulent viscosity
- $\bar{U}\alpha$ is the α component of the filtered velocity
- Sij is the strain tensor

The turbulent viscosity is expressed as

$$\nu_t = (C_{Smago}\Delta)^2 \left(2\bar{S}_{ij}\bar{S}_{ij}\right)^2 \tag{5.2.2}$$

where C_{smago} is the Smagorinsky constant and Δ the filter width. The Smagorinsky constant C_{smago} is unfortunately not constant. It depends on simulations and to distance to obstacles but it is usually close in a range $[0.1, 0.2]$ Hence, the new element (τ_{ij}^r) which appeared under the filtering operation is computable and the system closed.

Model comparison

There are many kinds of flows and many problems to solve. First, for example one can mention a turbulent flow, at Reynolds number sufficiently low, for which the interest could be to compute the fluctuation of the velocity. In this case a DNS is probably adapted. A second example could be the determination of the center of a vortex at high Reynolds number. This is an example of adequate use of LES. These examples highlight

that there is no application perfectly adapted to models but rather models adapted to applications.
Criteria indicating which model is preferable to select for a given application are needed. Pope [54] defines five criteria for appraising models. These criteria are:

- level of description: indicates the quality of the flow description
- completeness: points out if the model constituent equations are free from flow-dependent specifications
- cost of use: describes the computational difficulty
- range of applicability: indicates the kind of applications which can be addressed by the model
- accuracy: gives an appreciation of the model accuracy

5.3 Lattice Boltzmann approach applied to Computational Fluid Dynamics

The main topic of the thesis is a numerical approach known under the name of lattice Boltzmann method to simulate snow transport by wind. This method is relatively new and contrasts with the traditional approach to CFD by adopting a bottom-up approach to fluid modeling. CFD is the numerical simulation of fluid flows represented by a partial differential equation (PDE) widely known as the Navier-Stokes equation, which expresses a local conservation law for the momentum in the system. Lattice Boltzmann method describes the fluid at a kinetic level consisting of fictitious particle distributions, and proposes models for consecutive collision and propagation process between particles over a discrete lattice. The full continuum-level physics of the fluid is implicitly contained in this model, the concept is thus complementary to the classical CFD. Indeed, the various physical ingredients contained in the model need to be identified one by one and properly explicated in order to allow for a segregation between relevant and negligible properties. Based on those considerations, the collision-propagation model is substantially simplified for the needs of the numerical treatment.
In the next chapter will be present a compact explanation of the developed "Virtual-Snow" model with the lattice Boltzmann approach.

6 Simulation of fluid flow with the lattice Boltzmann approach

6.1 Introduction

The present chapter is devoted to present the 2D lattice Boltzmann model implemented to simulate snow transport by wind, the **VirtualSnow** model. The methods and algorithms are described in some detail. In particular, the conditions that model the behavior of the fluid and flow proprieties at boundaries are specified.
Below the various ways to settle a flow are briefly summarized. In fluid dynamics and finite-deformation plasticity the classical approaches to model solid particles behavior under the action of a fluid field can historically be split among two methods:

- the Lagrangian specification of the flow field is a way of looking at fluid motion where the observer follows an individual fluid parcel as it moves through space and time. Plotting the position of an individual parcel through time gives the pathline of the parcel. This can be visualized as sitting in a boat and drifting down a river.

- the Eulerian specification of the flow field is a way of looking at fluid motion that focuses on specific locations in the space through which the fluid flows. This can be visualized by sitting on the bank of a river and watching the water pass the fixed location.

Lattice Boltzmann approach is an Eulerian method that computes the dynamic evolution of the particle probability distribution function, as described by the Boltzmann kinetic equation discretized on a velocity lattice. Macroscopic flow-variables (velocity, pressure, density) are recovered as moments of the local and instantaneous particle probability distribution function, as is described in more detail in the next sections.

6.2 The Lattice Boltzmann method

6.2.1 Lattice Boltzmann ancestors

The first lattice Boltzmann modells have been derived from cellular automata (CA). Cellular automata represent a physical system in an idealized way where space and time are discrete, i.e., a fully discrete universe made up of identical cells. CA are defined by a regular lattice of cells characterized by a set of boolean state variables. The evolution rule, which is a function of the state of the neighboring cells, is the same for all cells and updating of the cells occurs simultaneously in discrete time steps.
A special class of CA [73], the lattice gas automata (LGA) [56], describe the dynamics of point particles moving and colliding in a discrete space-time universe. Lattice gas models with an appropriate choice of the lattice symmetry in fact represent approximated numerical solutions of the Navier-Stokes equations and are therefore able to describe macroscopic hydrodynamic problems [28]. However, lattice gas models suffer from some drawbacks: Statistical noise, non-Galilean invariance, a velocity dependent pressure and spurious invariants. Particularly, the statistical noise requires time and/or space averaging procedures to extract macroscopic quantities like density or velocity. These intrinsic properties of LGAs are the reason why they were not able to compete with conventional numerical methods of hydrodynamics.
The lattice Boltzmann method [17] historically developed from lattice gas automata McNamara and Zanetti [48] were the first who extended the boolean dynamics of the automaton to real numbers, the particle distribution functions, representing the probability for a cell to have a given state. The philosophy behind this procedure is that it is more efficient to average the micro dynamics before than after simulation. That is, the discrete nature of the fluid particles vanishes on the macroscopic level of observation.

6.2.2 Lattice Boltzmann method

The lattice Boltzmann method [68] can not only be seen as a successor of lattice gas automata (LGA). The equations can also be derived rigorously from the underlying physical model, the Boltzmann equation, and it can be shown that Navier- Stokes flow behavior is recovered in the macroscopic limit of small Knudsen- and Machnumbers [38], [68]. The following Figure outlines the major steps of the derivation of the relevant equations and relations of the lattice Boltzmann method (6.2.1).

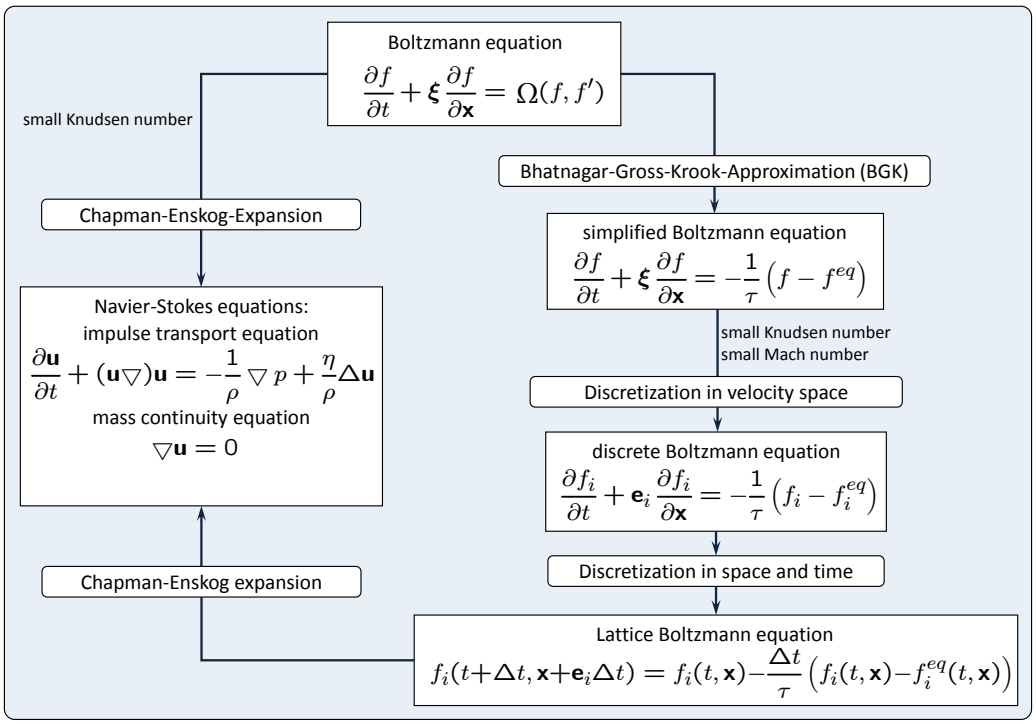

Figure 6.2.1 – Derivation of the equations and relations of the lattice Boltzmann method, [6]

The Boltzmann equation is a partial differential equation (PDE) describing the evolution of the single particle distribution function f in phase space.

$$\frac{\partial f}{\partial t} + \xi \cdot \frac{\partial f}{\partial x} + F \cdot \frac{\partial f}{\partial \xi} = \Omega(f, f') \tag{6.2.1}$$

This distribution function is defined in such a way that $f(x, \xi, t)$ is the probability for particles to be located within a phase space control element $(dxd\xi)$ about x and ξ at time t where x and ξ are the spatial position vector and the particle velocity vector, respectively. The macroscopic quantities, such as the density and the momentum, can then be obtained by evaluating the first moments of the distribution function f.
The right side of (6.2.1) is the collision operator $\Omega(f, f')$. A suitable simplification of the collision operator for the near-equilibrium state of low Mach number is the single relaxation time approximation, the so-called Bhatnagar-Gross-Krook (BGK) model, see Figure (6.2.1), where $f^{(eq)}$ is the Maxwell-Boltzmann equilibrium distribution function, and τ is the relaxation time which controls the rate of approaching equilibrium, which turns out to be linearly related to the viscosity of the fluid.

The BGK relaxation still fulfills Boltzmann's H-theorem.
To obtain the main equation of the lattice Boltzmann approach (6.2.3) see Figure (6.2.1), is discretized numerically in a very special manner. The discretization of space and time is accomplished by an explicit finite difference approximation. By scaling the lattice spacing, the time step and the discrete velocities appropriately.
To solve for f numerically, velocity space is discretized using a finite set of velocity vectors $\mathbf{e}_i (i = 0, ..., N)$ leading to the velocity discrete Boltzmann equation, where $f(x,t)$ is equivalent to $f(x, \mathbf{e}_i, t)$.
In our approach, the fluid is described with a population of particles density move synchronously, according to discrete time steps, along the links of a regular lattice. When bouncing into each other, these densities are redistributed among the lattice directions in such a way that mass and momentum are conserved. The quantities, mentioned before, $f_i(x,t)$ indicating the probability of presence of a particle entering site x at time t, with a velocity $\mathbf{e}_i$ pointing along the direction i. A lattice structure with q lattice directions, defined on a d-dimensional space, is commonly identified by the name "DdQq" lattice. Is discussed our case: a D2Q9 model, see Figure (6.2.2).

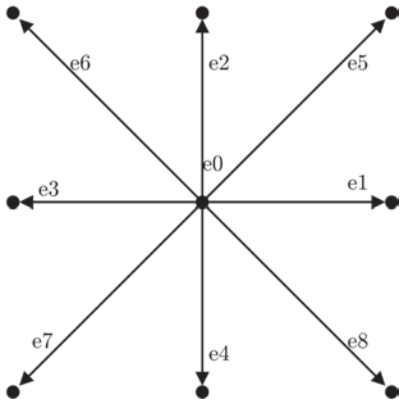

Figure 6.2.2 – Discretized distribution functions f_i for the D2Q9 model: eight distribution functions associated with the particles moving to the neighboring cells and one distribution function corresponding to the resting particles.

where $i = 1, ...8$ designates the geographical directions E, NE, N, NW, W, SW, S and SE in a two dimensional square lattice and $i = 0$ refers to a population of rest (R) particles $e_o = 0$.
Hence, the microscopic velocities of the 2DQ9 model are defined as

$$\{\mathbf{e}_i, i = 0, \ldots, 8\} = \begin{Bmatrix} 0 & c & 0 & -c & 0 & c & -c & -c & c \\ 0 & 0 & c & 0 & -c & c & c & -c & -c \end{Bmatrix} \tag{6.2.2}$$

generating a space-filling lattice with a nodal distance $\Delta_x = c\Delta_t$, where

- c is a constant microscopic reference velocity related to the speed of sound
- Δ_t is the time step.

The lattice Boltzmann equation is

$$f_i\left(t+\Delta t, x+\mathbf{e}_i, \Delta t\right) - f_i\left(t,x\right) = -\frac{\Delta t}{\tau}\left(f_i\left(t,x\right) - f_i^{eq}\left(t,x\right)\right) \tag{6.2.3}$$

the right hand side is usually called collision step and the left hand side streaming step; where

- f_i are the particle distribution functions propagating with speed $\mathbf{e}_i$,
- x is a point in the discretized physical space

For the collision step, the equilibrium distribution function has to be calculated at each cell and at each time step from the local density ρ and the local macroscopic flow velocity u. In particular when dealing with complicated formulations of the boundary conditions, it can be necessary to divide the update process into the following two equations

$$f_i{}^{out}\left(t,x\right) = f_i{}^{in}\left(t,x\right)) - \frac{\Delta t}{\tau}\left(f_i{}^{in}\left(t,x\right) - f_i^{eq}\left(t,x\right)\right) \tag{6.2.4}$$

$$f_i{}^{in}(t+\Delta t, x+\mathbf{e}_i) = f_i{}^{out}\left(t,x\right) \tag{6.2.5}$$

where f_i^{out} denotes the distribution values after collision (before propagation), and f_i^{in} are the values after collision and propagation, thus the values entering the neighboring cell as data for the next time step.
The simulation process, displayed in following the scheme, is an alternation between particle propagation and particle collision.

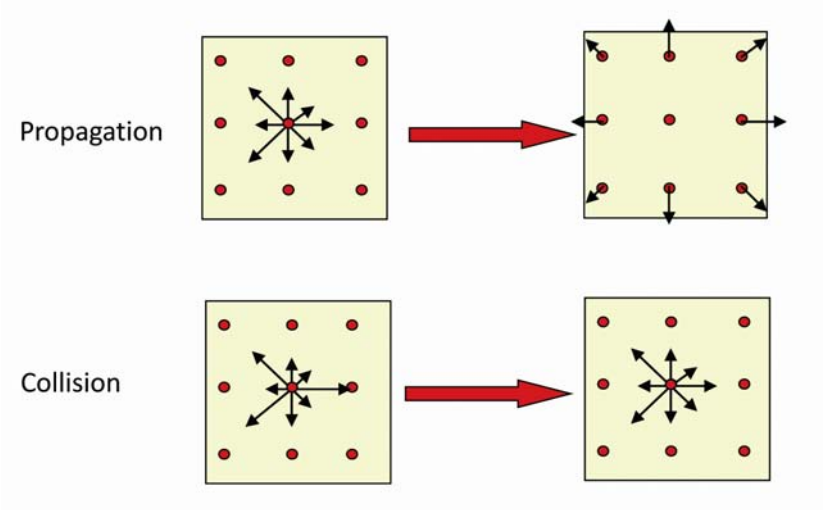

Figure 6.2.3 – Collision propagation processes.

We use a modified version of the Multi-Relaxation Time (MRT) model [20]. Considering the generalized lattice Boltzmann equation

$$f_i\left(t+\Delta t, x+\mathbf{e}_i, \Delta t\right) = f_i\left(t, x\right) + \Omega \tag{6.2.6}$$

where

- Ω is the collision operator

the collision operator of the Multi-Relaxation Time model is given by

$$\Omega = M^{-1}K \tag{6.2.7}$$

where

- M is the transformation matrix
- K is the change of distribution functions in moment space.

The moments m of the distribution functions are given by

$$m = Mf := (\rho, \rho_0 u_x, \rho_0 u_y, e, p_{xx}, p_{xy}, h_x, h_y, \in) \tag{6.2.8}$$

where

- ρ is a density variation
- $(\rho_0 u_x, \rho_0 u_y)$ is the momentum
- ρ_0 s a constant reference density

The moments e, p_{xx}, p_{xy} of second order are related to the strain rate tensor by

$$\partial_x u_x = \frac{S_e}{4c^2\Delta t}\left(3(u_x^2+u_y^2) - \frac{e}{p_0}\right) + \frac{3S_v}{4c^2\Delta t}\left(u_x^2 - u_y^2 - \frac{p_{xx}}{p_0}\right) \tag{6.2.9}$$

$$\partial_y u_y = \frac{S_e}{4c^2\Delta t}\left(3(u_x^2+u_y^2) - \frac{e}{p_0}\right) + \frac{3S_v}{4c^2\Delta t}\left(u_y^2 - u_x^2 - \frac{p_{xx}}{p_0}\right) \tag{6.2.10}$$

$$\partial_y u_x + \partial_x u_y = \frac{3S_\nu}{c^2\Delta t} u_x u_y - \frac{p_{xy}}{p_0} \tag{6.2.11}$$

where S_ν and S_e are relaxation rates. Moments h_x , h_y and $\in$ are of third and fourth order. Vector K is given with

$$K_1 = g_x \Delta_t \tag{6.2.12}$$

$$K_2 = g_y \Delta_t \tag{6.2.13}$$

$$K_3 = K_e = -s_e\left(e - 3_{\rho 0}(u_x^2 - u_y^2)\right) \tag{6.2.14}$$

$$K_4 = K_{xx} = -s_\nu\left(p_{xx} - \rho 0(u_x^2 - u_y^2)\right) \tag{6.2.15}$$

$$K_5 = K_{xy} = -s_\nu\left(p_{xy} - \rho 0 u_x - u_y\right)) \tag{6.2.16}$$

$$K_6 = K_{hx} = -s_h h_x \tag{6.2.17}$$

$$K_7 = K_{hy} = -s_h h_y \tag{6.2.18}$$

$$K_8 = K_\in = -s_\in \in \tag{6.2.19}$$

where

- $G = (g_x, g_y)$ is a body force
- $s_e s_h$ are relaxation rates related to the higher order moments.

The kinematic viscosity is related to the relaxation rate s_ν by

$$\nu = c^2 \Delta t \left(\frac{1}{3 s_\nu} - \frac{1}{6} \right). \tag{6.2.20}$$

The hydrodynamic pressure is given by

$$p = \frac{c^2}{3} \rho = c_s^2 \rho. \tag{6.2.21}$$

The collision rates s_e, s_h and $s_\in$ are not relevant for the incompressible limit of the Navier-Stokes equations and can be chosen in the range $[0, 2]$.
In Figure (6.2.4) the outline of the major components of the LB algorithm together with the relevant equations. Each "box" is executed for all cells during each time step. One sweep through all "boxes" represents one time step.

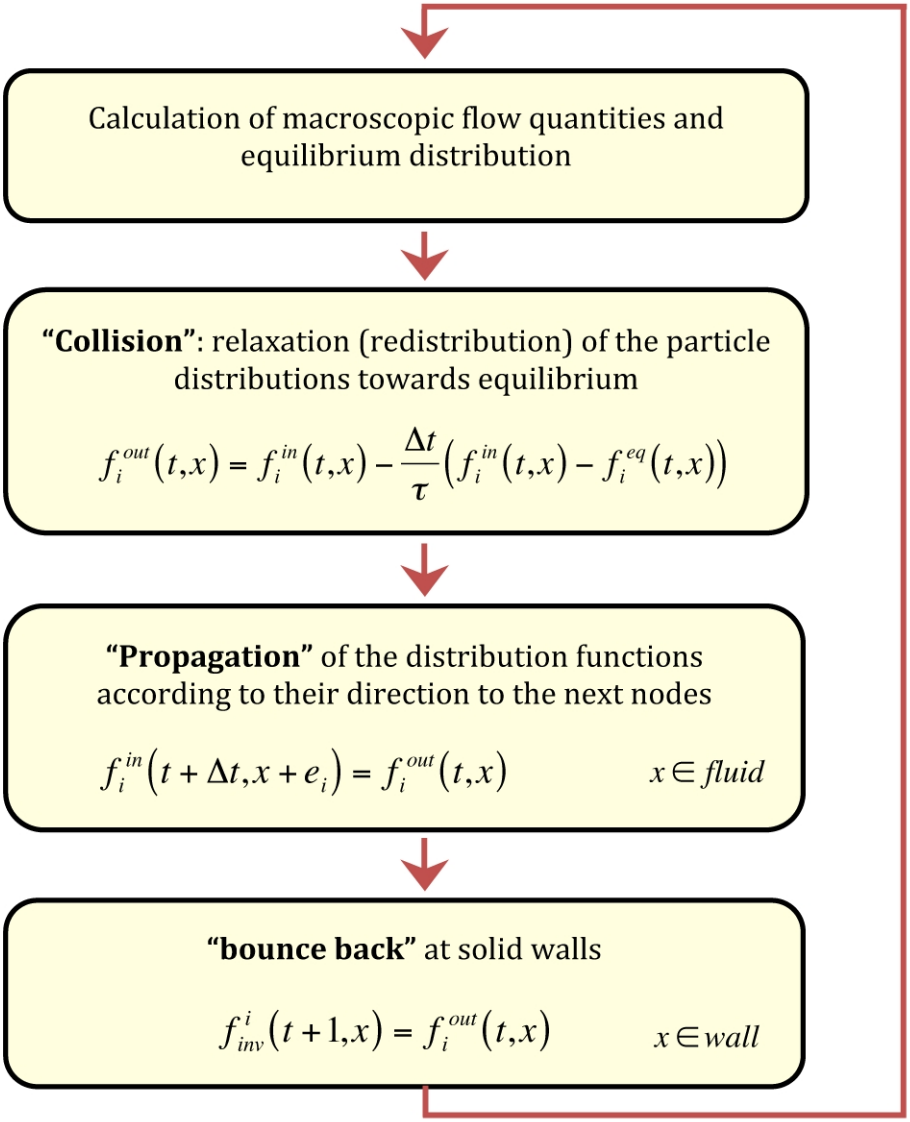

Figure 6.2.4 – Major components of the LB algorithm.

6.3 Turbulence: Large Eddy Simulation

"VirtualSnow" model adapts Large Eddy Simulation to the lattice Boltzmann scheme, modelling only the large eddies (larger than the lattice resolution), and trying to extrapolate what is happening at lower resolution scale (in fact modelling the effect of the unresolved scale on the effective ones). A model is needed for the unresolved physical scale, is used the so called Smagorinski subgrid model, [64]. One assumes that a turbulent viscosity ν_t results from the unresolved scales, that is the scales below the lattice spacing Δx. These scales are thus filtered. The main idea is to increase locally the relaxation time τ by defining a new space and time dependent relaxation time $\tau_{tot} = \tau + \tau_t$ where τ_t is the turbulent contribution. We assume a fixed value for τ . Then the total viscosity can be decomposed as

$$\nu_{tot} = \nu + \nu_t \tag{6.3.1}$$

where ν is the viscosity corresponding to the relaxation time τ and is given by following equation

$$\nu = c^2 \Delta t \left(\frac{1}{3 s_\nu} - \frac{1}{6} \right). \tag{6.3.2}$$

The new contribution νt is the so-called turbulent viscosity, see section (5.1.3) for details, resulting from the filtered scales. In the Smagorinsky model [64], it is expressed as

$$\nu_t = C_{smago} \Delta^2 |S| \tag{6.3.3}$$

where

- Δ is the filter size, whose magnitude usually corresponds to Δx
- $|S|$ is the magnitude of the strain-rate tensor $S_{\alpha\beta}$

$$|S| = \sqrt{2 S_{\alpha\beta} S_{\alpha\beta}} \tag{6.3.4}$$

$$S_{\alpha\beta} = \frac{1}{2} (\partial_\beta u_\alpha + \partial_\alpha u_\beta). \tag{6.3.5}$$

Thus the turbulent viscosity increases with $|S|$, so that the total viscosity is larger in regions close to obstacles. It is illustrated in figure (6.3.1), that displays the turbulence viscosity around obstacles simulated with "VirtualSnow" model. The flow is settled from left to right by imposing a logarithmic velocity profile with: $U_0 = 2,2 m/s$, Reynolds number $R_e = 10^5$ and $C_{smago} = 0.1$.

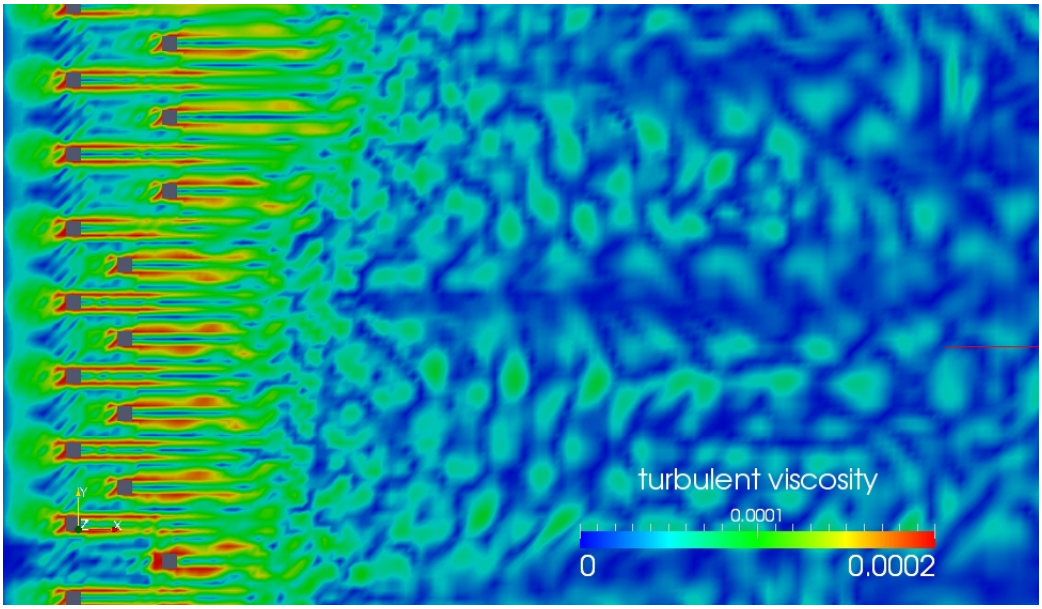

Figure 6.3.1 – Turbulence viscosity around obstacles simulated with "VirtualSnow" model.

The effect of the Smagoriski constant C_{smago} is to adjust the resolution scale flow. The filter size Δ is usually set to one lattice spacing. The quantity C_{smago} is typically smaller than 1/5.

6.4 Lattice Boltzmann approach for advection-diffusion

Advection-diffusion processes can also be simulated by the Lattice Boltzmann method. Different formulations have been proposed in the literature. Flekkoy [27] and Wolf-Gladrow [72] solved the advection-diffusion equation with lattice Boltzmann models on a uniform grid. Later, van der Sman and Ernst [70] developed a scheme which also works on irregular Bravais lattices. Recently, Ginzburg [32] described a family of lattice Boltzmann schemes for the advection-diffusion equation also allowing for anisotropic diffusion and providing many parameters allowing a fine tuning of the numerical properties of the method. In [66] a coupling algorithm is introduced which allows the extension of the advection/diffusion model to multiply locally refined grids.
In this section we describe the basic Lattice Boltzmann scheme for advection-diffusion equation.
The advection-diffusion process discussed in section 5.1.1 are expressed as

$$\frac{\partial s}{\partial t} + u_\alpha \frac{\partial s}{\partial x_\alpha} = \partial_\beta \left(D \partial_\beta s \right) \tag{6.4.1}$$

with an externally given velocity field $u(x,t)$ and diffusion coefficient $D(x,t)$.
The basis of the algorithm is one particular member of the family of advection-diffusion LB algorithms described in [27], where it was labelled the 'optimal convection solution'. Here we are using the D2Q9 set [55] of microscopic velocities ξ_q.

$$\vec{\xi}_q = c \begin{cases} (0,0) & : \quad q = 0 \\ (\cos\left[(q-1)\pi/2\right], \sin\left[(q-1)\pi/2\right]) & : \quad q = 1,2,3,4 \end{cases} \tag{6.4.2}$$

The collision operator reduces to a BGK-type [14] relaxation. Thus, the basic lattice Boltzmann algorithm is given as

$$f_q\left(x + \Delta t \xi_q, t + \Delta t\right) = f_q\left(,t\right) + \lambda\left[f_q\left(x,t\right) - f_q^{\mathrm{eq}}\left(x,t\right)\right], \tag{6.4.3}$$

which can be interpreted as a local collision step and propagation of the post-collision distributions to the neighboring nodes. Following [34], the collision eigenvalue λ is chosen as

$$\lambda = -3 + \sqrt{3} \tag{6.4.4}$$

to provide the optimal convection solution. The equilibrium distributions are given by

$$f_q^{\mathrm{eq}} = s\left(t_q + \frac{1}{3}a^{(e)}t_q^{(e)} + E_q^u + \frac{1}{2}\frac{u_\alpha \xi_{q\alpha}}{c^2}\right) \tag{6.4.5}$$

with

$$s = \sum_{q=0}^{q=4} f_q = \sum_{q=0}^{q=4} f_q^{\mathrm{eq}}. \tag{6.4.6}$$

$a^{(e)}$ is connected to the diffusion coefficient D via

$$a^{(e)} = \frac{6\sqrt{3}D}{c^2\Delta t} - 1. \tag{6.4.7}$$

The weights t_q are given by

$$t_0 = \frac{1}{3}, t_q = \frac{1}{6} \text{ for } q \neq 0. \tag{6.4.8}$$

$t_q^{(e)}$ is a basis vector which can be obtained from a second order polynomial in ξ_q:

$$t_0^{(e)} = -2, t_q^{(e)} = \frac{1}{2} \text{ for } q \neq 0. \tag{6.4.9}$$

E_q^u is used to remove a velocity dependent second order correction to the diffusion tensor:

$$E_0^u = -\frac{u_\alpha u_\alpha}{c^2}, E_q^u = \frac{1}{2}\frac{\left(u_\alpha \xi_{q\alpha}\right)^2}{c^4} \text{ for } q \neq 0 \tag{6.4.10}$$

The solution and validation of this approach has been presented in [66]. It is shown that this approach allows an efficient solution of advection/ diffusion problems on uniform grids and also on locally refined Cartesian meshes.

6.5 The snow model

The main difference between Bagnold´s approach, see section (3.3.2), and our model is the mass balance of a air-snow mixture, of the latter. We do not try to represent a specific grain of snow with relative particle diameter in a cell, but estimate the concentration of snow mass for each cell. Fictitious fluid and snow particles move on a regular lattice, synchronously at discrete time steps. The snow moves under the combined effect of the local fluid velocity field and gravity. Particles reaching the ground solidify, pile up and topple if necessary. Hence, they can change the shape of the boundary of the fluid. At the top of the deposition layer, erosion takes place and, if the fluid flows fast enough, it can pick up solid particles and transport them further away. A new simple set of rules, detailed below, is sufficient to catch the main ingredients of particles motion (saltation, creping, suspension) under the action of a fluid. The "VirtualSnow" model simulates dry snow. Our model includes the transient update of the snow surfaces during simulation after each time step, therefore, the snow cover is modeled dynamically coupling changes in geometry to the flow. To update the height of the surface cells as a function of local erosion or deposition, we estimate the erosive or accumulative snow mass flux contribution into or out of the computational cell. The accumulative or erosive snow flux is a function of the snow concentration, the surface normal and shear stress, the particle fall velocity and threshold surface shear stress for particle entrainment. In particular, the deposition flux is calculated as a function of the available snow concentration, the snow fall velocity and the velocity flow. It is assumed to reach its minimum value when the calculated shear stress is equal to the threshold shear stress.

$$q_{DepShear} = N_v * W_f * C \tag{6.5.1}$$

where N_v is surface normal velocity, W_f is the snow fall velocity and c is the concentration flow. The falling velocity is assumed constant at $w_f = 0.5m/s$ for the present analysis. The shear component of the erosive flux is a function of the available surface strain magnitude and the bonding strength of the snow pack. Neglecting the erosive flux from impacting particles one may deduce that this flux is,

$$q_{EroShear} = A * (Sm); Sm > Sm_{th} \tag{6.5.2}$$

$$q_{EroShear} = 0; Sm < Sm_{th} \tag{6.5.3}$$

where

- A is a proportionality coefficient representing the snow pack bonding strength
- Sm is strain magnitude
- Sm is strain magnitude threshold

The method employed here is based on the balance between erosion and deposition.

6.6 Boundary conditions

In addition to the governing equations of a flow problem, it is necessary to specify conditions that model the behavior of the fluid and flow properties at boundaries of various types. The boundary conditions that apply specifically to the velocity field are usually referred to as the no-slip boundary conditions.
Many boundary conditions for the Lattice Boltzmann method have been proposed in the past [16]. The most common and simple one is the bounce-back boundary condition, which is explained in the following. This condition is only first order in terms of numerical accuracy [75]. Hence, to improve it other boundary treatments have been proposed. Skordos [63] proposed to include velocity gradients in the equilibrium distribution function at the wall nodes. He et al. [39] extended the bounce-back condition for the non-equilibrium portion of the distribution. Inamouro et al. [41] suggested to cancel a slip velocity at the wall by using a counter slip velocity. Chen et al. [16] proposed to use a simple extrapolation scheme. Maier et al. [47] modified the bounceback condition to nullify the net momentum tangent to the wall and to preserve momentum normal to the wall. All these conditions deal with flat walls. Their action is to define the unknown distributions which would come from the solid. However, note that all these bounce-back condition improvements are difficult to implement for general geometries essentially because one has to know the wall orientation. With these boundary conditions, corner nodes - if present - require a special treatment.
Recently, some advances have been made in the treatment of curved and of lattice boundaries [49]. Indeed, curved boundaries are often approximated by a series of stairs (as e.g. in the case of simple bounce back). Depending on the simulation, this approximation leads to a consequential reduction of numerical accuracy.

The focus in this work aims on transport of snow particles in the atmospheric boundary layer. In order to conserve the accuracy of the geometric representation, we use the simple bounce back (the wall is located half-way between the last fluid cell and the first wall node) for the sedimentation (boundary condiction/field) and, the modified bounce back scheme developed in [15, 45] for the flow field which are second order accurate for arbitrarily shaped boundaries.

In most of the flows encountered in engineering the fluid does not move relative to a solid surface in the tangential direction right at the wall. The tangential component of velocity u_T is equal to the tangential component of boundary velocity U_T. This boundary condition

$$u_T = U_T \tag{6.6.1}$$

is called the no-slip condition in fluid dynamics. In lattice Boltzmann models the macroscopic flow quantities can only be set implicitly via incoming particle distribution functions on the boundary nodes. The easiest solution for introducing no-slip boundary condition (i.e a solid walls) is the introduction of the bounce back rule on wall nodes, as defines the following formula

$$f_i{}^{out}(t,x) = f_{\bar{i}}{}^{in}(t,x)) \tag{6.6.2}$$

with

- $x \in$ wall
- $\mathbf{e}_i = -\mathbf{e}_i$
- $f_i(t,x) = f(t,x,\mathbf{e}_i) = f(t,x,-\mathbf{e}_i)$

This rule can be seen as a replacement of (6.2.4). It reflects the distribution functions on the wall node and thus they return back to the fluid with opposite momentum in the next time step.
On a boundary site, one can easily observe that mass and momentum are conserved. Also, on average, the velocity on a boundary site is close to zero as any particle entering the sites with a given velocity leaves with the opposite velocity. It is important to clearly indicate how, and actually when, the velocity at the boundary is measured. In principle, without any other indication, we measure the velocity at the boundary after the application of the boundary condition (and the collision rule if there is any).
Unfortunately in this case, the simplest is not the best. One can demonstrate that the use of the fullway bounce-back usually generates a finite slip velocity and may lead to first order numerical accuracy in space [41].
In our case we use the simple bounce back for the sedimentation where the wall is located half-way between the last fluid cell and the first wall node.
The simple bounce back can be done in different ways. The following scheme shows the difference between the half-way and the fullway bounce back.

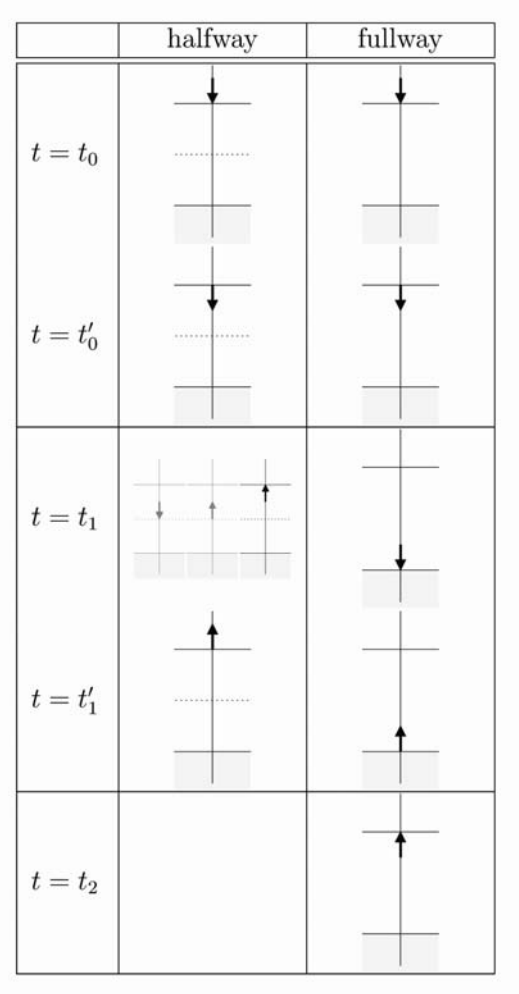

Figure 6.6.1 – Simple bounce back boundary conditions, [41].

For the flow field we use the modified bounce back scheme, which is of the second order accuracy. The distance between the last fluid node and the first solid wallis in a range from 0 to 1 (considering $\Delta x = 1$) an interpolation scheme on subgrid identifies the distance, as shows in Figure (6.6.2).

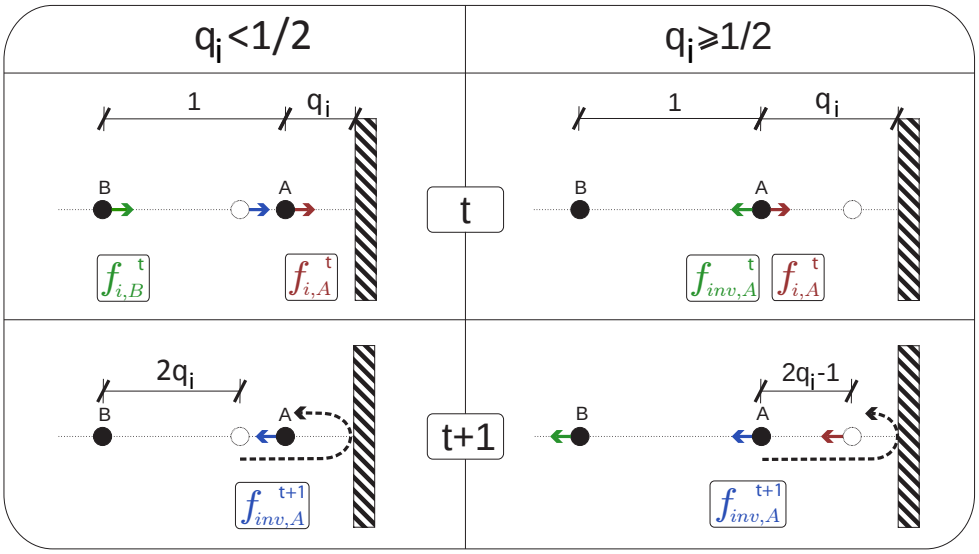

Figure 6.6.2 – Interpolation scheme based on subgrid distances for bounce back with second order accuracy, [6].

Here we identify two cases:

(i) the wall has a distance less than 0.5 $\mathbf{e}_i\Delta t$ from the node:

$$0.0 < q_i < 0,5 : \; f^{t+1}_{inv,A} = (1-2q_i)\; f^{t}_{i,B} + 2q_i\; f^{t}_{i,A} - 2\rho w_i\; \frac{\mathbf{e}_i\mathbf{u}_w}{c_s^2} \tag{6.6.3}$$

(ii) the wall has a distance between 0.5 and 1.0 $\mathbf{e}_i\Delta t$ from the node:

$$0,5 \leq q_i \leq 1,0 : \; f^{t+1}_{inv,A} = \frac{2q_i - 1}{2q_i}\; f^{t}_{inv,A} + \frac{1}{2q_i}\; f^{t}_{i,A} - \rho w_i\; \frac{\mathbf{e}_i\mathbf{u}_w}{q_i\; c_s^2} \tag{6.6.4}$$

The distributions at time $t/t+1$ are post/pre-collision values, $q\mathbf{e}_i\Delta t$ is the distance to the wall, $\mathbf{u}_w$ the velocity at the wall and ρ is constant because we are considering an incompressible flow. Therefore we obtain second order accurate results in space even for curved geometries [31]. For a detailed discussion of LBE boundary conditions we refer to [33]. In contrast to the simple bounce-back scheme, the use of this interpolation based no-slip boundary conditions result in a notable mass loss across the no-slip lines. To circumvent this problem the mass difference is transferred to the rest particle distribution. This results in a no slip scheme which is conservative in mass (and thus pressure) while introducing a higher-order disturbance of the stress tensor, however, this does not change the results significantly.
The boundary type for imposing motion is the velocity boundary conditions of Dirichlet type. The flow could be driven also by a body force. The outflow is defined via pressure boundary conditions, set by computing the distribution function in lattice Boltzmann for a density $\rho = p/{c_s}^2$.

7 Validation of the "VirtualSnow" model

This chapter will present the results of the numerical experiments performed to validate the LB model discussed in the previous chapter (6), in order to reproduce turbulent flow coupled to snow transport. If a new numerical model or a new extensions are introduced, even into a well known context or if an implementation has been changed it is in any case inevitable to validate model and tool. We shall therefore compare numerical results with real situations, either from numerical or an experimental point of view. In the course of this thesis an extensive validation process has been performed and evaluated. The method to validate the accuracy of the "VirtualSnow" model consists in a first phase of the comparison of numerical simulation results with well known properties of the system represented by that model and later the comparison the with real experiments. In particular, the parameters that control the fluid behaviour and transport mechanisms are optimized during the first phase of the validation process, whereas in the phase of the comparison between numerical and experimental results we investigate the accuracy of the grid refinement, the optimization of computational time and estimated the scale parameters between virtual situation and real situation. Therefore, after the set-up to define in the numerical model the similarity with the experimental situation, the same parameters that model fluid behaviour and snow transport are utilized for all building shapes tested.
In this chapter we present some examples of the test cases, which were carefully examined during the implementation and validation of the code. All simulations have been run with the 2D (D2Q9) model "VirtualSnow".
The chapter is mainly divided in two parts: in the first part, different steps necessary to set the flow field and mechanisms of snow transport are presented, and then the comparison between numerical and experimental results is shown.
The experimental results, used here, developed out in the "Jules Verne" Climatic Wind Tunnel of Nantes, France, under the commission of the European communities in 1997, [22]. A detailed explanation of the experimental tests is in chapter (4) .

7.1 Model assumptions

7.1.1 Initialization of the system: logarithmic wind profile

In laboratory wind tunnel experiments, the input flow is forced by a jet. The idea is the same here, as the fluid entry velocity is set by the user on the left hand column of the computational domain.

The "VirtualSnow" model sets the velocity, on the left hand side of the tunnel, via extended bounce back rule. The flow gets a momentum from the inflow wall, which is an additional term to the bounce back rule.
The density on the outflow boundary is set computing the equilibrium distribution function with the boundary density and the velocity from the node.
A specified wind velocity profile is implemented by settling the inlet fields with the logarithmic wind profile mentioned in section (3.1.2), and recalled here

$$u(z) = \frac{u_*}{k} \cdot \ln \cdot \frac{z}{z_0} \tag{7.1.1}$$

To create a fluctuating velocity we set a logarithmic velocity profile with a column of cylinders in the left side of the tunnel. The cylinders influences the turbulence intensity. An extensive investigation of the cylinders configuration is discussed in section (7.4.1). To achieve the similarity of the turbulence intensity profile with the real experiments, this section aims to describe the wind inflow.
Figure (7.1.1) shows a simulation with the "VirtualSnow" model the displays the effect of the imposed logarithmic wind velocity profile with the maximum equal to $u_0 = 4m/s$ on a tunnel of 16 x 4 m represented by a lattice of 128 x 512, the Reynolds number is $Re = 200000$. The field takes the influence of the obstacles within the tunnel, in this case a pitched roof building of 2 x 0.70 m.

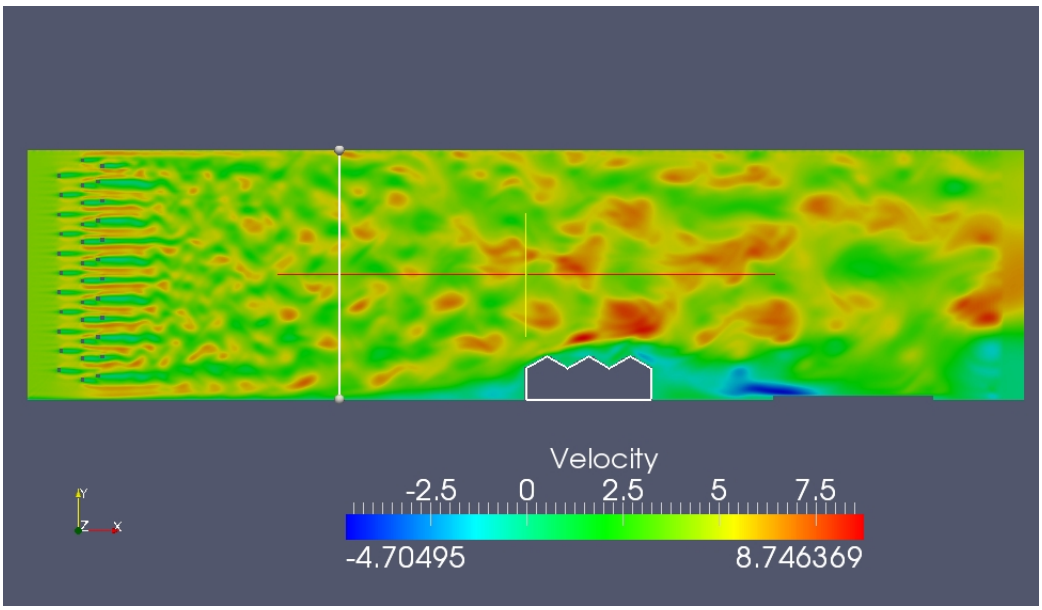

Figure 7.1.1 – Virtual wind tunnel computed with the "VirtualSnow" model, simulation displays the velocity x.

The graph (7.1.2) displays the average velocity profile in the white line of the previous image, along x-axis the height of the virtual tunnel and along y-axis the length.

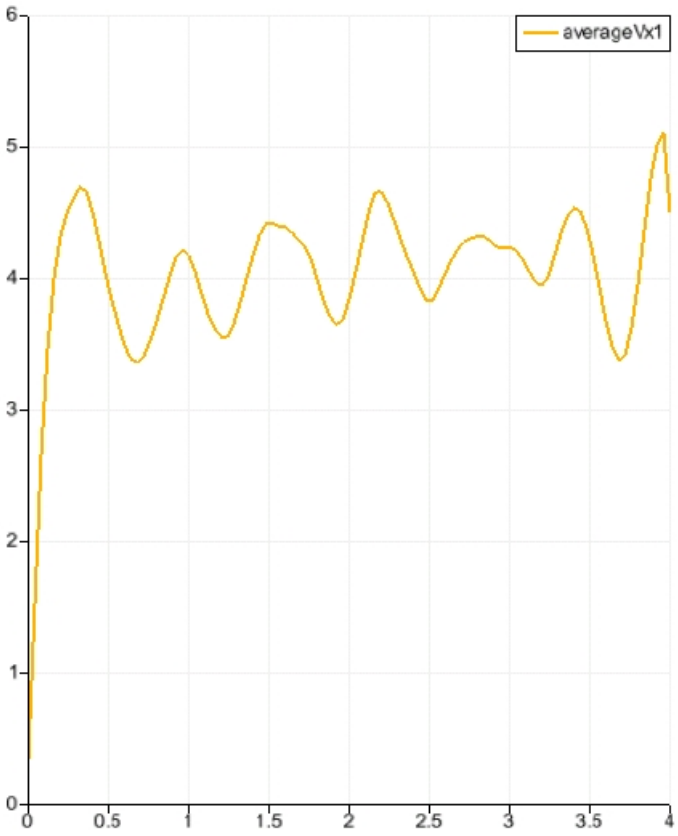

Figure 7.1.2 – Virtual wind tunnel computed with the "VirtualSnow" model, graph displays the average velocity x.

This section evidences the wind velocity profile used for all numerical experiments, in the next test cases the value of velocity initialization will be specified case for case.

7.1.2 Grid generation

Grid generation is the process of determining the coordinate transformation that maps the fluid, by transforming the non-uniform non-orthogonal physical space into the uniform orthogonal computational space. It is often considered as the most important and most time consuming part of CFD simulation. The quality of the grid chosen plays a

direct role with respect to the quality of the analysis, regardless of the flow solver used. The numerical solution of partial differential equations requires some discretization of the field into a collection of cells (considering lattice Boltzmann method).
In the "VirtualSnow" model, the discrete space Δx and time steps Δt are constants that can vary from one simulation to another but are fixed within a simulation. The grid spacing, of the cases presented in this chapter, is the same in all space directions, and it does not vary from one position of the discrete space to another.
The same can be said for the time step Δt, which does not change during the time evolution of the system.
The use of inhomogeneous grids simulates better the problem, pointers to other techniques can be found in [69]. Some parts of the simulated domain require a higher grid resolution than others in order to reach the required level of accuracy. The grid resolution needs for example to be increased close to an obstacle with complicated shape to ensure that the discretized version of the obstacle resembles the original one sufficiently well. In other cases, the resolution needs to be increased because the fluid flow exhibits small-scale patterns, such as the small vortexes generated close to the snow impact surface in the numerical experiment.
In order to overcome the limitation of a fixed grid spacing in the"VirtualSnow" model, a so called multi block technique was used, see the figure (7.1.3), the idea is to partition the domain of interest into rectangular subdomains, for each of which a different grid is used with local parameters Δx and Δt.

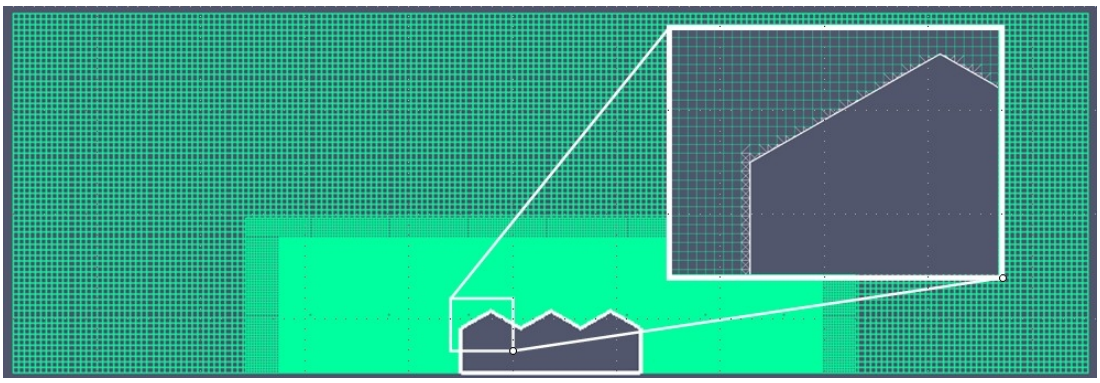

Figure 7.1.3 – Grid generation.

This extension of the model still has two difficulties that have to be investigated for diffusion. First, the data on the interface between two grids needs to be interpolated, and second, the data needs to be rescaled to account for the changing value of Δx and Δt. As a matter of fact, variables are not dimensionless with respect to a macroscopic system of units and thus depend on the particular value of the discretization parameters. In figure (7.1.4) the grid type considered for the next numerical simulations, the domain size will be specified case for case.

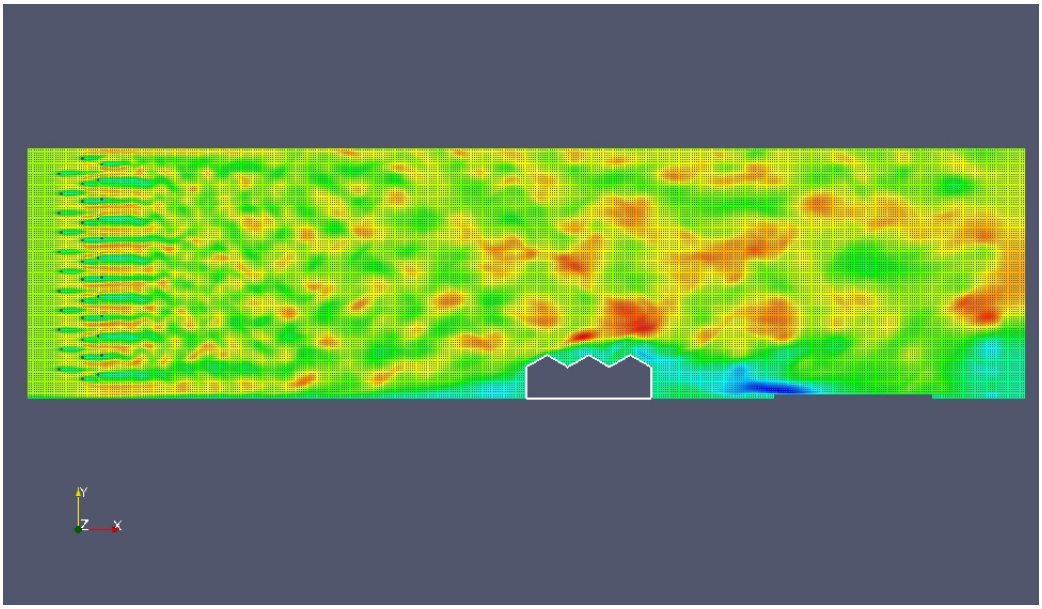

Figure 7.1.4 – Virtual wind tunnel computed with the "VirtualSnow" model, grid space discretization.

7.2 Validation of snow transport mechanisms

This section describes the process step by step in order to validate the snow transport mechanisms, the "VirtualSnow" model simulates dry snow. In the beginning we consider some oversimplified cases in terms of definition of flow, geometry and grid discretization. In this phase the mechanisms of erosion and deposition are not coupled. In the following are shown two test cases: the first validates the deposition process and the second validates the erosion process.

7.2.1 Deposition test case

This test case was performed to check the deposition process and the conservation of mass. In the fluid is defined a box with free boundary, as showed in red rectangular domain in figure (7.2.1), the domain is defined with a quadtree grid of 640000 nodes. In the first step the concentration flow is equal 0.1 for all box domain and equal 0 for the rest of the tunnel, advection-diffusion processes are activated. During the simulation time the snow is falling down due to gravity. The concentration flow is diffusing in the box domain and through the free boundary in the flow tunnel, as one can see from the images in the end of simulation the snow is completely deposited on the ground.

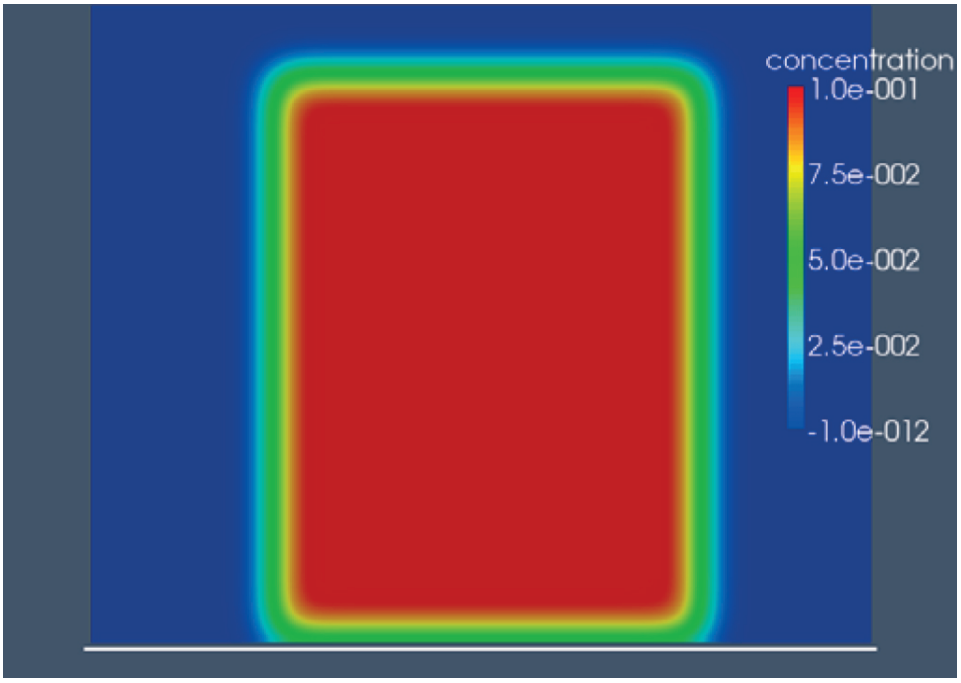

Figure 7.2.1 – Deposition test case, step 500.

The following figures show in different steps how the snow is depositing. The white line represents the sediment level over that, in the last simulation step, the snow is completely deposited on the ground. In the last step of simulation the total mass loss is $2,3\%$.

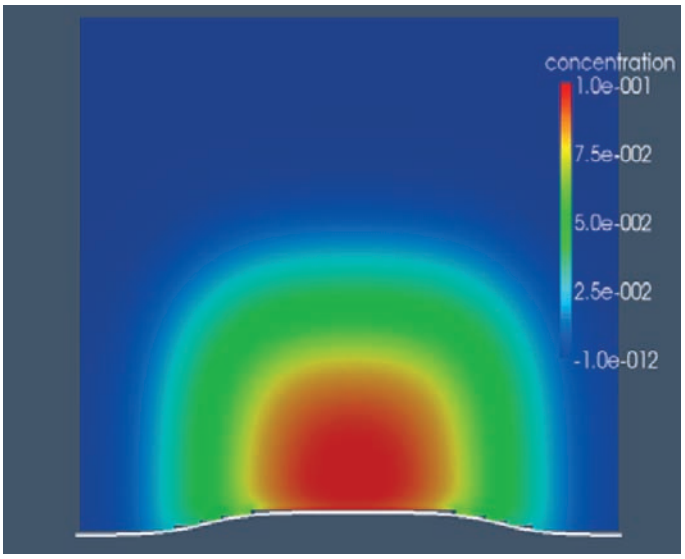

Figure 7.2.2 – Deposition test case, step 10000.

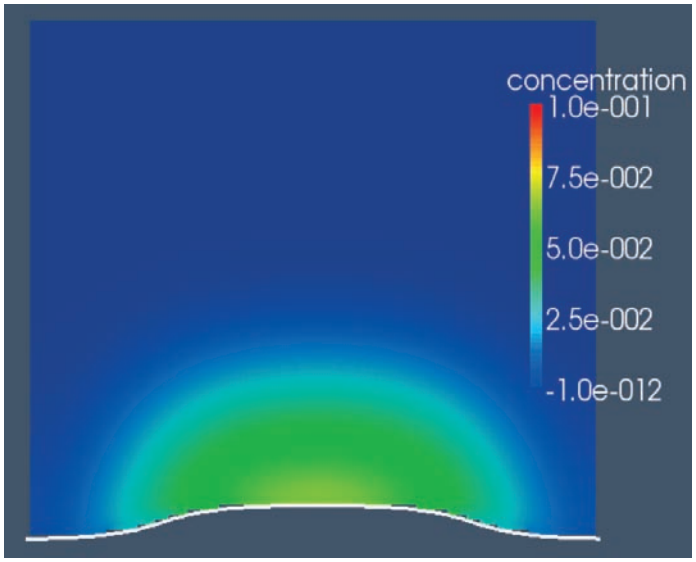

Figure 7.2.3 – Deposition test case, step 15000.

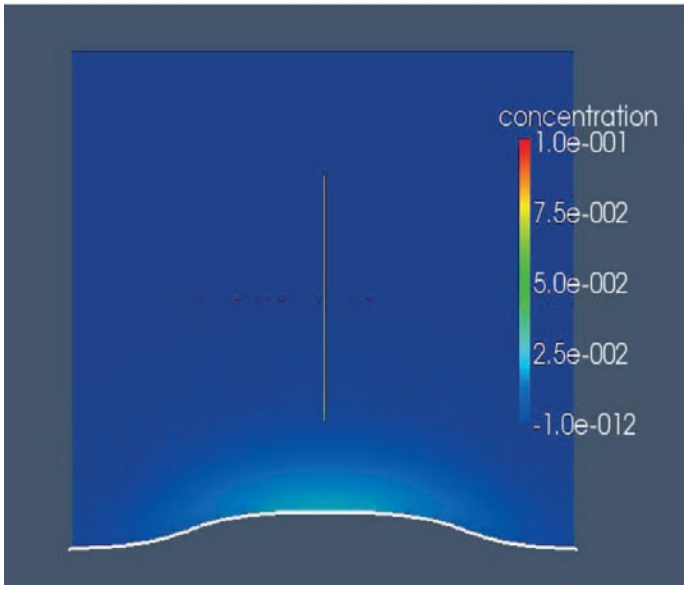

Figure 7.2.4 – Deposition test case, step 25000.

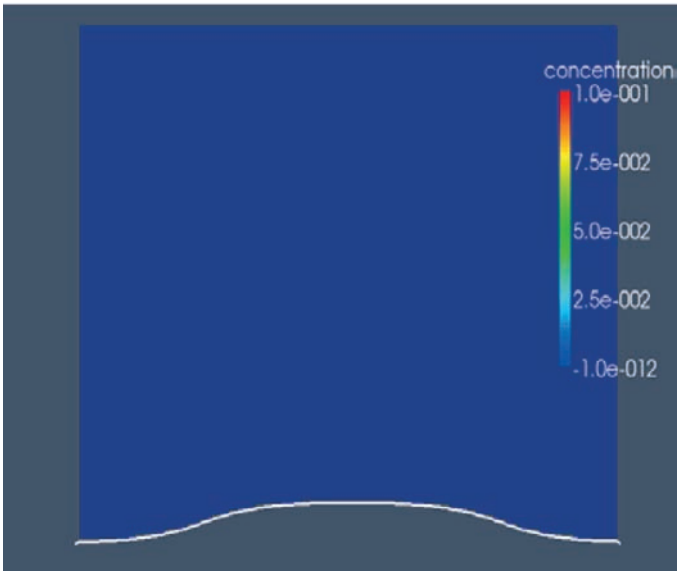

Figure 7.2.5 – Deposition test case, step 50000.

7.2.2 Erosion test case

Next test case shows how erosion process works individually. In this case we consider a layer of snow deposited on the square building, white line represents the sediment level over that the snow is completely deposited, see the first step of simulation (7.2.6). The wind inflow comes from the left side of the virtual wind tunnel and the snow inflow is set to be zero. During the simulation time the wind inflow erodes the snow deposited in agreement with the wind direction with an aerodynamic shape, in the last step is evident the erosion process of the snow layer and the diffusion of the snow in the flow. Figures (7.2.6), (7.2.7) show in different simulation steps of the erosion process.

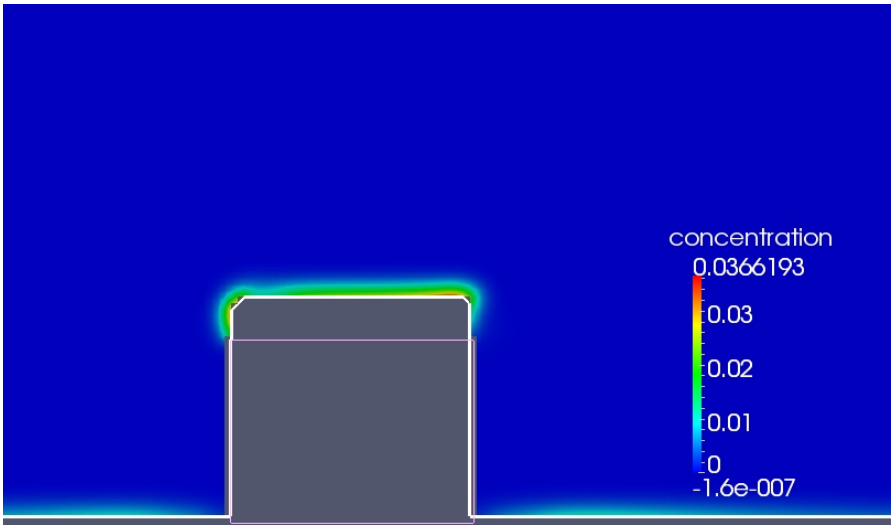

Figure 7.2.6 – Erosion test case, step 500.

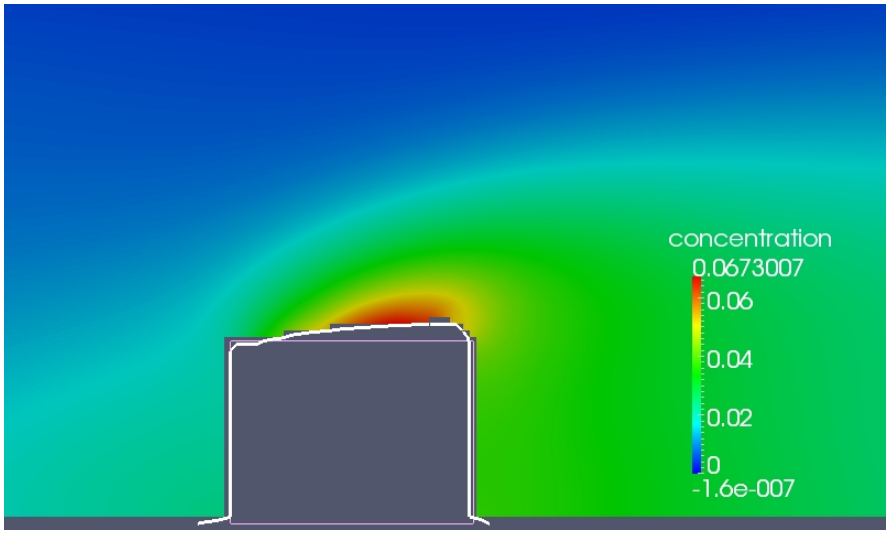

Figure 7.2.7 – Erosion test case, step 200000.

7.2.3 Deposition-erosion coupled mechanisms

The following images show the test case where all processes of snow transport are activated. The model calculates the turbulent flow with Large Eddy Simulation, the advection-diffusion with lattice Boltzmann approach, gravity, mechanisms of snow transport and others boundary conditions. Therefore, the developed code is able to simulate the coupled problem.
This test case considers the wind inflow introduced from the left side of the wind tunnel,

the snow from the top and left side and in the center of the tunnel there are two buildings with a pitched roof. The images present the flow concentration in a zoom view around the building in various steps during the simulation time.
The first imagine shows the initial state and the shape of buildings considered. In this test the parameters are set as follows: the Reynolds number is set $R_e = 100000$ (considering L_0 = height of building), the $C_{smago} = 0.1$ and $\nu = 0.0000152 m^2/s$

Figure 7.2.8 – Validation process of the "VirtualSnow" model, study case, step 0.

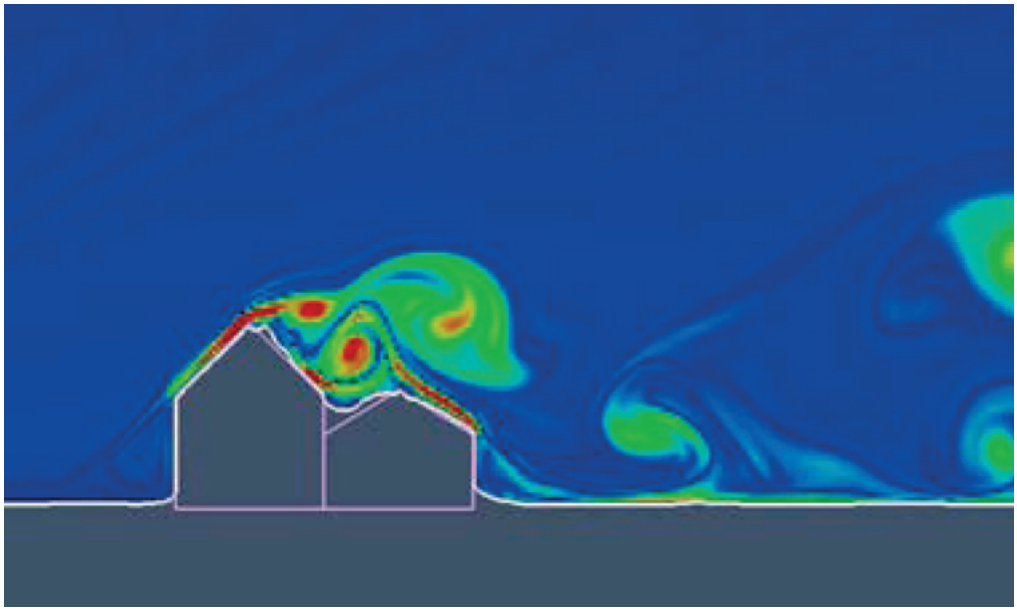

Figure 7.2.9 – Validation process of the "VirtualSnow" model, study case, step 10000.

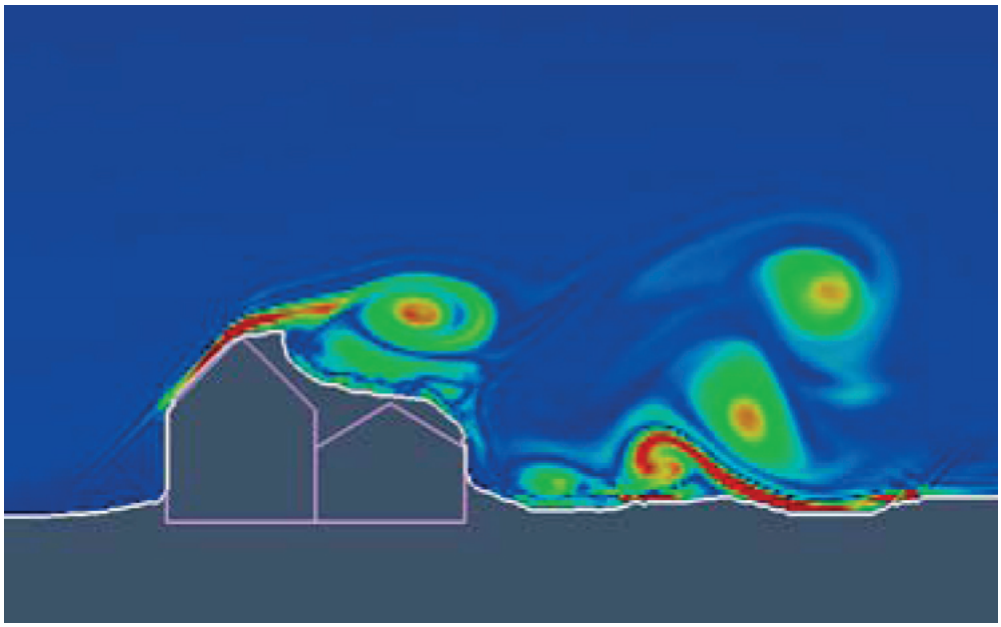

Figure 7.2.10 – Validation process of the "VirtualSnow" model, study case, step 2000000.

In the next paragraph results of simulations run with the "VirtualSnow" model will be compared with experimental results from "Jules Verne" Climatic Wind Tunnel presented

in chapter (4). A wide range of common roof types were examined, to optimize and validate the numerical model.

7.3 Numerical and experimental comparison results

The aim of this research work is develop a numerical model to determine the effect of wind on snow coverage on roofs (unbalanced roof loads) for a single snowfall. To validate and optimize several simulation parameters of the "VirtualSnow" model an extensive comparison campaign of numerical and experimental results has been performed.
The comparison study is subdivided in two sub-tasks. Earlier the numerical wind tunnel is calibrate to grant similar experimental conditions. The data obtained from typical and simple tests were used to set-up influence relationships between experimental and numerical parameters. After that, tests to compare numerical and experimental results of ordinary building configurations, which might be of primary importance in standard building codes, are performed.

7.4 Experimental-numerical set-up

7.4.1 Similarity of the mean and turbulent flow

In the real experiments the turbulence rate was adjusted over the snow mantle in the test section to be similar to the turbulence over an open field terrain (category II) of the European standard building codes, see Figure (7.4.1).

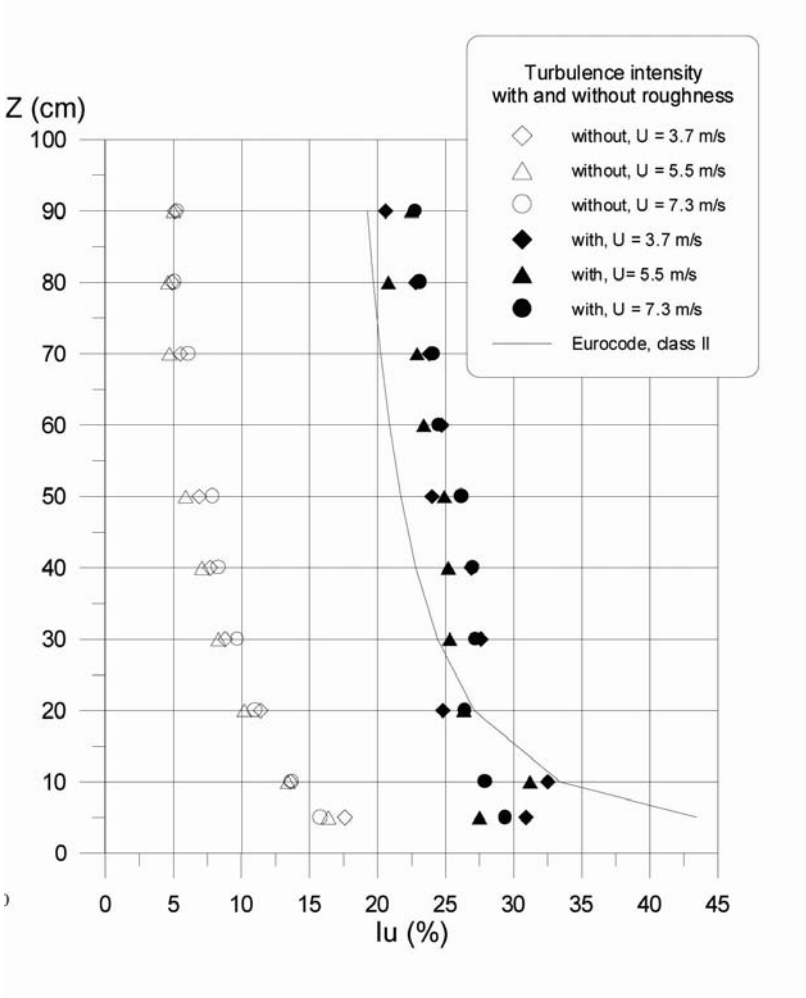

Figure 7.4.1 – Turbulence rate initial state (without roughness) and with roughnesses, [22]

To reproduce, in the numerical model, the vertical wind speed gradient and turbulence rate of the experiments has been conducted an investigation of the optimal location of a set cylinders in the first part of the test section, near the left inflow boundary. The wind speed and turbulence intensity calculations were made by using the following formula

$$I = \frac{u^{'}}{U} \tag{7.4.1}$$

where

- $u^{'}$ is the root-mean-square of the turbulent velocity fluctuations
- U is the mean velocity

$$I = \frac{\sqrt{\frac{1}{2}(rmsV_1)^2 + (rmsV_2)^2}}{\sqrt{((aveV_1)^2 + (aveV_2)^2)}} \tag{7.4.2}$$

where

- $\frac{1}{2}$ is 2D factor
- $rmsV_1$ is $\sqrt{\frac{\sum((u-U)^2)}{n}}$
- u is the velocity
- U is the average velocity
- n is number of time steps
- $aveV_1$ average of the velocity x mean $\frac{\sum(u_x)}{n}$

Numerous numerical experiments have been performed to achieve the flow similarity with the real experiments, in this paragraph we discuss only some of these. The configuration of cylinders, in terms of position and size, strongly influence the turbulence intensity profile. Several tests with different cylinders configuration, for various Reynolds numbers and building location has been investigate.
The first case is designed without cylinders at the left inflow boundary. In this case is imposed the wind inflow logarithmic profile at left boundary the maximum equal to $u_0 = 4m/s$ like in the real experiments, the tunnel of 16 x 4 m discretized with 512 x 128 lattice cells, and a pitched roof at 8 m from the inlet a building of 2 x 0.70 m, the Reynolds number chosen in the case is 200000. We performed several test case with the same configuration of cylinders but different Reynolds number and deducted an average velocity increase. Figure (7.4.2) displays the velocity field after 3 seconds of simulation and Figure (7.4.3) the turbulence intensity.

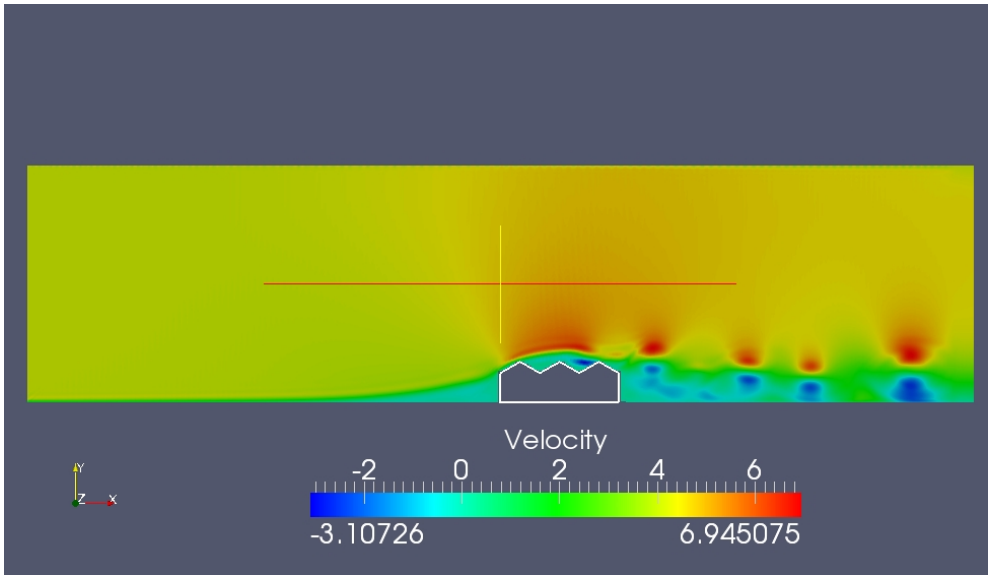

Figure 7.4.2 – Validation process of the "VirtualSnow" model, wind velocity field without cylinders.

In Figure (7.4.3) the turbulence intensity calculated with formula (7.4.2)

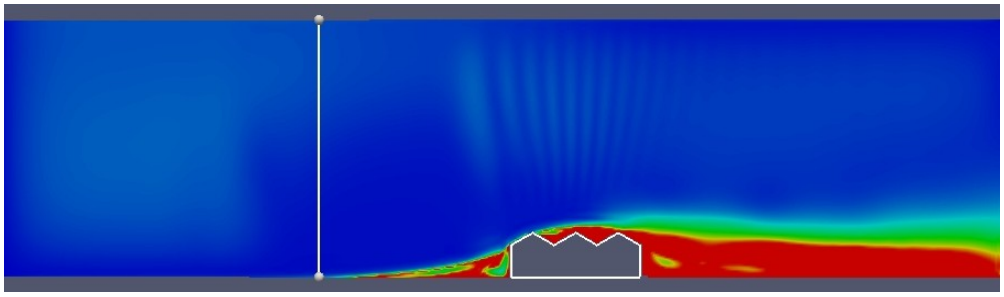

Figure 7.4.3 – Validation process of the "VirtualSnow" model, turbulence intensity without cylinders.

Graph (7.4.4) refers the data in reference to the white line in the previous image, with the height of the tunnel along x-axis its length along y-axis.

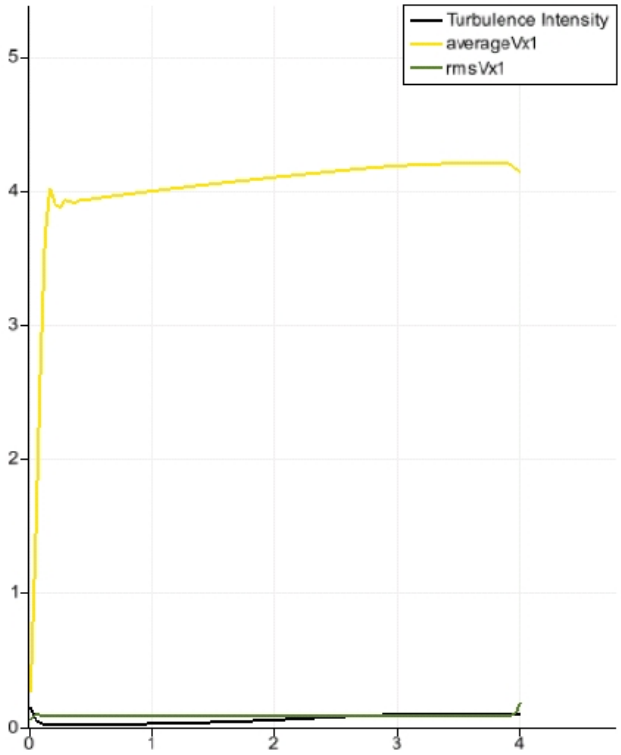

Figure 7.4.4 – Validation process of the "VirtualSnow" model. Profiles of turbulence intensity, average velocity and root mean square of velocity fluctuation without cylinders.

The result evidences that the absence of cylinders generates a smoother flow field, therefore we implemented a case with a vertical line of cylinders at the left beginning of the tunnel to disturb the flow, the dimensions of the tunnel, the model location and the Reynolds number are the same as the preceding case.
The first (7.4.5) image visualizes the flow field and image (7.4.6) the turbulence intensity.

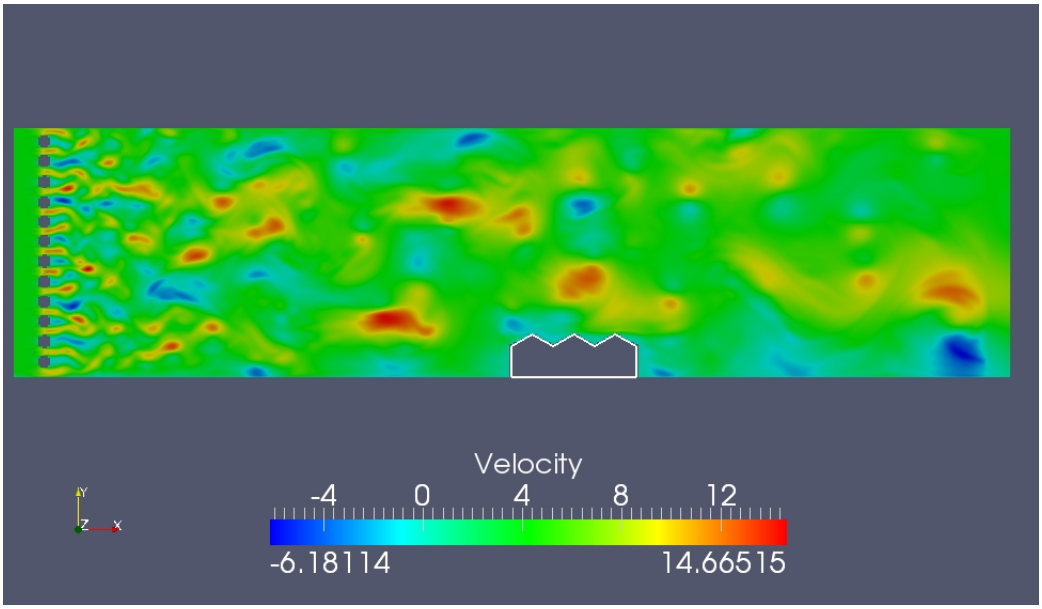

Figure 7.4.5 – Validation process of the "VirtualSnow" model, wind velocity field with one line of cylinders.

In Figure (7.4.6) the turbulence intensity calculated with formula (7.4.2)

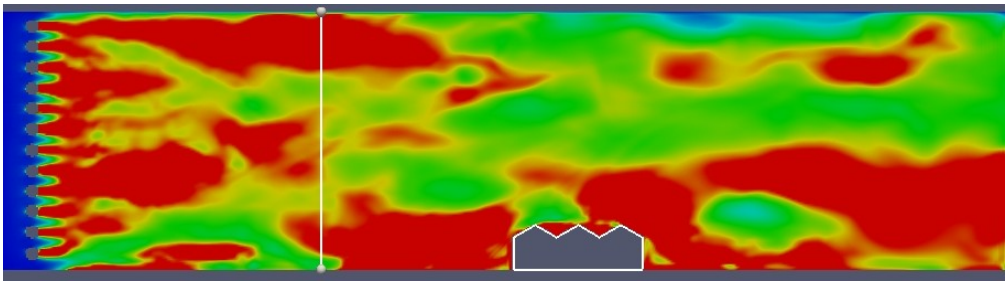

Figure 7.4.6 – Validation process of the "VirtualSnow" model, turbulence intensity with one line of cylinders.

The presence of cylinders near the inflow increases the formation of eddy. The profiles of average velocity and turbulence intensity in comparison the first study case are characterize of peaks, in this case is evident the influence of the single cylinder. In this case the values of average velocity and turbulence intensity increase in comparison the first case study. To reduce the influence in the flow of the single cylinder we decide to set a cylinder configuration with more cylinders randomized of smaller size as shown in figure (7.4.7) and (7.4.8)

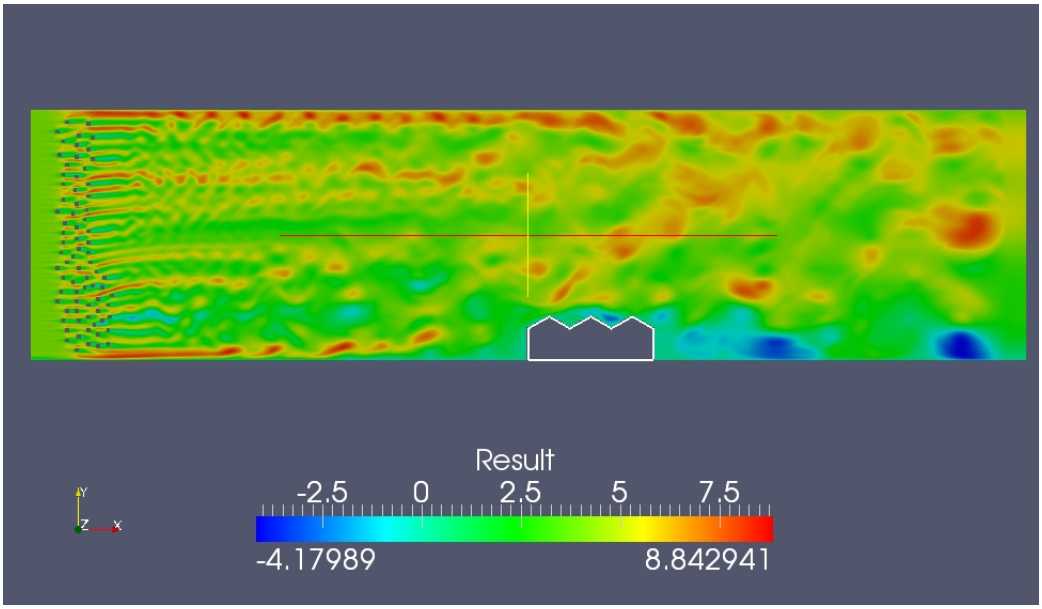

Figure 7.4.7 – Validation process of the "VirtualSnow" model, wind velocity field with randomized cylinders.

In figure (7.4.8) the turbulence intensity calculated with formula (7.4.2)

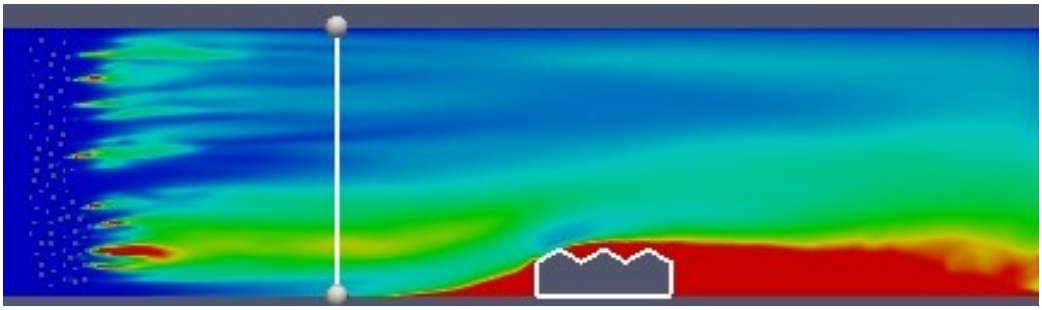

Figure 7.4.8 – Validation process of the "VirtualSnow" model, turbulence intensity with randomized cylinders.

Graph (7.4.9) selects the data in reference to the white line in the previous image, along x-axis the height of the tunnel and along y-axis its length.

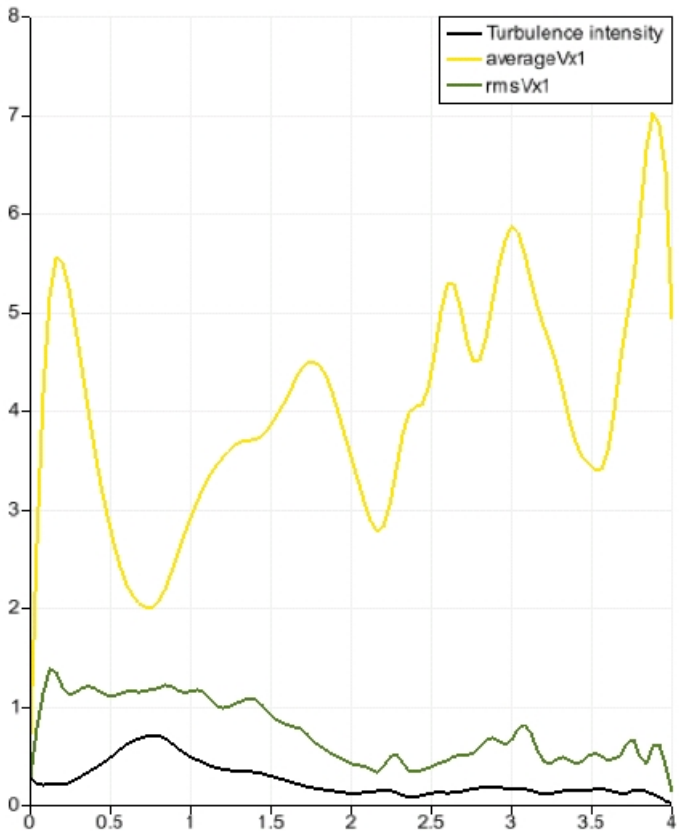

Figure 7.4.9 – Validation process of the "VirtualSnow" model, profiles of turbulence intensity and average velocity with randomized cylinders.

In these case the Reynolds number and the building location within the tunnel are the same but several cases are investigated during set up process, the results show that the average velocity increase quite regularly with the Reynolds number. The cylinders disturb strongly the intensity turbulence profile in the first part of the tunnel section but it is becoming smoother at 2/3 of the tunnel section, therefore the tunnel was extended horizontally and the building location was set at larger distance from the inflow in comparison of the real experiments. In addition a cylinders randomized distribution leads peaks in the intensity turbulence profile. For this reason, to compare the real experiments with the numerical model, the cylinders configuration was set in three vertical lines, the model was located at 8 m from the left boundary, and the Reynolds number set equal 184210, (7.4.3) is calculated as

$$Re = \frac{U * L}{\nu} = 184210 \tag{7.4.3}$$

where

- $U = 4m/s$ experiment fluid velocity
- $L = 0.7m$ building height
- $\nu = 0.0000152m^2/s$ viscosity

Figures (7.4.10) (7.4.11) and graph (7.4.12) show the configuration chosen to compare the numerical model to the experimental tunnel for all building shapes. The comparison with the turbulence intensity profile from the experiments (7.4.1) give a good level of approximation of the similarity condition of the flow.

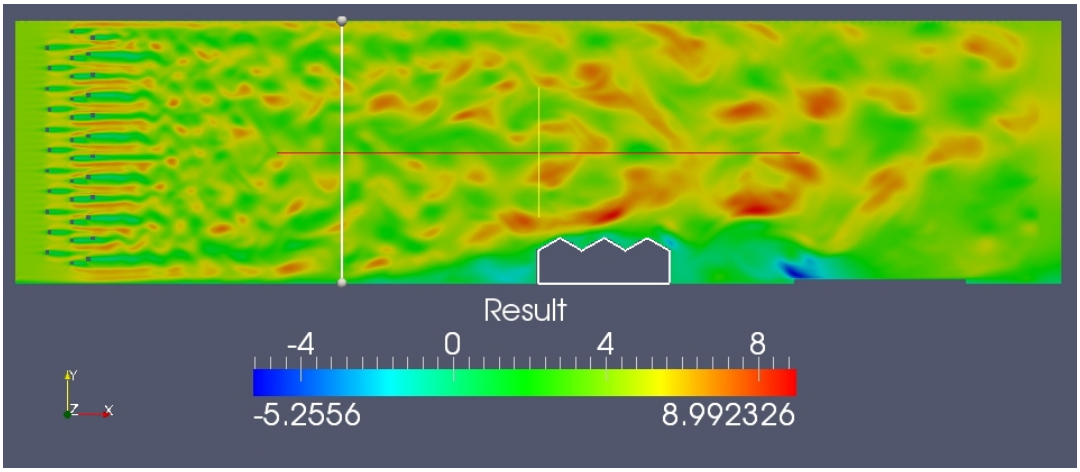

Figure 7.4.10 – Validation process of the "VirtualSnow" model, wind velocity field with three lines of cylinders.

In Figure (7.4.11) the turbulence intensity calculated with formula (7.4.2), and the graph (7.4.12) selects the data in reference to the white line in the previous image, along x-axis the height of the tunnel and along y-axis its length.

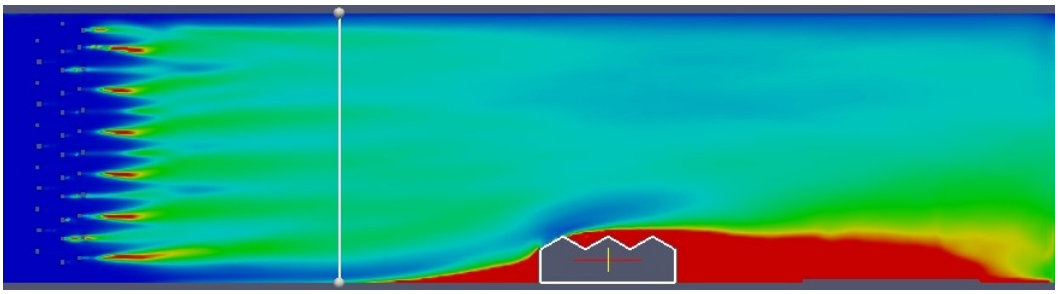

Figure 7.4.11 – Validation process of the "VirtualSnow" model, turbulence intensity with three lines of cylinders.

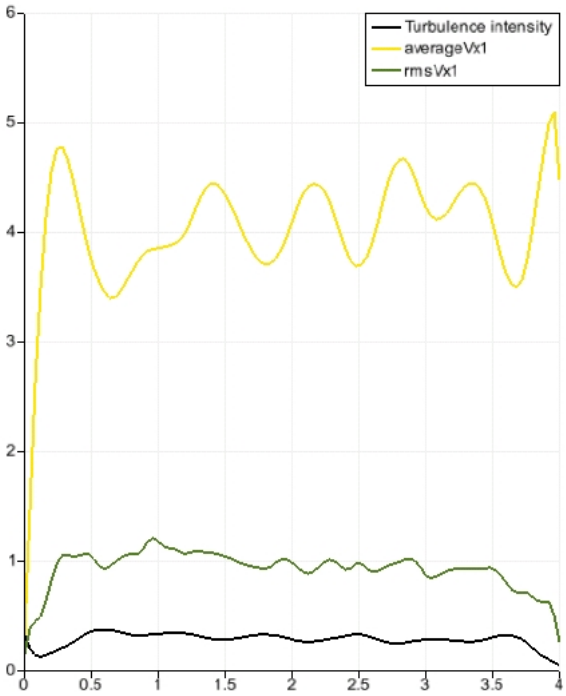

Figure 7.4.12 – Validation process of the "VirtualSnow" model, profiles of turbulence intensity and average velocity. and root mean square of velocity fluctuation with three lines of cylinders

In Table (7.4.1) are summarized the simulation parameters that have been used in the comparison between numerical and experimental tests. The parameters set in the previous section grant the similarity with the situation in the real wind tunnel. In the next paragraph we explain the procedure to set the snow similarity.

PAMAMETERS	value
inflow	logarithmic wind profile
outflow	density fluctuation =0
bottom walls	no-slip
top walls	velocity boundary $u_x = u_{inflow}$
u_o	4m/s
snowfall velocity	0
Re number	184000
C smagorinsky	0.1
viscosity	$0.0000152 m^2/s$
simulation time	3 seconds
number of nodes	65536
node distance	0.03 m

Table 7.4.1 – Simulation parameters.

7.4.2 Similarity of snow properties

In the real experiments, conducted in the "Jules Verne" Climatic Wind Tunnel, the snow storm event is simulated with snow guns that produce snow particles in flow field, the "VirtualSnow" model simulate a mix fluid of snow-air. Consequently to compare the two different models was found a compromise.
In the real wind tunnel the snow type can be adjusted from "wet" to "dry". For all experiments the wind tunnel was operated by keeping the humidity regulation systems off and at rather low ambient temperature (-10 °C). Snow density is about $360 kg/m^3$. The average liquid water content was 3.6% corresponds to an artificial "dry" snow. The wind tunnel accumulation rate of snow on the ground was, for a single snow event with wind velocity (4 m/s) of 1 hour: 15 cm/h. According to these values, in the numerical model, the inflow concentration (ratio of snow and air density) was adjusted equal 0.5% for all tests.
To increase the numerical efficiency the model was turned to higher concentration then the real situation, therefore the simulation time is faster. To compute 3 seconds real time, 200000 steps in the virtual model are necessary, with a single CPU $[2GHz]$ about one day of simulation is required. Other possibilities to adjust parametrs as well as grid refinement studies should be investigated.
Before we present the comparison of the numerical and experimental tests, the following table summarizes the similarity properties of the models:

PAMAMETERS	Experimental value	Numerical value
Test duration	1h	3sec.
Section dimensions	27x8m	16 x 4
Wind velocity	4m/s	4m/s
Fluid concentration	$1.34kg/m^3$	0.5%
Terminal fall velocity	$0.5to1.2m/s$	$0.5m/s$
Model location	16 m (from the nozzle)	8 m (from inflow)
Re	$>$ 10000(for sharp.edged buildings)	184000
Turbulence intensity	$\cong$ 20%	$\cong$ 20%

Table 7.4.2 – Numerical and experimental simulation parameters.

7.4.3 Case studies

In order to validate the "VirtualSnow" model several shapes of building has been tested and the results compared with the experimental tests. The selection of the building shapes is in agreement with the stability problem due to unbalanced snow load on buildings. In this section four various roof shapes are presented: a two-level flat roof with three different step configurations (length or high of the step), and a symmetric multi-pitch roofs with a pitch angle of 30°, in particular is investigated the case of multilevel roof because the deposition and erosion process near the step of the building is difficult to catch. For a complete explanation of the experimental results we refer to section (4). The input parameters that control the flow filed, the erosion and deposition processes are set equal for all the shape of buildings, this is an important point of evaluation of success of the numerical model.
The following scheme (7.4.13) shows the cross section and the plan view of the model tested in the "Jules Verne" Climatic wind tunnel. A more detailed explanation of the geometry definition is in paragraph (4.5.2), equal dimensions are used for the numerical simulations

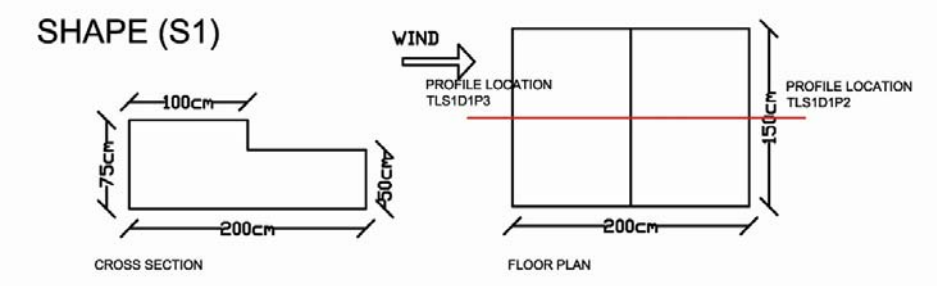

Figure 7.4.13 – Test case multi-levels roof (S1)

The test duration for the real experiments was set to one hour. Figure (7.4.14) shows the snow cover at the end of experiment.

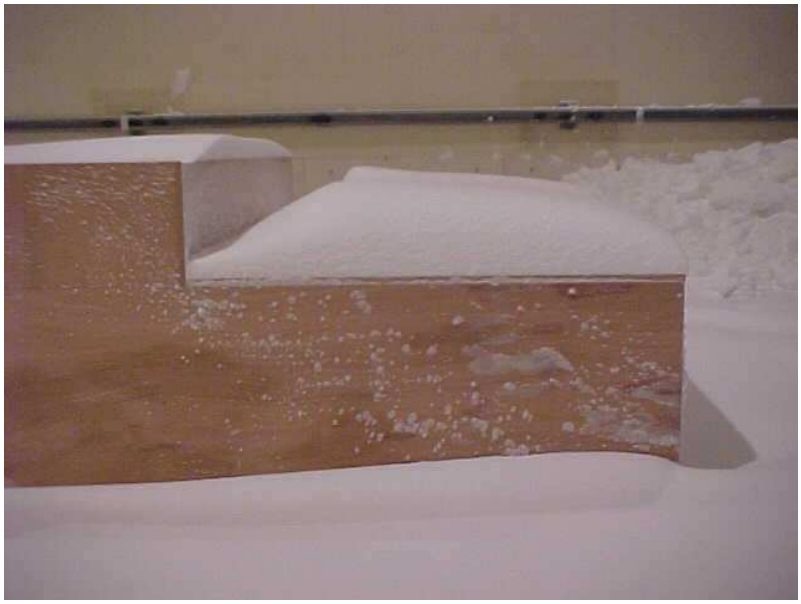

Figure 7.4.14 – Experimental result of test case multi-levels roof (S1) [57]

In following the multi-level roof (S1) shape is simulated with the "VirtualSnow" numerical model. In Table (7.4.3) are summarized some parameters of the simulation

PAMAMETERS	value
u_o	4m/s
snowfall velocity	$0.5m/s$
inflow concentration	0.5%
Re	184000
C smagorinsky	0.1
viscosity	0.0000152
simulation time	3 seconds
number of nodes	65536
node distance	0.03 m

Table 7.4.3 – Simulation parameters of test case multi-levels roof (S1)

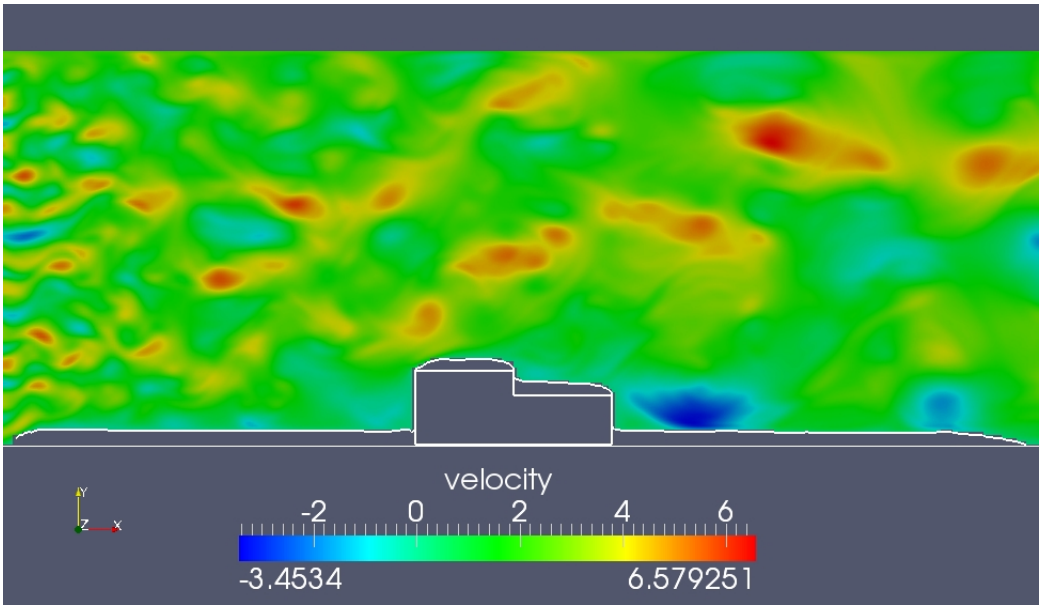

Figure 7.4.15 – Numerical simulation of test case multi-levels roof (S1).

Graph (7.4.16) shows the comparison of the experimental and numerical result, in the x-axis the length of the building and in y-axis the depth of snow. We observe that results are near to the real experiments except for the influence of the small eddies near the step of the building.

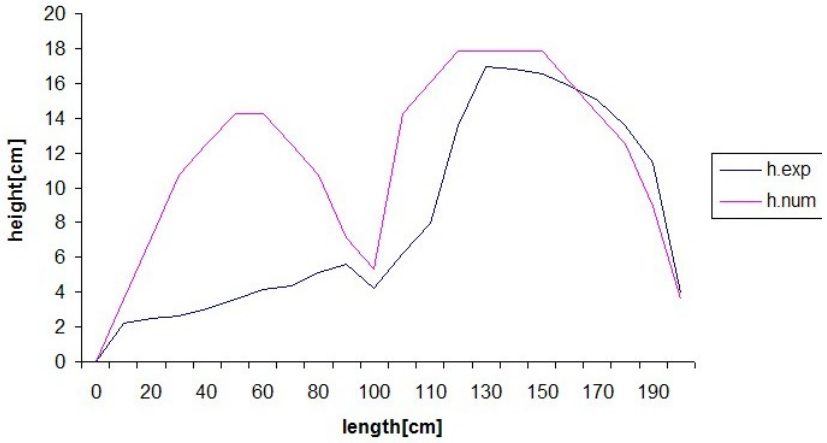

Figure 7.4.16 – Numerical simulation and real experimental results of test case multi-levels roof (S1).

The second case considered is a multi level roof with different position of the step. Figure (7.4.17) shows the cross section and the plan view of the model tested in the "Jules Verne" Climatic wind tunnel.

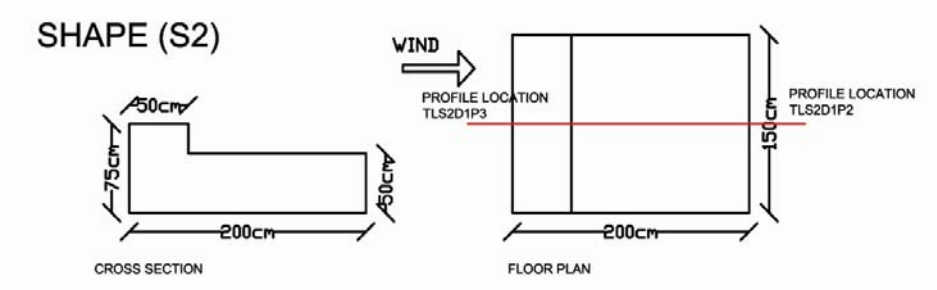

Figure 7.4.17 – Test case multi-levels roof (S2)

Figure (7.4.18) shows the snow cover tested in the Jules Verne Climatic wind tunnel after one hour of simulation

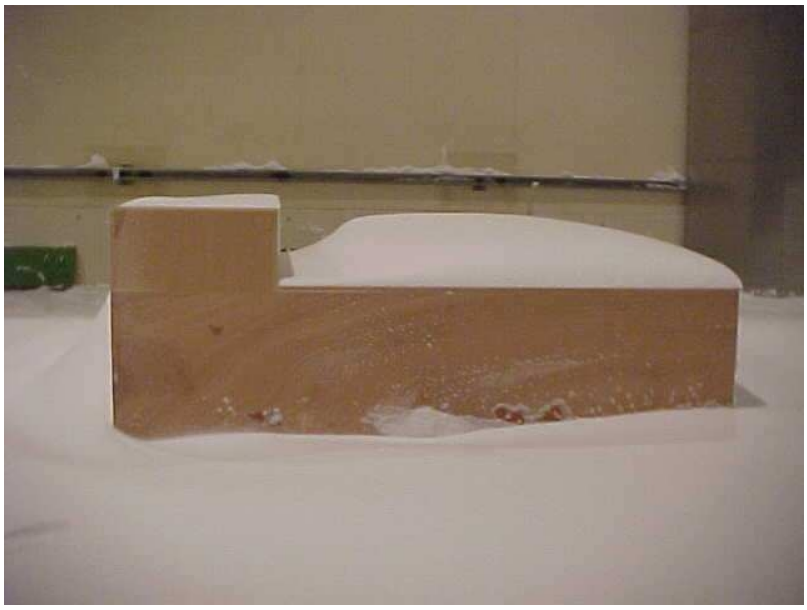

Figure 7.4.18 – Experimental simulation of test case multi-levels roof (S2) [57].

Following the simulation of the previous shape run with "VirtualSnow" numerical model the same parameters of simulation are considered for all shapes and are resumed in Table (7.4.4)

PAMAMETERS	value
u_o	4m/s
snowfall velocity	$0.5m/s$
inflow concentration	0.5%
Re	184000
C smagorinsky	0.1
viscosity	0.0000152
simulation time	3 seconds
number of nodes	65536
node distance	0.03 m

Table 7.4.4 – Simulation parameters of test case multi-levels roof (S2)

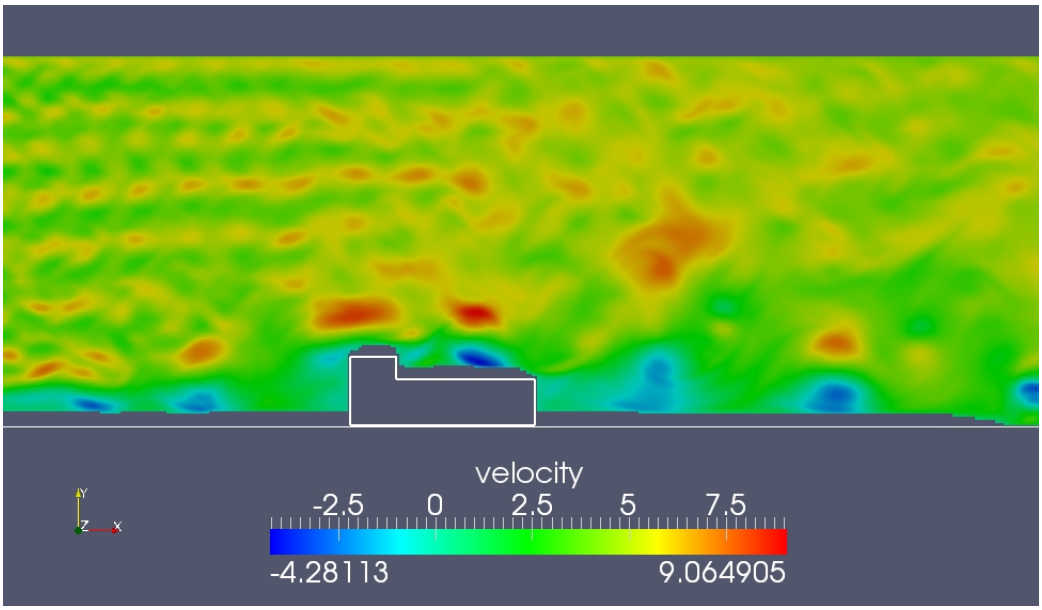

Figure 7.4.19 – Numerical simulation of test case multi-levels roof (S2)

Figure (7.4.20) shows the comparison of the experimental and numerical result, in the x-axis the length of the building and in y-axis the depth of snow.

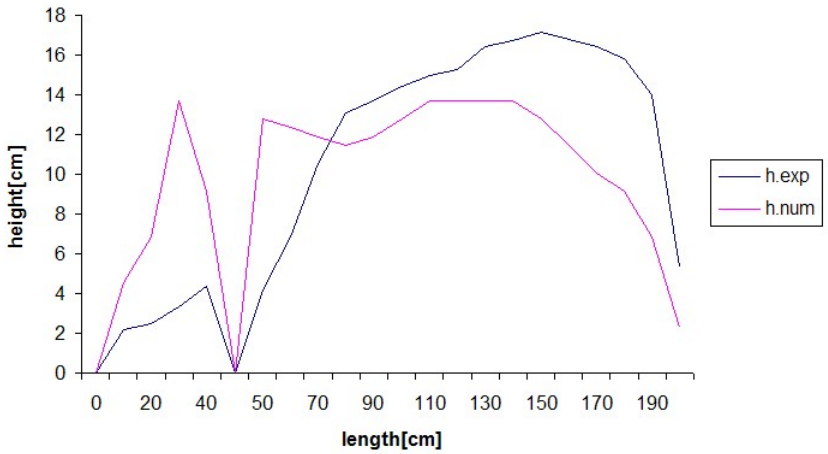

Figure 7.4.20 – Numerical simulation and real experimental results of test case multi-levels roof (S2).

In the third case considered is a multi levels roof with a central higher level and two step. The following scheme (7.4.21) shows the dimensions of the model tested in the Jules Verne Climatic wind tunnel.

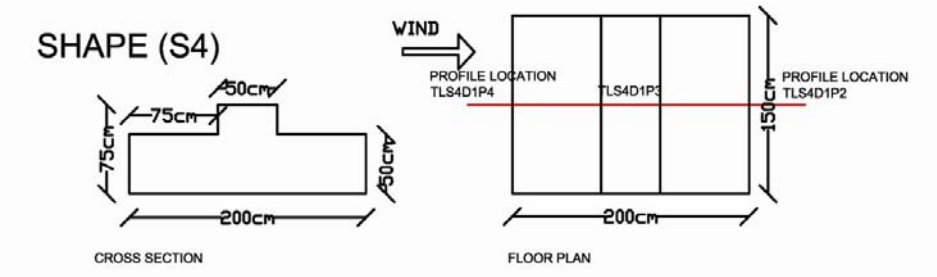

Figure 7.4.21 – Test case multi-levels roof (S4)

Figure (7.4.22) displays the snow cover in the experimental tunnel.

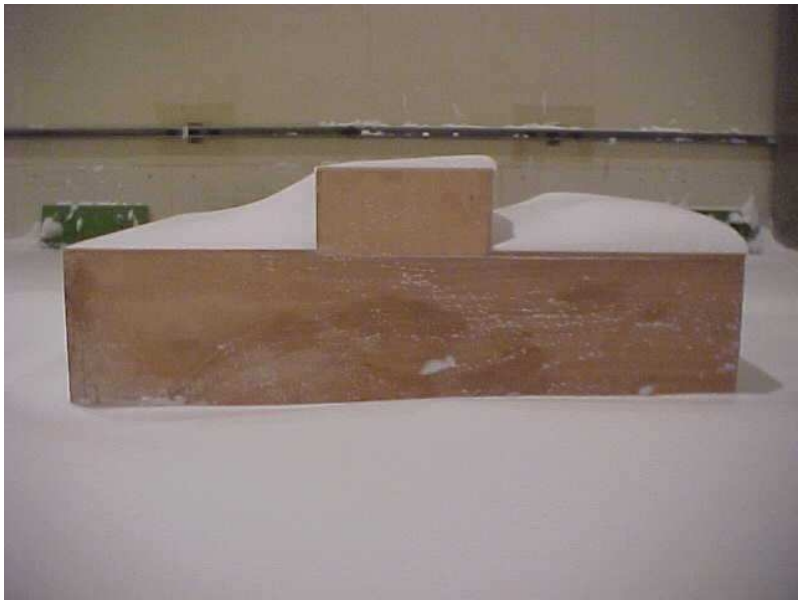

Figure 7.4.22 – Experimental simulation of test case multi-levels roof (S4) [57]

Following the same shape tested with the numerical model, as shown in Figure (7.4.23)

PAMAMETERS	value
u_o	4m/s
snowfall velocity	$0.5m/s$
inflow concentration	0.5%
Re	184000
C smagorinsky	0.1
viscosity	0.0000152
simulation time	3 seconds
number of nodes	65536
node distance	0.03 m

Table 7.4.5 – Simulation parameters of test case multi-levels roof (S4)

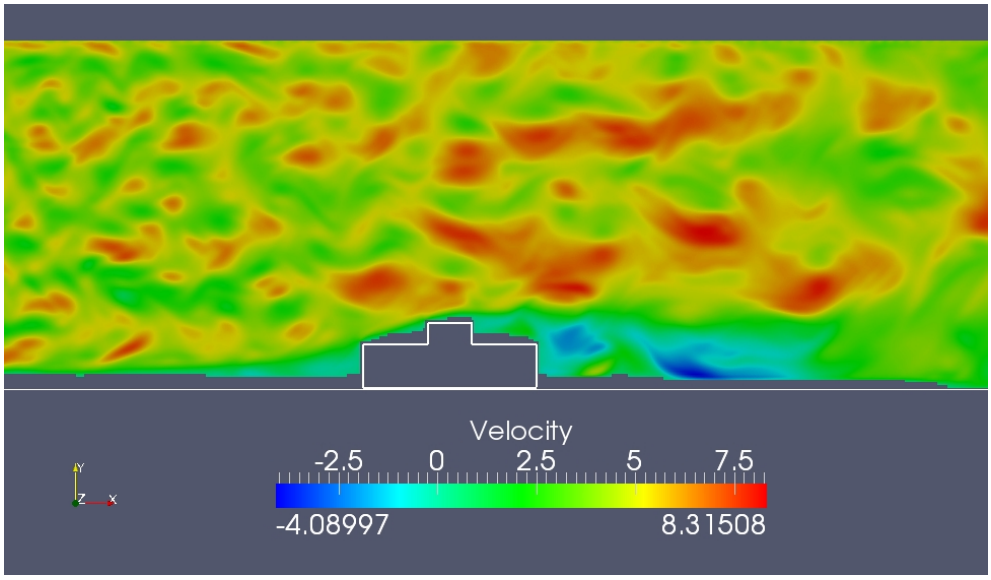

Figure 7.4.23 – Numerical simulation of test case multi-levels roof (S4)

Figure (7.4.24) shows the comparison of the experimental and numerical result, in the x-axis the length of the building and in y-axis the depth of snow.

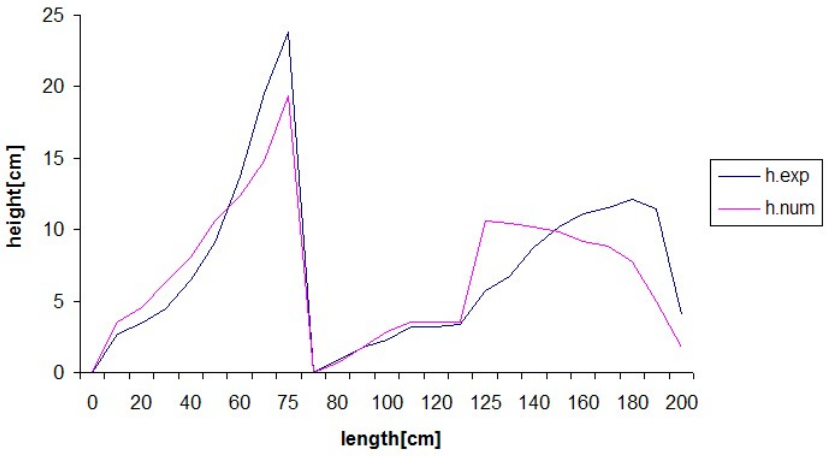

Figure 7.4.24 – Numerical simulation and real experimental results of test case multi-level roof (S4).

In the fourth case we considered a symmetric multi level roof. Figure (7.4.25) shows the cross section scheme of the model tested in the "Jules Verne" Climatic Wind Tunnel.

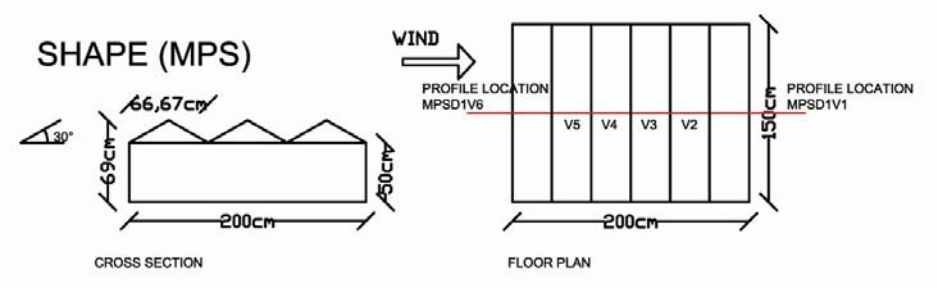

Figure 7.4.25 – Test case multi-pitched roof (MPS).

Figure (7.4.26) shows the snow cover from the real experiments.

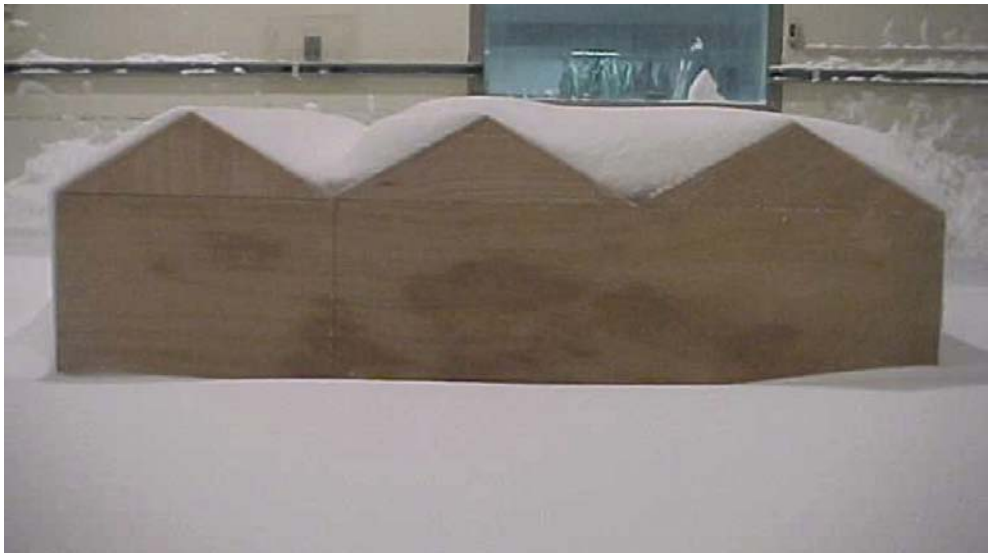

Figure 7.4.26 – Experimental simulation of test case multi-pitched roof (MPS) [57]

PAMAMETERS	value
u_o	4m/s
snowfall velocity	$0.5m/s$
inflow concentration	0.5%
Re	184000
C smagorinsky	0.1
viscosity	$0.0000152m^2/s$
simulation time	3 seconds
number of nodes	65536
node distance	0.03 m

Table 7.4.6 – Simulation parameters of test case multi-pitched roof (MPS)

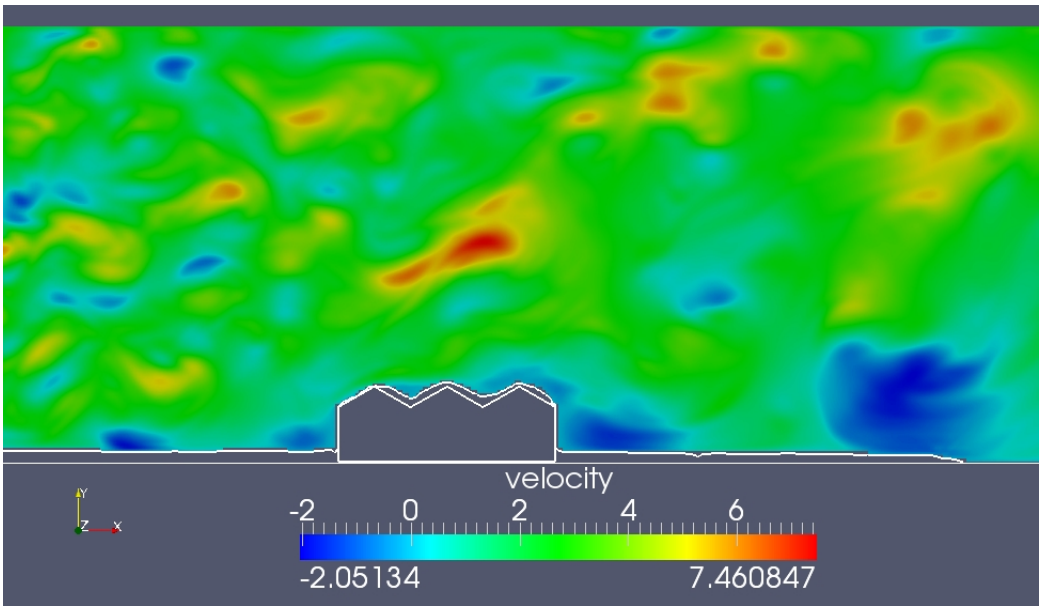

Figure 7.4.27 – Numerical simulation of test case multi-pitched roof (MPS).

Figure (7.4.28) shows the comparison of the experimental and numerical result, in the x-axis the length of the building and in y-axis the depth of snow.

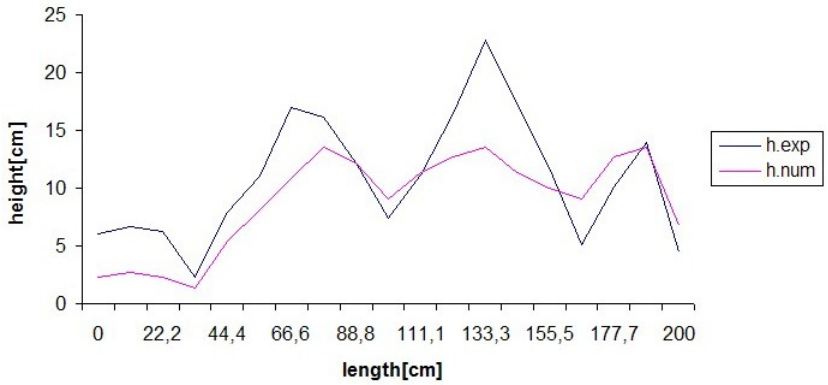

Figure 7.4.28 – Numerical simulation and real experimental results of test case multi-level roof (MPS).

7.4.4 Conclusion

The only and most convincing way to assess the validity of a numerical model is to compare its predictions with the real experiments. The "VirtualSnow" numerical model has been tested against a wide range of simulations and has shown to display some qualitative agreements to real experiments of very different building shapes.
In particular, it is observed that there is less snow on the upper part of the two-level flat roof than on the lower part situated either leeward or windward. Snow cover increase from the windward edge, where there is very little snow, to the leeward edge which is approximately the maximum snow depth. For two-level roofs values of maximum snow depth are close to the step height. For multi-pitch roofs, maximum snow depth occurs in the middle of the valley. Snow accumulation is greater in the leeward valley. Snow depth can be greater than the ridge height. In addition non-intuitive deposition-erosion patterns are observed and their time evolution where several regimes may be identified. In conclusion, a good qualitative agreement is observed between the numerical and real experiments.
The "VirtualSnow" model not only produces qualitatively similar deposition, but also provides, through simple and intuitive rules, a better understanding of the basic mechanisms that occur in snow transport. Creeping, saltation or suspension are no longer three phenomena requiring each a special treatment: they are all captured by the same erosion-deposition mechanisms. Our model thus offers unified view of the basic laws governing the formation of snow drift.

8 Concluding Remarks and outlook

The primary aim of this research work was to develop wind-snow risk mitigation strategies for the stability of buildings through load distribution profiles hazard assessment. In order to assess load distribution hazard on buildings with reasonable accuracy, a detailed computational fluid dynamics model was implemented and validated.
Redistribution of snow due to wind may produce substantial unbalanced snow accumulation on buildings. Inadequate analysis of loading configurations is considered to be a frequent cause of collapse. In many building standard codes, the design roof load consist of a uniform or balanced snow load that acts over the whole roof and, if applicable, a drift surcharge load. Insurance investigations show that the design rules led to reduced safety against collapse owing to snow loads. In order to increase the reliability level of the design process of building this work contributes as a sort of "pre-design" study concerning in load hazard assessment, which may be useful to enhance the building standard codes, as a measure of risk mitigation. The methodology developed by the International Graduate College is modified in a way to consider the load analysis resulting from Wind-Snow Hazard. Is difficult to estimate the Wind-Snow Hazard accurately because wind and snow during a storm event are strongly correlated and the effects and influence by the effects of structural shapes and terrain roughness. At present, Wind-Snow Hazard is investigated by snow wind tunnel tests, field measurements and numerical models. However wind tunnel tests and field measurements are not so easy to conduct. Furthermore, it cannot be said that the similarity law for snow wind tunnel test has been satisfactorily established yet, hence a numerical model may contribute to a better understanding of these phenomena.
Currently available computational fluid dynamics codes have either no implemented model or there are snow models with inaccurate prediction due to the use of empirical parameters, or models that require an interpretation of results which may exceed common engineering capabilities. As a final goal of this research a simplified tool is developed to estimate snow load profiles without performing expensive wind-tunnel tests or field measurements. Such a tool could be of great interest for structural engineering, especially concerning ordinary buildings, which are usually designed according to the standard codes. In addition a numerical model could be useful in the "pre-design" stages.
The numerical model for transient simulation of snow drift proposed in this thesis is based on the lattice Boltzmann approach to model fluid, unsteady turbulent flow is modeled by a MRT model and adapts a Large Eddy Simulation computing the resolved spatio temporal flow structures and models the effect of the unresolved scales on the effective ones.

The primary motivation, from a physics perspective, for pursuing new methods to simulating fluid dynamics that use a discrete, pseudo-microscopic approach, such as the lattice Boltzmann method and its derivatives, is the possibility to model coupled problems in a unified kinetic framework. By simplifying the underlying physics so that only the key elements (conservation laws, symmetry conditions, proper equilibrium distributions) needed to assure accurate macroscopic behavior are retained, a computational advantage over traditional methods can be achieved, especially when the inherently parallel nature of such methods is exploited.
This approach was therefore chosen to model snow transport by wind, as a description in term of microscopic rules is a very attractive alternative to the classical models based on the resolution of semi-empirical equations. Instead of extracting complex governing equations and later modeling them using complicated numerical schemes, it appears much easier to incorporate directly the phenomenon ingredients into intuitive evolution rules. The numerical model, called "VirtualSnow", considers the different particles transport modes (saltation, creep and suspension, (3.3)) not explicitely. Instead they emerge naturally on the macroscopic scale from the evolution rules. The model is one-way coupled, i.e. the air flow controls the snow drift within a Eulerian frame of reference.
To validate the new developed "VirtualSnow" model numerous simulations have been performed and the results are compared to experimental data obtained in the "Jules Verne" Climatic Wind Tunnel of Nantes. Predictions of load profiles are in reasonable agreement with these experimental data. Even if the proposed snow drift model presents discrepancies in comparison to the experiments, the results seem very promising for the development of a numerical design tool for engineering purposes. After all the numerical model is shown to be capable of simulating snow accumulations in a building step, which is a very complex problem. Although this is only a first step towards this ambitious goal, it shows some of the difficulties which have to be overcome but it also highlights some interesting and encouraging results.
Further developments are possible in several directions.
The lattice Boltzmann approach used in this thesis is based on uniform grids, therefore has limitations in terms of accuracy for example in the area close to the obstacle in same particular case sufferers of accuracy. This is caused by an insufficient grid resolution, thus the development of a non-uniform grid refinement with adaptive resolution of the system is mandatory.
In addition, more defined parameters sensitivity studies should be further investigated, identifying for example the cases for which the definition of the grid needs adaptive refinement or the case witch the concentration of snow could be increased in order to reduce the simulation time.
Finally, the development of a two dimensional model with a coupled approach of different sub-models and the success of each of them should be encourage the extension to three dimensions model that could be pursued in another project.

Bibliography

[1] GORDON B. Olson library acquisitions list February 2009.

[2] Semide/emwis (2009): Euro-mediterranean information system on know-how in the water sector.

[3] 1992., U. D. Suburban emergency management project - disaster dictionary, 1992.

[4] (2009):, F. Glossary. pub. by: School of civil engineering and geosciences at the university of newcastle.

[5] Abbott, M., and Basco, D. Computational fluid dynamics-an introduction for engineers. *NASA STI/Recon Technical Report A 90* (1989), 51377.

[6] Ahrenholz, B. Massively parallel simulations of multiphase-and multicomponent flows using lattice Boltzmann methods.

[7] Alexander, D. Towards the development of standards in emergency management training and education. *Disaster Prevention and Management 12*, 2 (2003), 113–123.

[8] Anderson, R., and Haff, P. Wind modification and bed response during saltation of sand in air. *Acta Mechanica Supple*.

[9] Anderson, R., and Haff, P. Wind modification and bed response during saltation of sand in air. *Acta Mech 1* (1991), 21–51.

[10] Anselmet, F., Gagne, Y., Hopfinger, E., and Antonia, R. High-order velocity structure functions in turbulent shear flows. *Journal of Fluid Mechanics 140* (2006), 63–89.

[11] Augusti, G., Borri, C., and Niemann, H. Is Aeolian risk as significant as other environmental risks? *Reliability Engineering and System Safety 74*, 3 (2001), 227–237.

[12] Bagnold, R. *The physics of blown sand and desert dunes*. Methuen, 1954.

[13] Barltrop, N., Adams, A., Hallam, M., Oil, A., et al. *Dynamics of fixed marine structures*. Butterworth-Heinemann, 1991.

[14] Bhatnagar, P. L., Gross, E. P., and Krook, M. A Model for Collision Processes in Gases. I. Small Amplitude Processes in Charged and Neutral One-Component Systems. *Physical Review 94* (1954), 511–525.

[15] Bouzidi, M., Firdaouss, M., and Lallemand P. Momentum transfer of a lattice-Boltzmann fluid with boundaries. *Physics of Fluids 13* (2001), 3452–3459.

[16] Chen, S., and Doolen, G. Lattice Boltzmann method for fluid flows. *Annual Review of Fluid Mechanics 30*, 1 (1998), 329–364.

[17] Chopard, B., and Droz, M. *Cellular automata modeling of physical systems*. Cambridge University Press Cambridge, 1998.

[18] Crank, J. *The mathematics of diffusion*. Oxford University Press, USA, 1979.

[19] Cushman-Roisin, B. Introduction to Geophysical Fluid Dynamics, 320 pp, 1994.

[20] d Humières, D. Multiple–relaxation–time lattice Boltzmann models in three dimensions. *Philosophical Transactions of the Royal Society of London. Series A: Mathematical, Physical and Engineering Sciences 360*, 1792 (2002), 437.

[21] Davidson, P. *Turbulence: an introduction for scientists and engineers*. Oxford University Press, USA, 2004.

[22] Del Corso, R., Formichi, P., and Stiefel, U. Recent European research advances in snow loading and their possible implementation in the Eurocodes. *Progress in Structural Engineering and Materials 2*, 4 (2000), 483–494.

[23] DHA, 1992.

[24] EEA. European environmental agency glossary, 2009.

[25] Einstein, H. Special lecture: Landslide risk assessment procedure. In *Proceedings 5th international symposium on landslides, Lausanne* (1988), vol. 2, pp. 1075–1090.

[26] ESPON. European spatial planning observation network - glossary of terms, 2009.

[27] Flekkøy, E. Lattice Bhatnagar-Gross-Krook models for miscible fluids. *Physical Review E 47*, 6 (1993), 4247–4257.

[28] Frisch, U., dHumieres, D., Hasslacher, B., Lallemand, P., Pomeau, Y., and Rivet, J. Lattice gas hydrodynamics in two and three dimensions. In *Modern approaches to large nonlinear physical systems workshop* (1986), vol. 27.

[29] Frisch, U., and Kolmogorov, A. *Turbulence: the legacy of AN Kolmogorov*. Cambridge Univ Pr, 1995.

[30] Gauer, P. *Blowing and drifting snow in alpine terrain: a physically-based numerical model and related field measurements*. PhD thesis, SWISS FEDERAL INSTITUTE OF TECHNOLOGY ZURICH, 1999.

[31] Geller, S., Krafczyk, M., Tölke, J., Turek, S., and Hron, J. Benchmark computations based on Lattice-Boltzmann, Finite Element and Finite Volume Methods for laminar Flows. *Computers & Fluids 35* (2006), 888–897.

[32] Ginzburg, I. Equilibrium-type and link-type lattice Boltzmann models for generic advection and anisotropic-dispersion equation. *Advances in Water resources 28*, 11 (2005), 1171–1195.

[33] Ginzburg, I., and d'Humières, D. Multi-reflection boundary conditions for lattice Boltzmann models. *Physical Review E 68* (2003), 066614.1–066614.30.

[34] Ginzburg, I., Verhaeghe, F., and d'Humières, D. Two-relaxation-time lattice Boltzmann scheme: About parametrization, velocity, pressure and mixed boundary conditions. *Communications in Computational Physics 3* (2008), 427–478.

[35] Grothmann, T., and Reusswig, F. People at risk of flooding: why some residents take precautionary action while others do not. *Natural Hazards 38*, 1 (2006), 101–120.

[36] Hammer, W. *Handbook of system and product safety.* Prentice-Hall, 1972.

[37] Hauke, G. *An Introduction to Fluid Mechanics and Transport Phenomena.* Springer Verlag, 2008.

[38] He, X., and Luo, L. A priori derivation of the lattice Boltzmann equation. *Physical Review E 55*, 6 (1997), 6333–6336.

[39] He, X., Zou, Q., Luo, L., and Dembo, M. Analytic solutions of simple flows and analysis of nonslip boundary conditions for the lattice Boltzmann BGK model. *Journal of Statistical Physics 87*, 1 (1997), 115–136.

[40] Hodges, A. Emergency Risk Management. *Risk Management 2*, 4 (2000), 7–18.

[41] Inamuro, T., Yoshino, M., and Ogino, F. A non-slip boundary condition for lattice Boltzmann simulations. *Arxiv preprint comp-gas/9508002* (1995).

[42] Jeffery, C. *Statistical models of cloud-turbulence interactions.* PhD thesis, The University of British Columbia, 2001.

[43] Klein, G. Method of measuring the significant characteristics of a snow cover. *Technical Memorandum, Division of Building Research, National Research Council Canada* (2010), 1–38.

[44] Kron, W. Flood Risk, Hazard, Values, Vulnerability. *Water International 30*, 1 (2005), 58–68.

[45] Lallemand, P., and Luo, L.-S. Lattice Boltzmann method for moving boundaries. *Journal of Computational Physics 184* (2003), 406–421.

[46] Lynch-Stieglitz, M. The development and validation of a simple snow model for the GISS GCM.

[47] Maier, R., Bernard, R., and Grunau, D. Boundary conditions for the lattice Boltzmann method. *Physics of Fluids 8* (1996), 1788.

[48] McNamara, G., and Zanetti, G. Use of the Boltzmann equation to simulate lattice-gas automata. *Physical Review Letters 61*, 20 (1988), 2332–2335.

[49] Mei, R., Luo, L., and Shyy, W. An accurate curved boundary treatment in the lattice Boltzmann method. *Journal of Computational Physics 155*, 2 (1999), 307–330.

[50] Nishimura, K., and Hunt, J. Saltation and incipient suspension above a flat particle bed below a turbulent boundary layer. *Journal of Fluid Mechanics 417* (2000), 77–102.

[51] O'Rourke, M., and Wrenn, P. *Snow loads: A guide to the use and understanding of the snow load provisions of ASCE 7-02*. Amer Society of Civil Engineers, 2004.

[52] Pliefke, T., Sperbeck, S., and Urban, M. The probalistic risk management chain-general concept and definitions.

[53] Pomeroy, J., and Male, D. Steady-state suspension of snow. *Journal of hydrology 136*, 1-4 (1992), 275–301.

[54] Pope, S., and Pope, S. *Turbulent flows*. Cambridge Univ Pr, 2000.

[55] Qian, Y. H. Simulating thermohydrodynamics with lattice BGK models. *Journal of Scientific Computing 8* (1993), 231.

[56] Rothman, D., and Zaleski, S. *Lattice-gas cellular automata: simple models of complex hydrodynamics*. Cambridge Univ Pr, 2004.

[57] Sanpaolesi, L. *Scientific support activity in the filed of structural stability of civil engineering works snow loads*. Commision of the european communities DGIII-D3, University of Pisa, Department Structural Engineering, 1999.

[58] Sayers, P., Gouldby, B., Simm, J., Meadowcroft, I., and Hall, J. Risk, Performance and uncertainty in flood and coastal defence–A review. *DEFRA/EA R&D Tech. Rep. FD2302/TR1* (2002).

[59] Schneider, S. Can we estimate the likelihood of climatic changes at 2100, climatic change. *Climatic Change*.

[60] Schneiderbauer, S., Tschachler, T., Fischbacher, J., Hinterberger, W., and Fischer, P. Computational fluid dynamic (cfd) simulation of snowdrift in alpine environments, including a local weather model, for operational avalanche warning. *Annals of Glaciology 48* (2008), 1313–1340.

[61] SEMP. Suburban emergency management project - disaster dictionary, 2009.

[62] Simiu, E., and Scanlan, R. Wind effects on structures: an introduction to wind engineering.

[63] Skordos, P. Initial and boundary conditions for the lattice Boltzmann method. *Physical Review E 48*, 6 (1993), 4823–4842.

[64] Smagorinsky, J. General circulation experiments with the primitive equations. *Monthly weather review 91* (1963), 99–164.

[65] Smith, K. *Environmental hazards: assessing risk and reducing disaster*. Routledge, 2004.

[66] Stiebler, M., Tölke, J., and Krafczyk, M. An Advection-Diffusion Lattice Boltzmann Scheme for Hierarchical Grids. *Computers & Mathematics with Applications 55*, 7 (2007), 1576–1584.

[67] Stull, R. *An introduction to boundary layer meteorology*. Kluwer Academic, 1999.

[68] Succi, S. *The lattice Boltzmann equation for fluid dynamics and beyond*. Oxford University Press, USA, 2001.

[69] Tölke, J., Freudiger, S., and Krafczyk, M. An adaptive scheme for LBE multiphase flow simulations on hierarchical grids. *Computers & Fluids 35* (2006), 820–830.

[70] van der Sman, R., and Ernst, M. Convection-diffusion lattice Boltzmann schemes for irregular lattices. *Journal of Computational Physics 160* (1999), 766–782.

[71] Van Dyke, M. *An album of fluid motion*. Stanford, CA, 1982.

[72] Wolf-Gladrow, D. A lattice Boltzmann equation for diffusion. *Journal of Statistical Physics 79*, 5–6 (1995), 1023–1032.

[73] Wolfram, S. Cellular automaton fluids 1: Basic theory. *Journal of Statistical Physics 45*, 3 (1986), 471–526.

[74] Zhang, J., Hori, T., Tatano, H., Okada, N., Zhang, C., and Matsumoto, T. GIS and flood inundation model-based flood risk assessment in urbanized floodplain. In *Proceedings of the International Conference of GIS and Remote Sensing in Hydrology* (2003), pp. 16–19.

[75] Ziegler, D. Boundary conditions for lattice Boltzmann simulations. *Journal of Statistical Physics 71*, 5 (1993), 1171–1177.